Performance analysis of high-resolution and hyperspectral data fusion for classification and linear feature extraction

Shashi Dobhal

January, 2008

Performance analysis of high-resolution and hyperspectral data fusion for classification and linear feature extraction

by

Shashi Dobhal

Thesis submitted to the International Institute for Geo-information Science and Earth Observation in partial fulfilment of the requirements for the degree of Master of Science in Geo-information Science and Earth Observation, Specialisation: ("***GEOINFORMATICS***")

Thesis Assessment Board

Chairman: Prof. Dr. Ir. A. (Alfred Stein)
External examiner : Prof. P.K. Garg, IIT Roorkee
IIRS member : Mrs. Hina Pandey
IIRS member : Mrs. Poonam Seth Tiwari
IIRS member : Dr C. Jegannathan

Supervisors

IIRS: Mrs. Hina Pandey
Mrs. Poonam Seth Tiwari
ITC : Dr. Markus Gerke (EOS)

INTERNATIONAL INSTITUTE FOR GEO-INFORMATION SCIENCE AND EARTH OBSERVATION
ENSCHEDE, THE NETHERLANDS
&
INDIAN INSTITUTE OF REMOTE SENSING, NATIONAL REMOTE SENSING AGENCY (NRSA),
DEPARTMENT OF SPACE, DEHRADUN, INDIA

Disclaimer

This document describes work undertaken as part of a programme of study at the International Institute for Geo-information Science and Earth Observation. All views and opinions expressed therein remain the sole responsibility of the author, and do not necessarily represent those of the institute.

Abstract

Fusion of multispectral image with a hyperspectral image generates a composite image which preserves the spatial quality from the high resolution (MS) data and the spectral characteristics from the hyperspectral data. Despite the potential use of hyperspectral data to enhance the spectral information in the merged product, hyperspectral data has not been exploited to its extensive level. In fact, the fusion of multispectral data with hyperspectral data poses impasse due to large volume which in turn contribute to complexities in further processing. The objective of the present study was to analyse the Hyperion data for classification and feature extraction processes. To fulfil the objective, high resolution IKONOS data has been fused with Hyperion using three merging algorithms i.e. Gram-Schmidt, Principal Component and Colour Normalised transform. The outcomes of fusion have been compared with Hyperion data for the spectral evaluation. The spectral evaluation has been acquitted by analysing the spectral profiles of the various land use and land cover (LULC) classes. The spatial evaluation of the three fused products has been persuaded by the manual delineation of the various LULC classes in the original IKONOS and the three fused products. The quality measures of completeness and correctness has been utilized to meet the purpose of spatial evaluation.

The outcomes of the spectral evaluation confirm that the CN spectral sharpening is better in preserving the spectral properties in the fused product. The qualitative assessment of the various LULC classes illustrate that there is a remarkable gain in the spatial quality of the three fused products in comparison to the Hyperion data but no gain in comparison to the IKONOS data.

The consequences of FSA (Feature Space Analysis) have been intended to examine the separability of signatures before and after fusion. The results of FSA show that for some of the classes there is a remarkable increase in separability after fusion using any of the three techniques. As a result, the classification accuracy incurred for the GST and the PCT fused product is higher than IKONOS data. The results of classification for the CNT fused product are badly affected due to the spectral artifacts.

Keywords: Merging techniques Gram-Schmidt Transform (GST), Principal Component Transform (PCT), Colour Normalised Transform (CNT), Image fusion, Remote Sensing, Hyperspectral.

Acknowledgements

This thesis is the end of my long journey of 18 months in obtaining my degree in M.Sc "Geoinformatics". I have not travelled in a vacuum in this journey. There are some people who made this journey easier with words of encouragement and more intellectually satisfying by offering different places to look to expand my theories and ideas.

As a number of teachers, staff members and my colleagues have helped in completing my project, it is my duty to put on record my sincere thanks to all of them.

I express my sincere gratitude to my supervisors Ms. Hina Pandey and Mrs. Poonam Tiwari Seth (IIRS supervisors) and Markus Gerke for their joint contribution, support, invaluable guidance, great insight and encouragement throughout this research. I express my earnest gratitude to Ms. Hina Pandey and Mrs. Poonam Tiwari Seth (PRS), for their whole hearted support and introducing me to the subject of hyperspectral Remote Sensing that I seriously lacked and felt as though I am embarking on an unknown terrain. I am extremely grateful and wish to express my indebtedness to my ITC supervisor, Markus Gerke (EOS), for his noble guidance, keen interest and constant encouragement throughout the research. His unquenchable thirst for excellence is a perpetual source of inspiration. His in-depth knowledge in the field, creative and valuable comments in a simplified form were available so fast that I hardly felt him far away. His mails were constant source of inspiration during my research phase which has greatly helped n completing the thesis.

I am extremely grateful to Dr. V.K. Dadhawal, Dean, Indian Institute of Remote Sensing (IIRS), for his constant moral support throughout the research work. His valuable comments, in-depth knowledge in the subject, strong persuasion and constructive suggestions lead us to the successful completion of the project. I am thankful to Mr. P.L.N. Raju, Head of Geoinformatics, Dr. C. Jegannathan, Scientist 'E', Ms. Vandita Shrivastava, Scientist 'D', Mr. Ram Mohan Rao, Scientist 'D' Grade for their constant support, valuable suggestions and innovative teaching style. I extend my sincere thanks to all the faculty teachers of IIRS for their help, support, ideas, and valuable suggestions throughout my time at the institute. I want to thank all the non-technical staff members of IIRS, for their help and support throughout this programme.

I would like to thank ITC (International Institute for Geo-Information Sciences and Earth Observation, Enschede), for granting me fellowship for taking up studies at The Netherlands. I would like to thank and express my indebtedness to the then course coordinator, Ms. J.F. Stoter, mid-term evaluation committee members, Dr. Valentyn Tolpinkin and Mr. Nicholas Hamm (new course coordinator, GFM) for their critical reviews and suggestions. Even, I want to thank the teachers at ITC, Professor Stein, Mr. Elzakker, Dr. Tempfli, and Dr. Michael Morgan for they approved my research proposal during my proposal defending at ITC, Netherlands.

I am really indebted and extend my thanks to Mr. Milap Punia, JNU (Jawaharlal Nehru University, New Delhi) for introducing me to the subject of hyperspectral data and clearing my doubts through mails. I want to thank Mr. Uttam Kumar and Mr. Rishiraj Dutta, ex-students of IIRS, for their constant

help and valuable suggestions throughout my research work. I extend my thanks to Mr. Kapil Malik, Sierra Atlantic, Noida, for his innovative ideas and suggestions during my research work. I specially want to thank my colleagues Mr. Duminda Welikanna (from Sri Lanka) and Mr. Gurpreet Singh without whom this research work was impossible. They developed confidence in me to persuade the work with determination and helped me with software problems.

My sincere thanks to all the fellow participants of Geo-Informatics and Geo-Hazards course. I extend my thanks to Gurdeep Singh, Sandip, Samadrita, Chandan Nayak, Ambika, Rupinder, Sumana, Dr. Chand and Pravesh for the constructive discussions, criticism, cooperation and moral boosting during my entire time at IIRS. It was of immense help for me in my research work. I extend my sincere thanks to Miss Deepthi (M.Tech), whose precious suggestions during the work helped me a lot. I am indebted to Rinki Deo, Rahul (juniors) and Mahendra Singh Bisht (M.Tech) for their kind help and support.

I am really indebted to my parents to whom I dedicate this thesis. Without their support and help over the years towards my education, all this would not have been possible. I have gained great strength from them.

I am sure that the upcoming students would find the subject useful and informative. Despite all possible and sincere efforts any shortcoming in this research is regretted and is expected to be generously forgiven.

I dedicate my thesis to my grandmother who passed away recently. She was 92.....

Table of contents

Contents

List of figures

List of tables

1. Introduction

The introduction chapter provides an insight to the present research and its importance. This familiarises the reader with the overall objective and focuses on providing the glimpse of the fusion techniques that are used in the present work. The chapter begins with the general section addresses to the general idea behind the research.

1.1. General

Resolution can be defined as the fineness with which an instrument can distinguish between the different values of some measured attribute. When talking about resolution in remote sensing we talk about four types of resolutions i.e. spatial resolution, spectral resolution, radiometric resolution and temporal resolution. Where the spatial resolution refers to the area of smallest resolvable element (e.g. pixel); spectral resolution refers to the smallest wavelength which can be detected in the spectral measurement (Lillesand and Kiefer, 2000). Technically these two types of resolution can be inter-related so that one can be improved at the expense of the others. The two kinds of the sensors that are used for remote sensing in the past are panchromatic sensors and multispectral sensors, panchromatic in general refers to having broad spectral range, i.e. there spectral resolution is less, and have one band which generally shows the black and white image. Mostly panchromatic sensors have more spatial resolution as compared to multispectral sensors which have higher spectral resolution, in other words have more bands and show the coloured images. The information of an image is based on spatial and spectral resolution of an imaging system. To exploit and explore the benefit of enhanced spatial capability in panchromatic camera and enhanced spectral capability in multispectral camera, fusion techniques were developed to merge both the images. The fused image is a result of enhanced spatial information from the panchromatic image and enhanced spectral information from the multispectral image.

Fusion of multispectral and panchromatic image has been done in past times by many people for different purposes i.e. for feature extraction, 3D modelling (building extraction etc.). "Image *fusion is the combination of two or more images to form a new image by using a certain algorithm*".(Pohl and Genderen Van, 1998)

The image fusion technique is differentiated into three main categories according to the different levels of processing. The three levels of processing are the Pixel-based, the Feature-based and the Decision-based image fusion. Secondly, according to the domain model the image fusion process is divided into: Spatial-Based, Spectral-Based, and the Algebraic-Based. (Ali Darvishi et al., 2005)

The information of an image is based on spatial and spectral resolution of an imaging system. The image fusion technique is required to obtain both high spatial and high spectral resolution. The fused image is a result of enhanced spatial information from the panchromatic image and enhanced spectral information from the multispectral image.

"The "hyper" in the hyperspectral means "over" as in "too many" and refers to the large number of measured wavelength bands" (Shippert, 2008). Hyperspectral imaging in remote sensing was a major breakthrough that opened the avenues of research in various fields like mineralogy mapping for oil

exploration, environmental geology, vegetation sciences, hydrology, tsunami-aids, biomass estimation and many more due to its ample spectral information contained in hundreds of co-registered bands.

In terms of Earth observing also, hyperspectral studies have proved to be beneficial. In the geological studies including the study of the extra-terrestrial rocks, the hyperspectral sciences have opened the doors to horizons. In this regard, India's first lunar remote sensing satellite named Chandrayaan-1 will do the mineralogical mapping and study the rocks found on the surface of moon on the basis of the spectral responses. (Aarthy and Sanjeevi, 2007)

The fusion of hyperspectral with multispectral image results in a new image which has the spatial resolution of the high resolution image and all the spectral characteristics of the hyperspectral image. Hyperspectral data fusion is the latest approach to acquire significant and reliable information that can't be acquired with fusion of multispectral and panchromatic images. Hyperspectral remote sensing implies observation across full spectral region of 400-2500nm.

There are various image fusion approaches that are widely used to obtain complement the information. There are some algorithms used specifically to fuse and classify the Hyperspectral data with the multispectral data. Some of the algorithms are transformation based (e.g. Intensity, Hue, Saturation), wavelet decomposition, neural networks, knowledge-based image fusion, Colour Normalised Transform (CNT), Principal Component Transform (PCT) and the Gram-Schmidt Transform. (Ali Darvishi et al., 2005)

In the IHS transformation image fusion, the Intensity (I), the spatial component and the Hue (H) and the Saturation (S), the spectral components of an image are generated from the RGB image. The Intensity (I) component is then replaced by the high resolution panchromatic image to generate a new image in RGB, which is referred as the fused image or a sharpened image (Chen et al., 2003). In the wavelet-based image fusion technique, the image fusion is performed between the two spectral levels of hyperspectral image and one band of the multispectral image. The Colour Normalised Transform is another fusion technique that uses a mathematical combination of the colour image and a high resolution image. The Gram-Schmidt Transform is another fusion algorithm, used to fuse a multispectral image with a panchromatic image. This algorithm works in two modes that are "mode1" and "mode2" (Aiazzi et al., 2006). The Principal Component Transform works on the same basis as the Gram-Schmidt Transform, used to enhance a low resolution image using a high resolution data.

Apart from fusion, there are various techniques to classify a hyperspectral image. Some of the specialised techniques to classify a hyperspectral image are ANN (Artificial Neural Network), SVM (Support Vector Machine), whole pixel method, Spectral Angle Mapper, Spectral Feature Fitting, Sub-pixel methods, segment-based end member selection.

The detailed description of the various hyperspectral image fusion techniques and the classification will be covered in the next chapter.

1.2. Motivation and problem statement

Hyperspectral and Multispectral imaging systems are widely used in Earth observing systems and regional applications. A Hyperspectral imaging system provides detailed spectral information that enables the observer to detect and classify a pixel based on its spectral characteristics. However, in many cases, the spatial resolution of these systems is lower than a multispectral imaging system that has

less spectral channels. Combining hyperspectral and multispectral images can enhance the information content of the image thus helping in geospatial data extraction.

Fusion of multi-sensor image data has been widely used procedures now-a-days for complementing and enhancing the information content. The high-spatial resolution data is important in terms of getting the shape, size and orientation of the different features while high-spectral resolution data is needed in terms of spectrally distinguishing each and every pixel for classification and feature extraction. When high-spatial resolution data is merged with the high-spectral resolution data, the fused product we obtain is better in spatial and spectral resolution with enhancement in features. In fact, then there might be some loss in information in the fused image which must be comparable with the original image.

Already, there are various approaches of fusing a multispectral image with a panchromatic image like IHS (Intensity, Hue and Saturation), PCA (Principal Component Analysis), Brovey and many more. In fact, in precedent researchers have functioned in the regard of fusing multispectral image with a panchromatic image to interpret the image for spatial and spectral enhancement. Fusion of multispectral image with a hyperspectral image has been executed using wavelet-based algorithm. In the spectral domain, some of the algorithms that are specifically used to fuse a multispectral image with a hyperspectral image are the CNT (Colour Normalised Transform), GST (Gram-Schmidt Transform), and PCT (Principal Component Transform) to examine the eminence of the fused image. The purpose of the fused image for classification and feature extraction and exploiting the fused image for spatial and spectral enhancement has been the input facet which motivated the present research. The present work primarily focuses on the qualitative assessment of the fused image in terms of the spatial and spectral improvement.

The new thing in this research is the manual delineation of LULC classes (areal and linear features) in the original and the fused image and validation of the results to measure the improvement in the spatial quality after fusion using the three approaches of merging a multispectral image with a hyperspectral image.

1.3. Objective

The main objective of the present work is the analysis of the high resolution and hyperspectral data fusion using three different approaches (Gram-Schmidt, Principal Component, and Colour Normalised Transform) for classification and feature extraction.

Overall, the present work proceeds with an objective of:-

- The analysis of high resolution and hyperspectral data fusion for classification and linear feature extraction.

1.3.1. Sub-objectives

- Fusion of high resolution and hyperspectral data using the three merging techniques (GST, PCT & CNT).
- Performance analysis of the high-resolution and hyperspectral data fusion for Visual discrimination of features.
- Analysing effects of fusion on Digital Land cover Classification.
- Analysis of the fused images for linear feature extraction.

1.4. Research questions

The research questions which need to be answered in the present work are

- Is there a gain in classification and feature extraction from the fusion of high spatial resolution and hyperspectral data, i.e. is there a gain in geometric accuracy while the high thematic information is kept?
- What is the effect of fusion regarding the separability of classes in feature space?
- How do the results for classification and feature extraction depend on the selected algorithm?

All the above mentioned research questions mainly focus on the performance of the hyperspectral data fusion using the three merging techniques on feature extraction and classification. Another query in relation to the present work is the consequence of the three fusion techniques on the separability of the signatures in feature space.

1.5. Data used

1.5.1. HYPERION

Hyperion is an EO-1 (Earth Observation-1) sensor which was developed under NASA's new millennium program in November, 2000. The Hyperion image of Dehradun was acquired on 25th December, 2006. There are 224 bands with the spectral range of 355 to 2577 nm at 10 nm band width. The level 1 product used in the present study has 242 bands. Out of these 242 bands only 198 bands are calibrated. The bands which are not calibrated are set to zero. The reason for these non- calibrated bands is low sensor responsively.

Sensor altitude	705 Kms	**No. of rows**	256
Spatial resolution	30 mtrs	**No. of columns**	3128
Radiometric resolution	16 bits	**VNIR**	0.45-1.35
Swath	7.2 Kms	**SWIR**	1.40-2.48
IFOV (mrad)	0.043		

Table 1-1 Details of the Hyperion

1.5.2. IKONOS (MSS & Panchromatic)

IKONOS was the first commercial high resolution satellite to be positioned into the orbit. The IKONOS image used in the present work has been acquired in Feb, 2005. The IKONOS (MSS) image has 4

bands (red, green, blue, NIR) with 4m spatial resolution and IKONOS (Pan) has one band (.4-.9 μm) with 1m spatial resolution.

System	IKONOS
Orbit	681 km, 98.2° inclination, sun-synchronous, 10:30 am crossing, 14-day repeat cycle.
Sensor	Optical Sensor Assembly (OSA)
Swath width	11 Km
Off-nadir viewing	+-50° Omnidirectional
Revisit time	1-3 days
Spectral bands (μm)	0.45-0.52(1),0.52-0.60(2),0.63-0.69(3),0.76-0.90(4),0.45-0.90(PAN)
Spatial resolution	1m (PAN), 4m (bands 1-4)
Data archive	www.spaceimaging.com

Table 1-2 Details of IKONOS (mss) & IKONOS (Pan).

1.6. Study area

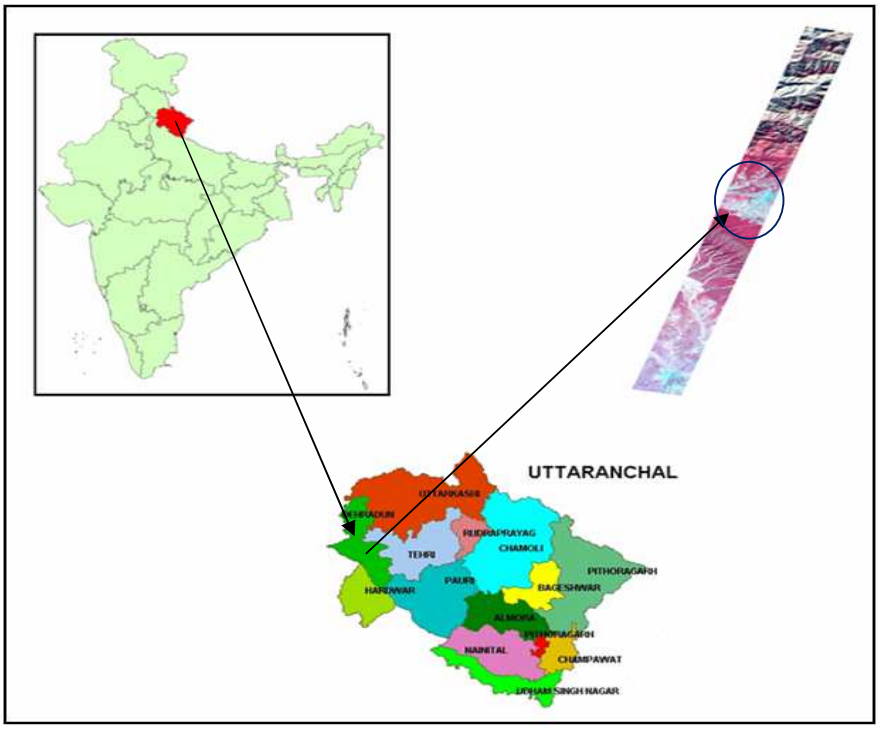

Figure 1-1 Study area (Dehradun city)

The city of Dehradun is situated in the south central part of Dehradun district. Dehradun city lies at 30°19' N and 78°20' E. The city is located at an altitude of 640 m above MSL. The lowest altitude is 600 m in the southern board is 38.04 sq. Km. The highest altitude is 1000 m in the northern part of the

city. The site where the city is located slopes gently from north to south direction. The northern part of the region is heavily dissected by a number of seasonal streams.

The study strip can be divided into two distinct land cover classes:

1) The western portion is dominated with varied vegetation of Sal, Teak, Bamboo, etc.
2) The southern part with the urban and some patches of vegetation. The urban pattern in Dehradun city is rather scattered and irregular.

The northern part again consists of varied LULC classes like the crop fields, fallow land, urban, grassland, shrubs, and vegetation of mix type. A seasonal river named Tons flows from North East to South West direction. Geomorphically, the northern part of the region is occupied by piedmont fan of post-Siwalik Dun gravels called the Donga fan. Donga fan is a region in the Dehradun city that consists of the varied LULC classes.

1.7. Chapter schema

The thesis starts with the introduction chapter which gives an insight to the image fusion technique and its benefits. The chapter gives a general introduction of the various image fusion algorithms used in remote sensing. The chapter more or less talks of the objectives and the research question to be answered in the present study. Also, the chapter gives a brief account of the study area and the data sets used. The second chapter is the literature review. This chapter covers more or less the conclusions drawn from the various papers I have gone through the research phase. The third chapter is the data preparation chapter, which in general will describe the pre-processing done to the datasets like the georeferencing, atmospheric correction, spatial and spectral subset. The fourth chapter is the methodology chapter which gives the general approach followed in the present work with a detailed workflow diagram. The fifth chapter is the results and discussion chapter followed by conclusion and further recommendations.

2. Literature Review

The chapter explorers the profundity of the various phenomenon covered in the present research like the atmospheric correction to the Hyperion data, classification, image fusion and various approaches of hyperspectral image fusion. The literature review done to get the general idea about the research is highlighted in the general section of the chapter. It talks broadly about the concept used in the research and tells the reader what he can expect further in the chapter. The chapter follows this section and provides the literature review done on the various other concepts like atmospheric corrections, band selection, classification, image fusion approaches used to achieve the desired.

2.1. General

Image fusion aims at integrating the spatial characteristics from the high resolution data and the spectral content from the lower resolution data. The process of image fusion caters and allows the user to interpret the image for further analysis depending up on various applications. Pohl and Genderen Van, 1998 proposed that image fusion is a tool to combine the multisource imagery using the advanced image processing techniques. According to Pohl and Genderen Van, 1998, the main objectives of image fusion are to sharpen images, improve geometric corrections, enhance certain features that are not visible in either of the images, replace the defective data, complement the data sets for the improved classification, detect changes using multitemporal data and, substitute the missing information in one of the image with the signals from another source image.

According to Varshney and Arora, 2004, merging methods are often divided into two categories: first method simultaneously takes into account all bands in the merging process e.g. Hue-Saturation-Value transformation, Principle-Component transformation, Gram-Schmidt transformation technique; the second category deal separately with the spatial information and each spectral band e.g. Brovey transformation, High-Pass-Filter transformation technique.

In the context of the present work, the fusion of the multispectral data with the hyperspectral data is executed using some algorithms to investigate the performance of the hyperspectral data for classification and feature extraction and also to examine the effect of the algorithms on the fusion outcomes.

2.2. Review on radiometric corrections to the Hyperion data

San and Suzen, 2007 pointed out that although the technical specifications of the Hyperion sensor are reasonably advanced but in the operational mode due to the some atmospheric effects of scattering, aerosols and water vapour the quality of the Hyperion image acquired is badly affected. Thus, to render

accurate and reliable outcomes the radiometric correction of the Hyperion data is a compulsory pre-processing step.

According to Bakker et al., 2004, the pre-processing of the imaging spectrometer data necessitates the radiometric correction which in turn postulates the use of some function to convert the DN (Digital number) into the at-sensor radiance. The at-sensor radiance should be calibrated by the end user to minimise the atmospheric effects to obtain the at-sensor or the surface reflectance data.
Conversion of the DN values to the radiance values can be performed by utilizing the following equation:

$$L_\lambda = \left[\frac{L_{MAX} - L_{MIN}}{Q_{CALMAX} - Q_{CALMIN}}\right] \times (DN - Q_{CALMIN}) + L_{MIN}$$ .....***equation 2. 1***(Owojori and Xie, 2008)

Where DN = Digital Number for each pixel of the image.

L_{MAX} and L_{MIN} = calibration constants.

Q_{CALMAX} and Q_{CALMIN} = the highest and the lowest points of the range of rescaled radiance in DN.

According to Bakker et al., 2004 the improvement of the signal as compared to the noise from the background materials can be done in three ways in the visible part of the spectrum. The three ways to correct the signal are cosmetic corrections, relative Atmospheric Correction methods based on the ground reflectance properties and Absolute Atmospheric Correction methods based on atmosphere process information.
Bakker et al., 2004 postulated that the cosmetic correction counterbalances the visible faults and noise in the image data. According to them, usually these are not the real atmospheric correction methods as these do not allow running any model. Some special filters, image stretching and enhancement procedures are required to perform the cosmetic corrections. The cosmetic corrections are required to minimise the problem of periodic line dropouts, line striping and random noise.
Usually, the ***periodic line*** dropout is an outcome of the error in any of the detectors of the sensor. Periodic drop out can be traced in an image by the presence of some black lines in the image data. The error of ***line striping*** is an outcome of non-identical detector response. The result of the error in the image file can be described by some bright and dark scan lines. The third cosmetic correction is the ***random noise*** which occurs due to the inaccuracy in the transmission of the data. The occurrence of some bright and dark spots in the image file is the consequence of this error which hinders in the information extraction processes.
Generally, atmospheric correction (AC) methods are of two types: Relative AC methods that are based on two methods i.e. two reflectance measurements and the two reference surfaces. Another method of atmospheric correction is the use of ***absolute atmospheric processes.***
Basically, the ***absolute atmospheric processes*** need to define the elements necessary in the atmospheric profile. The absolute atmospheric correction methods are based on some AC models that require the information regarding the atmospheric condition, altitude, geometry between sun and the satellite, aerosol level, water absorption, time of acquisition of the image and more details. The absolute AC methods have the advantage over other methods that these can be run under any atmospheric condition.

- San and Suzen, 2007 have compared the various techniques of atmospheric correction done to the Hyperion data. The work compared the results of the four models namely ACORN (Atmospheric CORrection Now), FLAASH (Fast Line- of- Sight Atmospheric Analysis of Spectral Hypercubes) and the ATCOR 2-3 (Atmospheric CORrection) on the Hyperion data for the test site of Central Anatolia having sparse vegetation cover. The resultant images obtained after running the models and the spectral signatures collected from the field were compared in the spectral domain. In the spectral range between 1300-1400 nm and 1740-1990 nm certain anomalies were encountered due to the water vapour and the aerosols cover in the atmosphere. Due to the reason, these regions were omitted for the analysis. As the ATCOR 3 algorithm uses the DEM (Digital Elevation Model) for the correction, the capacities of the three models that is ACORN, FLAASH and ATCOR 2 were compared. Then, the best output according to the ability of the three models has been compared to the ATCOR 3 model. The results of the various models run for the atmospheric correction of the Hyperion data show beneficial results. As the ATCOR 3 algorithm requires a DEM, which was not available for the region, ATCOR 2 model was used for this purpose. The results of the ACORN and the FLAASH model show comparable spectral curves. The wavelength regions of 1305.95 to 1396.73 nm and 1749.79 to 1991.95 nm were set to zero due to water absorption bands in the ACORN model. The same sort of suppression due to the water absorption bands was observed after running the FLAASH model but here the wavelength range was quite narrower i.e. in between 1366.44 to 1396.73 nm and 1830.57 to 1941.56 nm. The results of the ATCOR 2 and ATCOR 3 model were similar to the FLAASH. The study concluded that ACORN algorithm is best for the atmospheric correction of the Hyperion data.
- Shih, 2004 has performed the atmospheric correction for the Hyperion scene of Taiwan region. FLAASH model was used for the purpose. A water content and the cloud mask generated image was compared to an optical image .The spectral polishing effect is also studied with the spectra obtained after running the model. The radiance values were compared with the corrected spectra. The results of the study show that the image obtained after running FLAASH closely matches with the reflectance spectra. The original 196 bands have been reduced to 167. The cloud mask image generated after running FLAASH shows high agreement with the clouds observed in the optical image.
- Owojori and Xie, 2008 carried out a work on the LANDSAT image-based Land Use Land Cover changes in the San Antonio region of the United States, using atmospheric correction and an object-based image classification and finally the validation of the results. Here the atmospheric correction of the LANDSAT image has been done using FLAASH (Fast Line-of-Sight Atmospheric Analysis of the Spectral Hypercubes) model. The results of the FLAASH model run for the LANDSAT image showed the enhancement in the spectral resolution. "*Dark Object Subtraction (DOS) is the simplest and most widely used image-based relative atmospheric correction approach for classification and change detection applications*".
- Eckert and Kneubuhler, 2004 has done some radiometric calibration to the Hyperion data for the agricultural land classification and vegetation properties estimation in the Limpach Valley of Switzerland. The level 1B1 product has been used here consisting of the 198 spectral bands in the wavelength range of 400-2500 nm with a spatial resolution of 30m. The pre-processing of the Hyperion data is done by correcting the striping error. The strips caused by the calibration differences are removed by using a correction algorithm to improve the dataset. The

algorithm works in a horizontal manner and checks for every DN value with its immediate left and right pixel DN value. The pixel DN value is designated as an abnormal DN if its value is quite lower than its neighbouring DN value. The abnormal DN values are corrected by taking the average of the neighbouring pixel DN values. This algorithm works best for most of the bands except for the bands which are intensively striped one. After the strips are removed the atmospheric correction is performed using the ATCOR-4 algorithm which is based on the look-up tables generated with a radiative transfer code (MODTRAN-4). The results of the atmospheric correction done to the Hyperion data showed enhancement in the spectral resolution thus helping in better classification of the agricultural fields.

In the present work, FLAASH model is run to remove the atmospheric effects because FLAASH consider the properties of water vapour, aerosol distribution and elevation and as a consequence FLAASH module of ENVI provides the most accurate and reliable method of compensating for the atmospheric effects.

2.3. Review on band selection

According to Huang and He, April 2005, hyperspectral data consists of high number of the correlated bands in the wavelength range of 400-2500 nm. The large data volume helps in differentiating among various signatures in a scene but at the same time add to the problem of heavy computation and redundancy. To solve or minimise this problem one needs to reduce the number of bands, the process to do the same can be termed as "***dimensionality reduction***" or "***band selection***".
Generally, band selection is the process of compressing the information in less number of bands. The process of band selection is done for the data having hundreds of bands containing redundant information and is highly correlated. Band selection is an important step in hyperspectral data processing because the large volume of data poses challenging problems for information processing which tend to complicate the interpretation results.

- Huang and He, April 2005, analysed the band selection in the hyperspectral data using the process of feature weighing. The band selection in the hyperspectral data has been done by using the pair wise separability criterion and matrix coefficient analysis. The criterion values were evaluated for the individual new bands from the decorrelation of each class using the Principal Component Transform (PCT), evaluating the coefficients of the PCT and also the criterion values, determination of the final weights of the original bands and removal of the redundant bands by giving a threshold value. The results proved that the present method of band selection is better through the comparison of the two sequential search algorithms and the four feature weighting algorithms.

In the context of the present work, band subsetting is performed on Hyperion because it tries to identify the subset of the original Hyperion bands for the given task without affecting the band physical means.

2.4. Review on Land Use / Land Cover classification

Classification is the process of assigning a thematic class to an individual pixel that represents the radiance detected at the sensor. The result of classification is a transformed image consisting of the discrete values for the classes of interest instead of the continuous values, which are measured in terms of the DN (Digital Number) or the Brightness Value (BV). Generally, image classification is the phenomenon to reduce the number of bands into a single band raster file.

Image classification is employed for extracting the information classes of the interest. Land cover classification of the image data depend on the diverse circumstances of the image acquired. Different conditions like the sun illumination, snow cover, other atmospheric conditions, crop growth in a particular season etc. conditions effect the classification process.

Image classification or the 'partition of the feature space' can be done in two ways: Supervised and Unsupervised classification. In the ***supervised classification***, the operator defines his classes of interest by selecting the training samples in an image on the basis of his/her knowledge of the area. In the ***unsupervised classification***, the image is partitioned into homogenous spectral clusters using some clustering algorithm. These spectral clusters are accomplished on the basis of some spectral similarities.

According to Anderson et al., 1976, during 1970s the USGS invented a land use and land cover classification system for use with remote sensor data. The basic concepts and structure of the system is still applicable today. Even in the recent times for the LULC mapping, the people still follow the basic structure originally invented by the USGS. (Lillesand and Kiefer, 2000)

The basic USGS Land Use and Land Cover mapping method utilize the concept and have designed to use four "levels" of information. Level 1 was originally designed for the use with the low to moderate resolution satellite data such as Landsat Multispectral Scanner (MSS) images. The images with resolutions of 20 to 100 m are more suitable for this level of mapping. Level II was invented for the use with the small-scale aerial photographs. The images with resolutions of 5 to 20 m are relevant for this level of mapping. The most suitable and widely used image type for this level has been high altitude colour infrared photographs. The other data sources in which level II LULC mapping can be utilized are Landsat Thematic Mapper and the Enhanced Thematic Mapper Plus (+), SPOT, IRS (Indian Remote Sensing) satellite. For mapping at Level III, supplementary information, in addition to that rendered from the medium-scale images is required. The image data sets with resolution of 1 to 5 m is relevant in this category. Mostly, high-spatial resolution images and the aerial photographs can be used as the data sources at this level. The last level of mapping that is of Level IV requires substantial amounts of additional information in addition to that obtained from aerial images. The images having resolutions of .3 to 1.0 m is appropriate in this level. The image data sources that come under this category are large-scale aerial photographs.

Land Use/Land Cover Classification Level	Representative Map Compilation Scale	Approximate Minimum Size Area Mapped (ha)
I	1: 500,000	150
II	1: 62,500	2.5
III	1: 24,000	0.35

Table 2-1 Table giving the classification level with minimum size of the area mapped (Lillesand and Kiefer, 2000)

The table given gives the minimum size of the Land Use/Land Cover units mapped at various classification levels. The calculations are established on the minimum map unit size of 2.5 * 2.5 mm.
There are various algorithms available to classify specifically a multispectral image like the Box classifier, Minimum Distance to Mean Classifier and the Maximum Likelihood Classifier. The ***box classifier*** takes the maximum and minimum limits of a class. Basically, it defines the mean and standard deviation per class to acquire a box-like area in the feature space. The ***Minimum Distance to Mean Classifier (MDM)*** defines the cluster centres. When the classification is carried, the Euclidean distance from an unknown pixel to various cluster centres is computed. The pixel is assigned to a class to which the distance to the mean DN value of that class is least. The ***Maximum Likelihood classifier*** takes the class variability in to account. The MLC classifier considers the cluster centre, its shape, size and orientation. This can be executed by computing a statistical distance recognized on the mean values of the classes and the covariance matrix of the clusters. The pixel is assigned to the class to which it has the highest probability.

2.4.1. Review on Hyperspectral classification

Classification of the hyperspectral data like Hyperion is an important research area now-a-days because of the high spectral variability among different classes. Hyperspectral classification can be beneficial for better discrimination among a single class, as for example, the urban feature (building tops) can be classified according to the different material types like silica or clay; vegetation can be classified into more than one type according to the variable spectral reflectance in the near infrared range; likewise other classes can also be distinguished depending on the spectral variability. Due to large number of co-registered and narrow bandwidth bands, hyperspectral data has the key potential to better discriminate among diverse classes with additional information.
The classification executed on the multispectral data grades in clustering the image into very broad categories of the classes but the hyperspectral data allows the prospects of classifying the image data into various classes according to the spectral variability. Hyperspectral analysis can be done in the spectrally similar classes and the sub-pixel scale information can be extracted. There are various methods of classifying the hyperspectral data. According to Shippert, 2008 the spectral analysis of the hyperspectral data is done by comparing the pixel spectra with the reference spectra, also called the target spectra. The target spectra can be derived using some of the spectral libraries or region of the interest in the spectral image. The hyperspectral data classification can be divided into two broad categories: spectral matching approach and the sub-pixel classification. (Shippert, 2008)

2.5. Spectral matching algorithms

2.5.1. SAM (Spectral Angle Mapper)

According to Bakker et al., 2004 the spectra are addressed like vectors in space with the dimensionality equal to the number of bands, n. The SAM rule figures the spectral similarity between the unknown

reflectance spectrum, e (consisting of the band values e_i), and a reference reflectance spectrum (received from the field or the laboratory), r (having band values r_i). The spectral similarity between the unknown spectrum and the reference spectrum is expressed in terms of the vector angle, ø, between the two spectra as calculated using all the bands, i. Then, the SAM-score can be calculated by:

$$\cos\ \varphi = \frac{\sum_{i=0}^{n} e_i r_i}{\sqrt{\sum_{i=0}^{n} e_i^2}\ \sqrt{\sum_{i=0}^{n} r_i^2}}$$ .....***equation 2.2*** (Greiwe and Ehlers, 2008)

φ = Spectral angle

e = Given image spectra

r = Reference spectra (end member)

n = Number of classes

The SAM-score is compared in terms of the angular difference, measured in radians ranging from zero to Π/2. The smaller the spectral angle, the more similar is the unknown pixel to the reference (target) spectra.

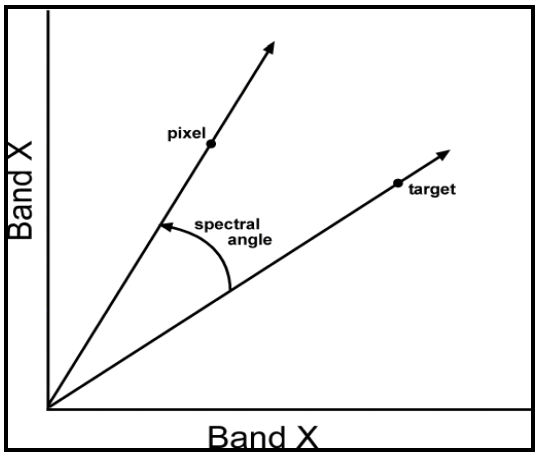

Figure 2-1 Spectral angle between target and the pixel spectra in two-dimensional space (Shippert, 2008)

Shippert, 2008 proposed that the spectral angle between the unknown and the reference pixel is insensitive to the changes in pixel illumination because the increase or decrease in the pixel illumination does not accounts for the change in vector direction but in the magnitude (i.e., a darker pixel will plot along the same vector, but closer to the origin). In the case of a hyperspectral image, the SAM rule of classification computes the "hyper" angle between the pixel and the target.

2.5.2. Spectral Feature Fitting

According to Shippert, 2008 in the Spectral Feature Fitting, the user specifies a range of wavelength within which the unique absorption feature exists for the selected target. Then, the unknown pixel spectrum is equated with the reference target spectra on the ground of two measures: 1) depth of the feature in the pixel is compared with the depth of the feature in the reference pixel and, 2) the shape of the feature in the unknown pixel is compared with the shape of the feature in the target pixel using a least square technique.

2.6. Sub-Pixel methods

2.6.1. Spectral unmixing

According to Bakker et al., 2004 generally the pixel spectra, consist of the spectral mixture of a number of the ground classes present in a sensed surface. The various factors which contribute to the spectral mixing are: the imaging systems of the sensor mixes the reflected light from various ground features, secondly, the materials present in the field of view of the sensor impart to the mixed reflectance for an individual pixel, and thirdly, difference in the illumination conditions due to topographic effects may also account for the mixed reflectance.

Spectral unmixing is a type of image classification approach which recognises the composition nature of the ground feature and classifies the pixel on the basis of the varied reflectance, instead, of just assigning the individual pixel to the fixed number of classes. The reflectance of a single pixel of a hyperspectral data is composed of the mixture of reflectance given by the ground features for a scene area. The spectral unmixing procedure endeavours at finding the relative or absolute fractions of the set of the spectral components that together contribute to the observed reflectance of pixels. The set of spectrally unique surface materials existing within a scene are often referred to as the spectral ***end-members*** for that scene. The spectral unmixing intents at gaining the fractions of the pure end-members from the mixed pixel. This mixed pixel is also called as the 'mixel' or the signal.

A linear combination of spectral end-members is chosen to decompose the mixed reflectance spectrum of each pixel, $\vec{R}$, into fractions of its end-members, $\vec{\mathrm{Re}}_j$, by

$$\vec{R} = \sum_{j=1}^{n} f_j \, \vec{\mathrm{Re}}_j + \vec{\in} \text{ and } 0 \le \sum_{j=1}^{n} \mathrm{f_j} \le 1 \text{ .....} \textbf{\textit{equation 2.3}} \text{ (Bakker et al., 2004)}$$

Where $\vec{R}$ = reflectance of mixed spectrum of each pixel.

f_j = fraction of each end-member j.

$\vec{\mathrm{Re}}_j$ = reflectance of the end-member spectrum j.

and 'j' indicates each of the 'n' end-members, and $\vec{\in}$ is the residual error.

The SAM approach of supervised classification is preferred over other classification approaches for the present study because we wanted the pure unique pixels that cluster the image on the basis of the spectral variations among the various LULC classes. Also, the SAM approach of classification when

used on the calibrated reflectance data is insensitive to the illumination and albedo effects which makes it more efficient way for classifying the image data.

2.7. Review on validation of land use/land cover classification

According to Jensen, 1996 accuracy assessment is a general term for comparing the classification to the geographical data that is assumed to be true, in order to determine the accuracy of the classification process. The true data is assumed to be taken from the ground truth data. But, sometimes it's not practical and assessable to get the ground truth data or test each and every pixel to the ground truth; therefore a set of reference pixels is always used.

There are diverse ways of obtaining the classification accuracy of a classified image. The outcomes of the image classification are established on samples of the classes (training sites) collected from the ground or from image itself to quantify the classification and assess it for further interpretation. This can be done by the sampling techniques that are anticipated to select the pixels to be tested. There are various sampling schemes that are used to quantify the classification accuracy.

In context to the simple land use and land cover classification, the two schemes of rendering the classification accuracy are: ***Random sampling*** and the ***Stratified random sampling***. In the ***random sampling*** technique, some random points are generated for every class in the classified image with class labelled to them. The interpreter has to identify each and every pixel and assign the pixel to the class to which it actually belongs in the reference image or with the ground truth information. The random sampling technique may undersample small but possibly very important classes unless the sample size is significantly large. In the ***stratified*** or the systematic sampling technique, uniform distribution of the points is done, i.e., equal number of points is randomly generated for every class in the classified raster file. Likewise, the interpreter after going through every pixel assigns it to the actual class (derived from the high-resolution image or the ground truth data) and produces the contingency matrix or error matrix.

An error matrix is a square array of numbers laid out in rows and columns that extract the number of sample units (i.e. pixels, cluster of pixels) deputed to a particular category in proportion to the actual category as affirmed from the field. The columns generally represent the reference data, while the rows indicate the classification generated from the satellite images. An error matrix is a very efficient way of exemplifying accuracy because the accuracy of each class is clearly described, along with both the error of omission (error of exclusion) and error of commission (inclusion errors). Error of omission denotes those samples that are omitted in the interpretation result. This error initiates from the reference data and therefore is related to the columns in an error matrix. The error of commission is generated by the incorrectly classified samples which refer to the rows in an error matrix. Error of omission is a result of the producer accuracy which is defined as the probability of a sampled point on the map is one particular class. The error of commission is a result of the user accuracy which is the probability that a certain reference class has also been marked that class.

- Greiwe and Ehlers, 2008 analysed the combined effect of the hyperspectral and the high resolution image for object-based classification. The study area for the present work is the central part of the City of Osnabrueck (Northwest Germany), which consists of different urban surface types. In the present work, the fusion is performed on the feature-level. Hyperspectral data (HyMap) has been fused with the high resolution imagery (digital orthophotos) for

classification using the end member selection. After this segmentation is performed on the high spatial resolution data, the segments has been used to find the end members in the hyperspectral data which helps in the classification phenomenon.

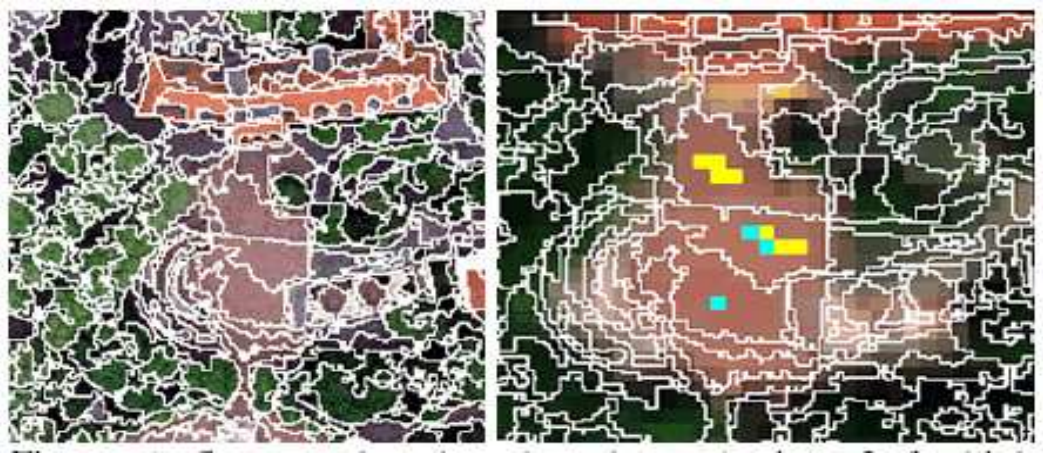

Figure 2-2 Segmented image of the high-resolution data (left) and the representative end members (yellow coloured) in the hyperspectral data (HyMap) (right)

The results show the differentiation in different material classes, like the "red roof top" were discriminated into "red roof concrete" and "red roof clay". In the present work three different classification approaches have been taken to evaluate the performance. The three approaches are minimum distance classification of the RGB image, the SAM-score method of classification and an additionally combination of the segment's elevation. The classification accuracy from the three methods has been compared which shows a low overall accuracy for the RGB phenomenon due to spectral similarity in the defined classes. There was an increase of 20% due to the addition of the hyperspectral information in the classification process. This is due to the discrimination of the surfaces with similar features but into different materials. The work proved that the integration of the hyperspectral characteristics together with the high spatial resolution data results in better discrimination and classification of the different urban surfaces based on material differentiation.

- Lee and Davies, 2004 carried out a study on the autonomous vegetation cover scene classification of the EO-1 Hyperion data. In this study an algorithm to locate the extent of lava and its initial location and vegetation cover based on the spectral shape is compared. This is called as L-V (Lava- Vegetation) algorithm. The algorithm has been developed under the ASE (Autonomous Sciencecraft Experiment) that is set onboard on the EO-1 sensor for the automatic data processing based on the change detection from observation to observation. The L-V algorithm has been developed for the differentiation into the vegetated and the non-vegetated regions in the volcanic regions. The algorithm has been developed taking the six day time images of the Hyperion data for the volcanic regions; two images of the Kilauea in Hawaii, two of Mt. Etna in Sicily, Italy and two of Erta'Ale in Ethiopia. The spectra from the forty randomly chosen pixels on one Kilauea image were investigated. A strong absorption of the red light was examined at band 34, hence called as "red edge". Thus, the pixels having the "red edge" were classified as the vegetated part and the pixels without the "red edge" were put into

the non-vegetated category. The two bands were investigated for this purpose that is band 34 and 41. The two bands were chosen because the "red edge" can be seen in these two bands and the DN value of band 34 is equal to or lower than the value of band 41. Likewise, the spectral information was taken for the rest of the five images. A condition has been developed in this work like if 34< or =41, then vegetation or otherwise if 34>41, then its non-vegetated region (or the lava). The algorithm proved to be very accurate and efficient for the classification in the volcanic regions into vegetation and non-vegetation (lava) category.

- Eckert and Kneubuhler, 2004 analysed the potential of the Hyperion data for the agricultural landcover classification and the vegetation properties estimation in the Limpach valley of Switzerland. The two approaches for classifying the Hyperion data of the agricultural land in Switzerland has been examined in this study namely the SAM (Spectral Angle Mapper)-score and the multiresolution object- based classification. The results of classification have been influenced by the low spectral variations among various agricultural types due to the late phonological stage of the cultivars at the time of data acquisition. The results of the SAM rule approach of classification of the agricultural fields has been influenced by the spectral mixture due to the small-spaced pattern of the fields. Also, due to the late phenological changes, there is a spectral similarity in the various landcover classes. Even, the results of the object-oriented approach of classification produced disappointing results due to many reasons like low spectral variations in the crops due to the reason of the time of acquisition of the Hyperion data, spectral mixture due to small-spaced fields in the region and low textural differences in the Hyperion datasets. The factor that influenced the most in the classification process is the time of acquisition of the Hyperion data. The study concluded on the note that for the classification of the agricultural fields the data should be taken during the time of the year from the spectral point of view like the growing season.

2.8. Review on manual classification

As generalised by Bakker et al., 2004 the phenomenon of delineation or manual classification is mainly based on the geomorphological characteristics using a structured legend. The process of delineation can also be termed as mapping which in general, requires a generalisation of the real world. The simplest way to do this is by introducing classes or the categories. Then, the manner to introduce the classes can be hierarchal which provide an easy way to aggregate data to the high level classes.
According to the USGS, for mapping the Land Use and Land Cover at Level I and Level II, for most of the classes the minimum mapping unit of 16 ha was utilized. The work was carried out for most of the coterminous United States and Hawaii at a scale of 1:250,000. The polygons delineating the natural area have a minimum size of 4 ha. Even for the man-made features like roads and highways the minimum size of the polygons has been 4 ha, with a minimum feature width of 200 m. (Lillesand and Kiefer, 2000)

Generally, manual delineation of the land use and land cover classes is done on the basis of the visual interpretation of the input images. Feature extraction from the remote sensing images based on visual interpretation is the most intuitive way of rendering information. Generally, visual inspection of the various land use and land cover classes is based upon the ability of a man to pertain and connect colours and patterns in an image to real world features. For this purpose, a skilled photo-interpreter is required.

The visual inspection of the diverse land use and land cover classes is done to obtain spatial information for various applications like the vegetation mapping, soil mapping, urban planning, cadastral mapping, LULC (Land Use and Land Cover) mapping and many other areas. Mostly, the interpretation of the results is done by explicitly digitising the geometric and the thematic data of the features of interest.

Usually, while examining the images (from the remote sensing satellites) for the purpose of visual interpretation the image interpreter is between two situations i.e. ***spontaneous identification*** and by ***logical assumption***. In the spontaneous identification, the interpreter at the first look can infer about the various land use and land cover classes present in an image while in the logical assumption, the image interpreter applies his analysis and logical thinking to conclude about the various land cover and land use classes present in satellite imagery.
For the visual interpretation of the various land use and land cover classes in satellite imagery, we require a set of key factors to express and draw conclusions about the classes. These set of factors are termed as the interpretation keys or elements. There are 7 interpretation keys. ***Tone*** is defined as the relative brightness of a black/white image. ***Hue*** pertains to the colour of the image in IHS (Intensity Hue Saturation) space. ***Shape*** is the characteristic factor to define most of the classes in an image (crop fields are usually rectangular, roads are linear). ***Size*** is considered in the relative or absolute terms. The width of the road is examined in relative terms and compared to the size of the other features. ***Pattern*** relates to the spatial arrangement of the various classes. ***Texture*** pertains to the gradient in the tone (e.g. course or smooth, even or uneven). ***Site*** relates to the topographic or the geographic location. ***Association*** is the grouping of similar features in to one class.

In the context of the present work, the land use and the land cover classes delineated from the data sets is based on the above mentioned 7 interpretation keys. In the course resolution data of Hyperion, the 7 interpretation keys aided in delineating the land use and land cover features because any of the class was hardly recognizable.

2.9. Review on validation of manual classification

According to Bakker et al., 2004 the results of the manual classification are validated using the ground data or the high-resolution data. This is performed for the qualitative assessment of the features delineated from the image files. Usually, the quality of the extracted features can be assessed using the quality measures of completeness and correctness.

According to Weidemann et al., 1998 before computing the completeness and correctness, we require the TP (True Positive), FP (False Positive) and the FN (False Negative) areas. The area of the delineated feature which is common and correctly matched in both the ***test*** (input image) and the ***reference*** image (usually a high-spatial resolution image) is termed as the TP (True Positive) area. The area of a delineated feature which is covered in the reference image but does not match to the area of the same feature delineated in the test image is termed as the FN (False Negative) area. The area of the delineated feature in the test image which does not match to the area of the same delineated feature in the reference image is termed as the FP (False Positive) area.
Completeness is the ratio of the matched extracted data to the total number of the relevant records within the ground truth data.

Completeness = TP / (TP+ FN) where completeness Є (0, 1).....***equation 2.4*** (Wiedemann et al., 1998)

Correctness is the ratio of the matched extracted data to the total number of the relevant and irrelevant data obtained.

Correctness = TP/ (TP+FP) where correctness Є (0, 1).....***equation 2.5*** (Wiedemann et al., 1998)

The quality of the extracted feature is computed by combining the completeness and correctness as a single measure.

Quality = TP/ (TP+FP+FN) where quality Є (0, 1).....***equation 2.6*** (Wiedemann et al., 1998)

- In the paper, Wiedemann et al., 1998 studied the road axes and compared the quality of the roads extracted with the reference data. The automatically extracted roads from some algorithms have been compared with the manually delineated roads as the reference data. The comparison is done on the two bases: firstly, matching the extracted road to the reference network and secondly using some quality measures like the completeness, correctness, redundancy, planimetric RMS differences and the gap statistics. The aim of the study is to evaluate the geometric accuracy of the extracted roads. The results of the validation of the extracted data from the quality measures of correctness and completeness are of no more significance because the vector layer obtained (by manual delineation) is no correct and complete.

In the present context, the quality measures of completeness and correctness are used to validate the results of manual classification using a high-spatial resolution image as the reference image because of the unavailability of the ground truth data.

2.10. Review on Image fusion

Image fusion is the combination of two or more images to produce a single sharpened image that is used for further interpretation. Pohl and Genderen Van, 1998 conceptualised that "*Image fusion is the combination of two or more different images to form a new image using a certain algorithm*".

According to the different processing level the image fusion is divided into three categories:

(i) Pixel-Based image fusion.
(ii) Feature-Based image fusion.
(iii) Decision-Based image fusion.

According to the domain model, image fusion is divided into three categories:

(i) Spatial-Based image fusion.
(ii) Spectral-Based image fusion.
(iii) Algebraic-Based image fusion.

2.10.1. Processing levels

2.10.1.1. Pixel-Based image fusion

Pohl and Genderen Van, 1998 inferred that the pixel-based image fusion is based on the pixel-by-pixel fusion or through the fusion of the associated local neighbourhood of the pixels in each of the images used for the fusion. This is the lowest level of processing. In the pixel-based image fusion the data used should be properly co-registered or otherwise the new image suffers from misregistration. Pixel-based image fusion requires appropriate resampling of the image data to a common pixel spacing and map projection.

2.10.1.2. Feature-Based image fusion

Pohl and Genderen Van, 1998 generalised that the feature-based image fusion is the second level of processing. In the feature-Based image fusion technique various features documented in the different data sources are sorted together and then fused feature wise to get a new image. In the feature-based image fusion, the various classes are sorted by utilizing the components of edge matching, shape, size, orientation, and features with similar intensity in the images to be fused. In feature-based image fusion, less meticulous co-registration is required.

2.10.1.3. Decision-Based image fusion

According to Pohl and Genderen Van, 1998 in the decision-based image fusion, value-added data is employed where the individual images are refined for information extraction. Then some decision rules are applied to combine the extracted information to build up a common understanding of the features. Hence, this level of processing is also called as interpretation-level of image fusion.

2.10.2. Fusion algorithms

2.10.2.1. IHS (Intensity Hue Saturation)

According to Chen et al., 2003 in the IHS transformation image fusion, the Intensity (I), the spatial component and the Hue (H) and the Saturation (S), the spectral components of an image are generated from the RGB image. The Intensity (I) component is then substituted by the high resolution panchromatic image to render a new image in RGB, which is referred as the fused image. This is also called as a sharpened image. In the IHS transformation the three bands of the lower resolution image is utilized to translate it into the IHS space. Then, a contrast stretch is applied to the high resolution image, so that the stretched image has the same variance and average as the intensity component image. The stretched image that is the higher resolution image substitutes the intensity component before the image is metamorphosed to original colour image.

2.10.2.2. Colour Normalised Transform

The Colour Normalised Transform is another fusion technique that uses a mathematical grouping of the colour image and a high resolution image. The Colour Normalised Transform is also named as the Energy Subdivision Transform that employs a high resolution image to sharpen a low resolution image. This algorithm is also called as Brovey Transform, the outcome of this transform is the DN of the fused (DN fused) which is incurred from the input data in 'n' multispectral bands b_1, b_2……b_n multiplied by the high resolution image DN higher.

DN fused = [DN b_1/ (DN b_1 + DN b_2+…….DN b_n)] * DN higher (ENVI help guide)

The Brovey Transform algorithm uses a formula that normalises multispectral bands used for a RGB (Red Green Blue) display and multiplies the result by high resolution data to add the intensity or the brightness component of the image. Brovey Transform is used to increase the contrast and intensity in the low and high ends of the histogram and for producing visually appealing images. (Sanjeevi, 2008)

2.10.2.3. Wavelets-Transform image fusion

According to Gomez et al., 2001 the wavelet concept is utilized to fuse the two spectral levels of a hyperspectral image with one band of multispectral image. Wavelets generally mean "waves". Image fusion by Wavelet-based method involves two processing steps: first step consists of extracting the details or the structures. The extracted structures are decomposed into three wavelet coefficients based upon the direction that is the vertical, horizontal and the diagonal. Thus, in combining the high-resolution image with a low-resolution image, the high-resolution image is first reference stretched three times, each time to match one of the low-resolution band histograms while, the second step necessitates the introduction of these structures/details into each low-resolution image band through the inverse wavelet transform. Thus, the spectral content from the low-resolution band image is preserved because only the scale structures between the two different resolution images are added. (Sanjeevi, 2008)

2.10.2.4. Gram-Schmidt Transform

Aiazzi et al., 2006 described that the Gram-Schmidt Transform (GST) is another fusion algorithm which is used to fuse a multispectral image with a panchromatic image. The Gram-Schmidt Transform was invented by Brover and Laben in 1998 and patented by Eastman Kodak. This algorithm works in two modes: "mode1" and "mode2". The "mode1" takes the pixel average of the multispectral (MS) bands. The spatial quality in "mode1" is better but suffers from the spectral distortions due to the radiometric difference of the average of the MS bands and the panchromatic image. While, in "mode2" the spectral distortions are not present but suffer from poor enhancement and low sharpness.

2.10.2.5. Principal Component Transform

The Principal Component Transform (PCT) used to enhance a low resolution image using a high resolution data. The PC band1 is replaced with a high resolution band, which is scaled to match the PC band1. Hence, there is almost no distortion in the spectral information in the fused output image. The

low resolution image is sharpened to high resolution image using nearest neighbour, bilinear cubic or cubic convolution technique. (ENVI help guide)

- Ali Darvishi et al., 2005 analysed the capability of the two algorithms that is Gram-Schmidt and the Principal Component transform in the spectral domain. For this purpose two datasets have been taken (Hyperion/ Quickbird-MS and Hyperion/ Spot-Pan). The main objective of the study was the investigation of the two algorithms in the spectral domain and the statistical interpretation of the fused images with the raw Hyperion. The study area was Central Sulawesi in Indonesia. The results of the fusion show that the GST and PCT has almost similar ability in protecting the statistics as compared to the raw Hyperion. The correlation analysis show poor correlation between the raw Hyperion and the fused image bands. The results of the analysis show that the bands located in the high-frequency area of the spectrum better preserve the statistics as compared to the bands located in the low-frequency region. Different statistical parameters like the standard deviation, mean, median, and mode, maximum, minimum values of the raw Hyperion and the two fused images (GST & PCT) were compared for the analysis.
- Gomez et al., 2001 has studied the fusion of the hyperspectral data with the multispectral data using the Wavelet-based image fusion. In the present study, two levels of hyperspectral data were used in fusion with one band of multispectral data. The fused image obtained had a RMSE (Root Mean Square Error) of 2.8 per pixel with a SNR (Signal to Noise Ration) of 36 dB. The results show that the fusion of hyperspectral data with the multispectral data produced a composite image of high spatial resolution of the multispectral data with all the spectral characteristics of the hyperspectral data with minimum artifacts. The study concluded that more than two datasets can be fused using the Wavelet transform image fusion technique.
- Chen et al., 2003 carried out a study which took the hyperspectral data, AVIRIS (Airborne Visible/ Infrared Imaging Spectrometer) to fuse with TOPSTAR (Topographic Synthetic Aperture Radar) which provides the textural information to get a composite image to study the urban scene. The study has been conducted for the urban area of Park city, Utah. The composite image obtained has been superimposed on the DEM (Digital Elevation Model) generated from the TOPSTAR data to get a 3D perspective. The transformed image obtained was interpreted for the visual discrimination among various urban types. This was possible after fusion of AVIRIS and TOPSTAR data using IHS (Intensity Hue Saturation) transform, which resulted in an image having high spatial and spectral resolution. The objective of the study was to study the areas which are at a risk due to the geological hazards like the avalanches, mudflows etc. The fused image was interpreted for information extraction for assessment and mitigation of these hazards in the area. The results of the fusion of the AVIRIS and TOPSTAR data show better enhancement in the urban features. The spectral resolution of the AVIRIS data helped in better discriminating among various urban features like the buildings and the mining tailings. The MNF-transformed bands of the AVIRIS data also improved the discriminability among the various features. The combined use of the HIS fused data, the MNF-transformed bands and the DEM of the area provided for better understanding of the urban features.
- Ling et al., 2006 has analysed the results of fusing the high resolution data like the IKONOS and Quickbird using the FFT (Fast Fourier Transform) - enhanced HIS method. The study aimed at evaluating the ability of the traditional methods like the HIS and the PCA (Principal

Component Analysis) in fusing the high resolution data to preserve the colour and spectral information in the fused product. The study integrated the HIS transform with the FFT filtering of both the panchromatic and the intensity component of the multispectral image. The study has been done using the IKONOS and the Quickbird data. The analysis prove that the HIS transform using the FFT filtering improved the results in preserving the high spatial quality and the spectral characteristics.

In the present work, the GST (Gram-Schmidt Transform), PCT (Principal Component Transform) and the Colour Normalised techniques are utilized to fuse the multispectral image with a hyperspectral image to assess the fused images for spatial and spectral enhancement.

2.11. Summary

The chapter more or less talks of the different concepts like the atmospheric correction, the various image fusion methods including hyperspectral image fusion algorithms, landcover classification, quality assessment. Most of the work carried till now in the hyperspectral data perspective is regarding atmospheric correction or the fusion of the hyperspectral data with the multispectral data using some algorithms. Some of the work has been carried out in the direction of land cover classification of the hyperspectral data and then the validation of the results by the accuracy assessment. The present research integrates the different phenomenon of atmospheric correction and land cover classification of the Hyperion data, fusion of Hyperion with the high resolution data and assessing the quality of the fused image by visual discrimination and even the statistical analysis, into one. The present work adds a new attribute to the hyperspectral work that is manual delineation of some of the land cover classes and linear features in the original and the fused images and then validating the results by utilizing the quality measures of completeness and correctness.

3. Data preparation

This chapter goes to the depth of the literal work persuaded with the IKONOS (mss), IKONOS (Pan) and the Hyperion data in context of the present research. The chapter caters and allows the reader with the knowledge of all the pre-processing steps and experiments carried out on the original data sets i.e. Multispectral (MS) data, IKONOS (mss) and hyperspectral data of Hyperion.

3.1. Pre-processing

The pre-processing stage can be considered as the first step to work with the data sets available and acquire the valuable information from the same. The data sets that are available to the user initially are in the raw form and most of the datasets are not geo-referenced or geometrically calibrated to the ground. These datasets can also have errors due to atmospheric effects and need atmospheric corrections or radiometric calibrations. The users have data that contains lot of information and often user does not require the whole of it, therefore spatial and spectral subsetting of the data is required, which also helps in reducing the complexities and the processing time on the image used.
The pre-processing stage has been further divided into the steps like the geometric calibration, the radiometric correction or the atmospheric correction of the Hyperion data, spectral subsetting of the Hyperion data or the band selection. These steps have been further tinted in the upcoming paragraphs.

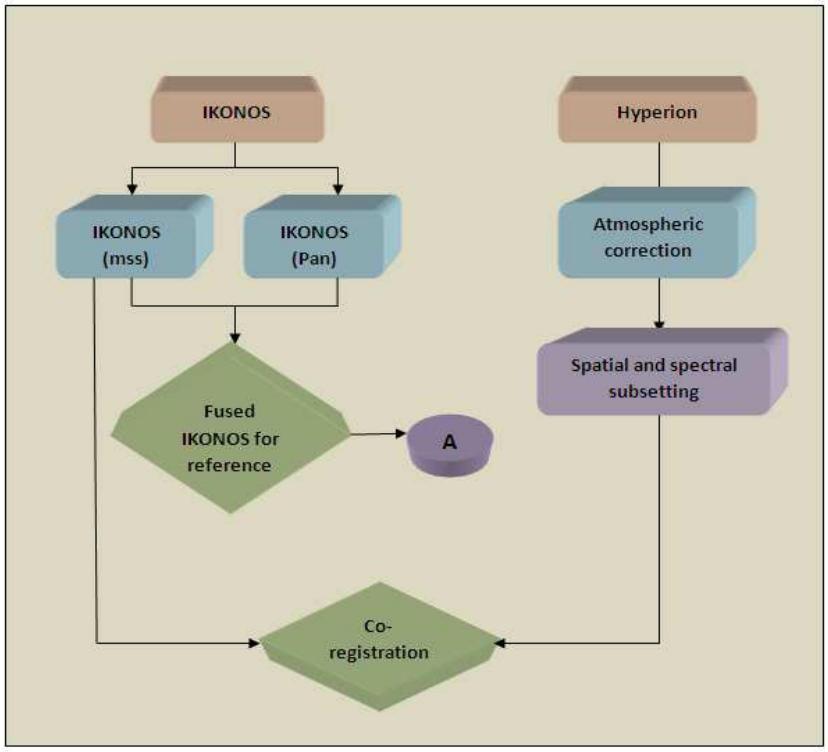

Figure 3-1 Different pre-processing levels

The various pre-processing steps carried out here are as follows:
Step 1: Atmospheric correction of the Hyperion data.
Step 2: Extracting the spatial and the spectral subset of the Hyperion data.
Step 3: Fusion of the IKONOS (mss, 4m) and the IKONOS (Pan, 1m) for reference data.
Step 4: Geometric correction or georeferencing the Hyperion data

3.1.1. Atmospheric correction of the Hyperion data

The radiometric calibration of the hyperspectral data is needed in order to allow the retrieval of pure ground radiances from the target materials.
The Hyperion image for the study area (Dehradun) is badly affected due to the time of acquisition i.e. 25th December, 2006. During this time of the year, the northern part of India suffers from severe cold and haziness in the atmosphere. The haziness in atmosphere accounts for the reduced radiation from Sun reaching the Earth surface causing blurriness in the image. Also, there is spectral variation in the vegetation and agricultural fields due to phenological changes. Due to all these reasons, the atmospheric correction for the Hyperion image was considered important in the present study.
Hyperion acquires the data in the pushbroom mode with two spectrometers; one in the VNIR range and the other in the SWIR range. In the present work, Hyperion data of Level 1R has been taken that became effective on December, 2001. Hyperion data has 242 bands of which only 198 are calibrated (band 8 to 57 for VNIR and 77 to 224 for the SWIR range). Because of the overlap between the focal planes of the VNIR and the SWIR, there are only 196 unique channels. The bands that are not calibrated are set to zero. The reason for not calibrating the 242 bands is low detector responsively.
The steps in the pre-processing of Hyperion for the radiometric correction of the Level 1R include Short Wave Infrared (SWIR) smearing, removal of the bands having no information, removal of the line dropouts, removal of the line striping in the various bands, and removal of the absorption bands. The SWIR and the VNIR (visible near-infrared) bands are scaled; subsets of the bands are specified; abnormal pixels are corrected and finally geometric correction is done.

3.1.1.1. Removing the absorption bands and the bands having no information

The Hyperion Level 1R product consists of the 242 bands of which 198 are nonzero. This is due to the heavy water absorption in the VNIR and the SWIR region and also due to the spectral overlap between the two spectrometers set in the VNIR and the SWIR region.
In the present work, the bands from 126-176 (mostly in the 1400-1900 nm) have been dropped due to the heavy water absorption in the VNIR and SWIR region. The Hyperion bands have been resized taking into history of the information content in the different image bands because some of the Hyperion bands (Level 1R product) of the Dehradun scene do not have any information while some of the bands suffer from the negative values for the wavelengths. Accordingly, the image bands were finally resized into 149 bands by excluding the bands having no information, bands having negative values for the wavelengths and bands falling in the water absorption range.

Bands	
0-8	No information
9-11	Negative values
70,71,72	No information
73,74	Negative values
76	Negative values
68,69	Negative values
80,81	Negative values
83	No information
85,86,88	No information
120-130	No information
165-181	No information
185,186	Negative value
Above 224	No information

Table 3-1 List of the bands excluded from the Hyperion (242) Level 1R product

3.1.1.2. Balancing vertical stripes in the VNIR and the SWIR range

In a pushbroom sensor, an inadequately calibrated detector in any of the VNIR or the SWIR range leaves high-frequency errors called as the "vertical stripes". These vertical stripes badly affect the image bands. In the Hyperion striping pixels have been classified into four categories: i) continuous with atypical DN values, ii) continuous with constant DN value, iii) intermittent with atypical DN values and, iv) intermittent with lower DN values. Out of the above four categories, the first two are acute, as they contain very low or no valid and effectual data about the features on ground. The level 1R product consists of the bands affected with the vertical stripes, which are left untouched, thus allowing the user to handle or replace according to the requirement. In order to render calibrated Hyperion image bands, we need to cautiously balance these vertical stripes.

In the present work, these vertical strips were minimised by checking each band for the vertical stripe, and replacing the DN value for the affected column by the average of the DN values of the adjacent columns. This was done for most of the image bands because whole of the calibrated bands were seriously affected by these vertical stripes.

3.1.1.3. Identifying and removing the bad columns

In order to counterbalance for the striping in the Hyperion datasets global and local de-striping approaches have been proposed. In the present work, the bad columns were identified visually in order to avoid imposing severe changes in the spectra. A total of the 36 bad columns were identified in the 13 VNIR bands of the Dehradun (scene area). No bad columns were identified in the SWIR region.

Bands	Bad column in Dehradun
8	6,68,114,125,132,141
9	6,68,114,119,125,246
10	6,68,114,199
11	6,68,114,199
12	6,114
13	114
15	114
27	47
28	47,114
31	114
54	13,17,20,32,39
55	13,17,20,32,33,39
56	13,17,20,32,33,39
57	8,13,17,20,33,36,38

Table 3-2 Location of the detected bad columns in the Hyperion Level 1R product.

These bad columns once identified were reduced by checking each band for the bad column, and replacing the DN value for the affected column by the average of the DN values of the adjacent columns.

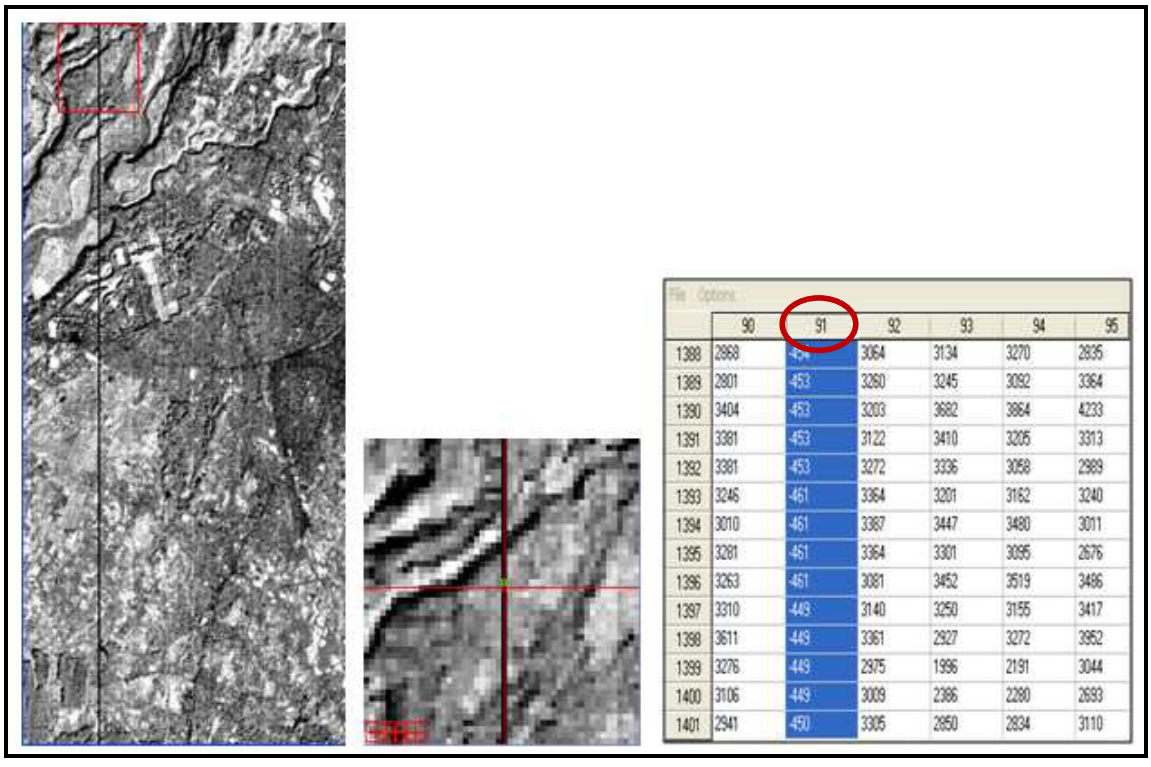

Figure 3-2 A bad column (column number 91) recognised in the 99th band of the Hyperion image (Before correction)

Above is seen a Hyperion image band number 99, of which 91th column is affected from negative DN value for that column. After correcting the column by replacing the existing DN value with the average of the DN value of the adjacent columns, the error is reduced to some level. After the correction, the same image band is seen as shown downwards.

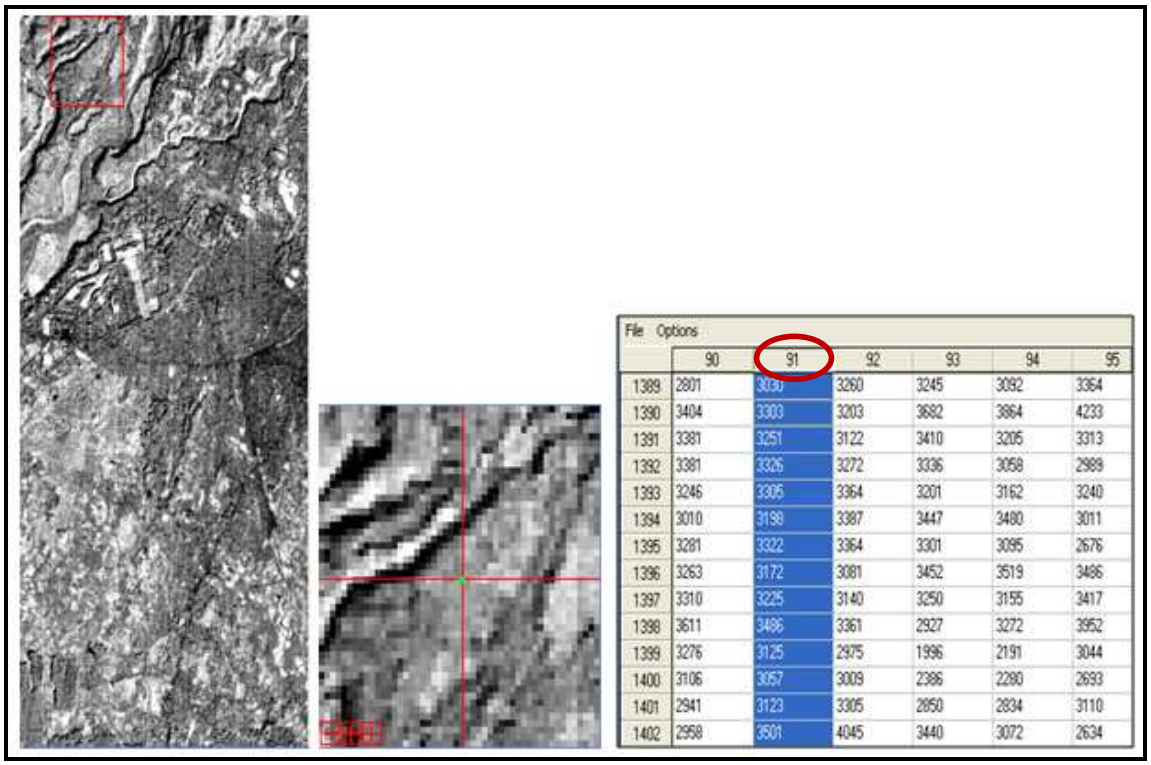

Figure 3-3 Image after the bad band column removal

After the image bands are corrected, for the different errors like the bad band removal, removal of the absorption bands, removal of the non-calibrated bands, and reduction of the vertical stripes, the 242 bands image has been reduced to 149. Now on these resized 149 bands, the FLAASH (Fast Line-of-Sight Atmospheric Analysis of the Spectral Hypercubes) model is run.

In the present work, the FLAASH model is chosen because of the following reasons:

- FLAASH uses a more recent version of MODTRAN (Moderate Resolution Atmospheric Radiance and Transmittance Model) with a newer spectral database.
- It uses a reflectance ratio-based method for visibility retrieval.
- FLAASH performs the MODTRAN calculations on-the-fly, supporting off-nadir geometries and all the MODTRAN aerosols types.
- FLAASH provides the compensation for the "adjacency effect" (pixel mixing due to scattering of surface reflected radiance) and the automated wavelength calibration.
- The results from FLAASH and other Radiative transfer model tend to be similar in the dry, clear atmospheres but significant differences can occur under moist and hazy conditions.

The specifications for the FLAASH model to run are as follows:

Lat - 30º 20' 24.72"	**Flight time (GMT) (HH:MM:SS)** 5:10:23
Long -78° 0' 23.76"	**Atmospheric model**- Tropical
Sensor type- Hyperion	**Water Absorption Feature-** 1135nm
Sensor altitude -705 Km	**Aerosol model**- Rural
Ground elevation- .600 Km	**Aerosol Retrieval**- 2-Band (K-T)
Pixel size- 30m	**Initial visibility**- 20 Km
Flight data- 25th December	**Modtran Multiscatter Model –**Scale DISTORT

Table 3-3 Specifications of FLAASH model

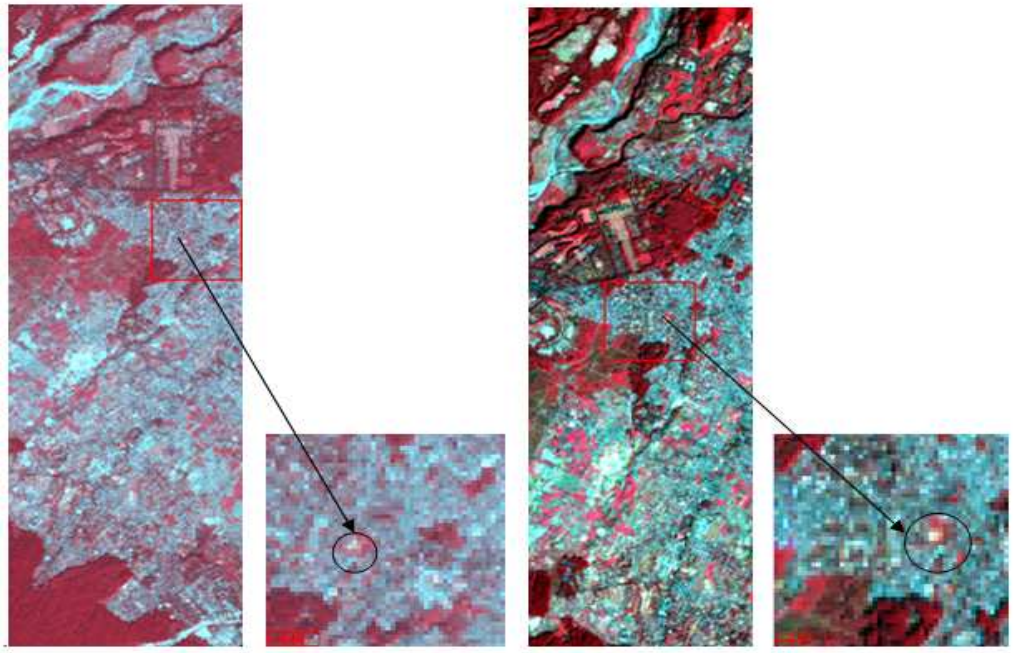

Figure 3-4 Urban feature (building) seen before and after running FLAASH.

In the above figure one can trace out visually, the difference in the urban feature seen before and after running FLAASH model. After running FLAASH model, the haziness in the image is minimised to a certain level and the features are sharpened with increased brightness. This can be interpreted statistically also, by observing the profile (graphs showing the variation of Wavelength, bands vs. Reflectance value) of the feature before and after running FLAASH.

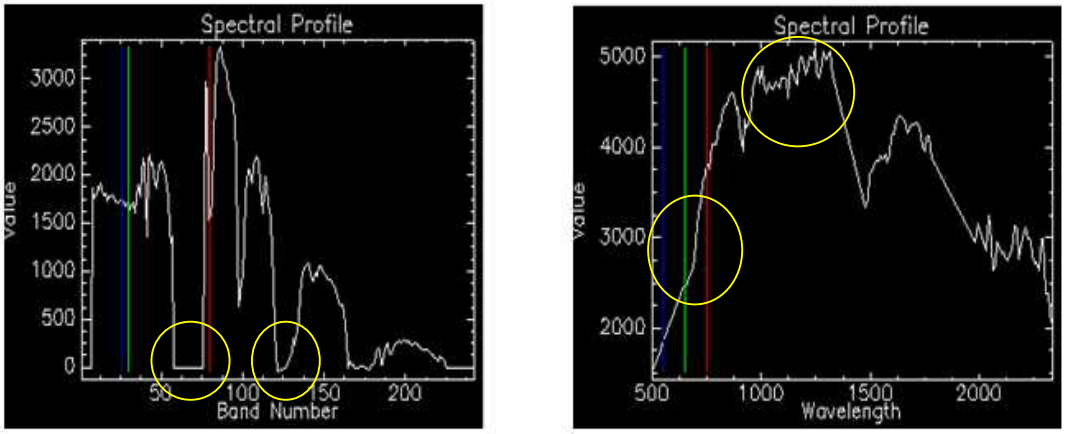

Figure 3-5 Spectral profile of the urban feature before and after FLAASH

From the above profile, one can observe the enhancement in the feature class after running the model. We can well observe that the dips present in the profile between the band number 57 to 85 (approximated) and also at 120-130 range are completely reduced after the atmospheric correction. Instead, we can see a sharp rise in the value starting from the blue region and a steep slope in the atmospherically corrected profile. Also, we can observe in the profile of the atmospherically corrected image, the presence of a number of narrow contiguous peaks in the wavelength range of 900-1350 nm range.

3.1.2. Georeferencing of the Hyperion data

The geometric calibration of the image data can be done by the georeferencing. It is the simplest way of linking an image data to a projection system. Geometric correction is undertaken to avoid geometric distortions from a distorted image, and is achieved by establishing the relationship between the image co-ordinate system and the geographic coordinate system using calibration data of the sensor, measured data of position and attitude, the ground control points, atmospheric conditions, etc.

The geometric calibration is usually achieved by the process of geocoding which is done by applying two methods as given below:

1. ***Image to map registration****:* The base reference data used here is survey of India toposheet for image to map geometric correction. To select the Ground Control Point (GCP), permanent features like bridges, road crossings, railway lines, reservoirs etc. which were easy to locate on both map and IKONOS image were used. For this purpose, first order transformation was used and therefore, 4 GCPs were taken for image to map registration. The root mean square error (RMSE) for the geo-corrected image was 0.52 pixels. Geo-correction also involves selection of the transformation projection and the Datum which were taken as Universal Transverse Mercator (UTM) and WGS 84 respectively.
2. ***Image to image registration****:* In the image to image registration the base referenced data used is an image, during the project geo-referenced IKONOS is used as the base image for the co-registration of the other data i.e. Hyperion in our case. Image to image registration was an important step in the research as we know that the basic objective of the research is to fuse the IKONOS data with Hyperion, so pixel to pixel matching of the two images was important. This

could be achieved if we could co-register both the images together. The root mean square was tried to be kept as low as possible. Affine transformation was applied as the area was not very large to do the registration however fifty well distributed GCPs were taken to do the registration as any misregistration could lead to erroneous results later in the research. The RMSE recorded for the Hyperion image was equal to .9254 pixels with respect to the IKONOS image. It was ascertained that geo-co-registration should lie within the sub pixel level through the visual inspection of the geo-linked pixels in both the images. The correctness of the registration was also further verified by using different tools like swiping and flickering in ERDAS.

3.1.3. Spatial and the spectral subsetting of the Hyperion image

3.1.3.1. Spatial subset

The spatial subset of the image is the process of extracting the significant area from the image file and removing the extraneous part for better and fast processing. In the remote sensing domain, we talk of subsetting an image according to the area of interest of the user.

In the present work, the spatial subset has been prepared to extract the common area in both the datasets (IKONOS, mss and Hyperion), since here the core idea is to fuse the two images using the three algorithms i.e. Gram-Schmidt Transform, Colour Normalised Transform and the Principal Component Transform. Thus for fusion common areas are required in both the datasets.

The raw Hyperion image file for the Dehradun scene initially consisted of 256 samples and 3407 lines. On applying the radiometric corrections and running the FLAASH model on the raw Hyperion image, the image file has been broken down into 197 samples and 399 lines. Hyperion is further reduced to 45 samples and 340 lines to get a common area, in both IKONOS and Hyperion. The IKONOS (mss) image file, primarily consisted of 2548 samples and 3141 lines which was decomposed to 362 samples and 2796 lines.

3.1.3.2. Spectral subset

The spectral subset is an important phenomenon in the hyperspectral data perspective because of the high dimensionality of the data which caters challenging task and the computational complexity due to the numerous bands. Thus, the number of bands should be reduced in order to allow for better outcomes and faster processing.

In the present work, the Hyperion data taken consists of 242 bands with the spectral coverage range of 400-2500 nm. While, the spectral range of the IKONOS (mss) data is from 400-900 nm. As the mainstay thought of the research is image fusion, for which we require the two datasets to be fused in almost similar spectral range, the spectral subsetting of the Hyperion dataset has been a compulsory step in the present work.

The spectral subsets for the Hyperion data have been created in the same wavelength range as that of the IKONOS i.e. 400-900 nm. The bands taken for the spectral subset are from the band number 15 (498.0400 nm) to band number 34 (691.3700 nm) and from band number 41 (762.6000 nm) to band

number 55 (905.0500 nm). So, in total, the Hyperion image file has been reduced from resized 149 bands to 34 bands.

3.1.4. Fusion of the IKONOS (mss) and IKONOS (Pan) for the reference data

Fusion is the process of integrating two or more images of same or different resolutions using certain approach to acquire a composite image with high degree of information.
In the context of the present work, image fusion of IKONOS, mss (4m) and IKONOS, Pan (1m) has been performed using PCA (Principal Component Analysis) using nearest neighbour resampling technique. This has been done to get a composite image in RGB, which has been used as the reference image for the manually delineated land cover/land use classes and the linear features. The composite image was required for the reference data because of the unavailability of the ground reference data for the evaluation of the geometric accuracy.

3.2. Summary

The data preparation chapter gives an overview of the various pre- processing measures carried out in the present context like georeferencing the Hyperion data, atmospheric corrections, spatial and spectral subsetting. The chapter was mandatory in the sense that it provides with the key inputs that were necessary for further processing and analysis of the data. The atmospheric correction of the Hyperion data has been performed by running the FLAASH model. The chapter is organized in a way to provide the reader with the preliminary experiments carried out specifically on the Hyperion data. Overall, the chapter caters and allows for the better understanding of the Hyperion data.

4. Methodology

The methodology chapter has been framed in a manner to achieve the research objectives and answer to the research questions. The chapter describes the processes that have been performed on the Hyperion and the high spatial resolution data, IKONOS (mss). The overall methodology adapted in the current work is as follows:

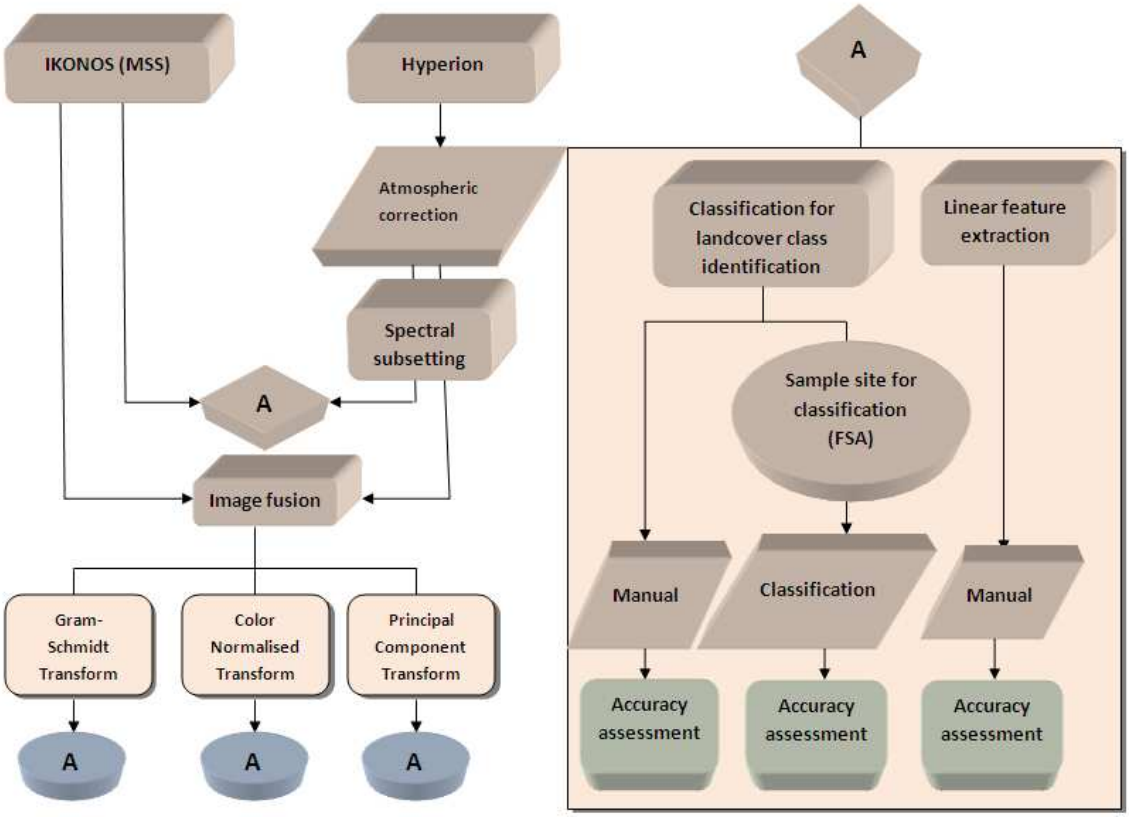

Figure 4-1 Overall methodology

The methodology adapted in the work is focussed on the steps to achieve the research objective i.e. performance analysis of the hyperspectral and high-resolution data fusion for classification and linear feature extraction and find out the answers to the research questions formulated in the present work. The research will investigate the effect of the three algorithms i.e. the GS (Gram-Schmidt), PC (Principal Component) and the CN (Colour Normalised) Transform on the fusion of Hyperion data with the high-spatial resolution IKONOS (mss) data. Also, the focus is on the classification and feature extraction processes in the three fused products. The overall methodology is shown by a workflow diagram in Fig 4.1.

Then, the overall methodology in brief can be summarised in the following steps:
Step 1: Extracting the common area (or subsetting) in both the datasets i.e. Hyperion and the IKONOS.

Step 2: Atmospheric correction of the Hyperion data.
Step 3: Spectral subsetting of the Hyperion image bands.
Step 4: Georeferencing the Hyperion data.
Step 5: Extracting visually interpretable land cover classes from the original data.
Step 6: Extracting linear features from the original data.
Step 7: Validation of the results of the manual classification using a reference image (obtained by the fusion of IKONOS, mss & IKONOS, Pan).
Step 8: Sample site selection for classification and feature space analysis.
Step 9: Supervised classification (using SAM approach) of the original data sets using the samples selected.
Step 10: Validation of the classification results using ground truth.
Step 11: Fusion of Hyperion with the IKONOS (mss) data using the three algorithms i.e. Gram-Schmidt Transform, Colour Normalised Transform and the Principal Component Transform.
Step 12: Extracting the same land cover classes and linear features in the three fused images.
Step 13: Validation of the results of manual classification using the same reference image.
Step 14: Feature space analysis (FSA) for the three fused images using the same samples (ROIs).
Step 15: Supervised classification (using SAM approach) of the fused images using the same samples (ROIs).
Step 16: Validation of the digital classification done to the three fused images using the samples collected from ground itself.
Step 17: Comparison of the results incurred with respect to classification and features extraction in the original and the three fused product.

4.1. Pre-processing stage

This is the preliminary step of the research work. In the context of the present work, the different processes persuaded out in this stage are the atmospheric correction to the Hyperion data, geometric correction of the Hyperion, spatial and spectral subsetting. All of the processes have already been described in more detail in the data preparation chapter.

4.2. Image fusion

Image fusion is the phenomenon of combination of one or more images using an algorithm to acquire a composite image which caters with better and enhanced spatial and spectral information.

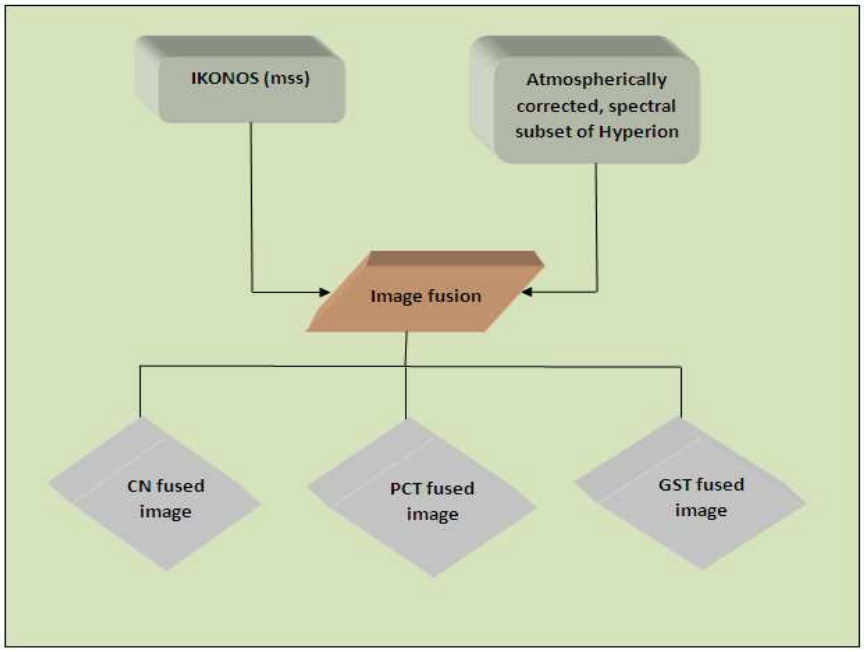

Figure 4-2 Image fusion process

4.2.1. Colour-Normalised Transform

The Colour Normalised Transform is a fusion technique that uses a mathematical combination of the colour image and a high resolution image.

The Colour Normalised technique of fusion has been used to merge the multispectral (IKONOS) with the hyperspectral (Hyperion) image. The CN spectral sharpening takes whole of 34 bands (spectral subset) of the Hyperion image to fuse with 4 bands of IKONOS image.CN spectral sharpening works only if the bands fall within the spectral range of one of the sharpening image's bands; all other input bands are unchanged in the output. The spectral range of the high-resolution image (IKONOS) is defined by the band centre wavelength and a factor called the Full Width-half Maximum (FWHM). This is the narrowest bandwidth in which the sensor can detect the change. The units of FWHM are watts per steradian micrometer square meter. For the Hyperion image the FWHM factor is defined using a toolkit (found from ITT visual basic site) and for the high resolution image (IKONOS) we have to define this factor in the header file of the image.

DATA (Resolution)	FWHM (watts per steradian micrometer square meter)
IKONOS(mss), 4m	.665 (Red),.5505(Green),.4805(Blue) and .83 (NIR)
Hyperion, 30m	10.90 nm (VNIR) and 10.14 nm (SWIR)

Table 4-1 The FWHM value of the IKONOS and Hyperion data (found from GeoEye IKONOS user guide)

4.2.2. Gram-Schmidt Transform

In the context of the original data used we first create separate spectral subsets of the Hyperion data for the red, green, blue and NIR bands and fuse them with the individual RGB and NIR bands of the IKONOS image. For the red band we make a spectral subset of 7 bands from the band number 28 to 34 (630-691 nm), for the green band the spectral subset of 8 bands from the band number 19 to 26 (538-609 nm), for the blue band the spectral subset of 4 bands from the band number 15 to 18 (498-528 nm) and for the NIR band the spectral subset of 15 bands from the band number 41 to 55 (762-905 nm) were made. After developing the spectral subsets for the R, G, B and NIR band from the Hyperion image file, the individual (R, G, B and NIR) band has been merged with the R, G, B and NIR band of the IKONOS data.

The merging of the spectral subsets of the Hyperion image file(R, G, B and NIR bands) with the IKONOS (R, G, B and NIR bands) produced four separate images i.e. for the red, blue, green and NIR (near infrared). These separate images were then stacked to get one single 34 band image which achieved the spatial resolution of IKONOS and the spectral characteristics of the Hyperion image.

4.2.3. Principal Component Transform

The Principal Component transform algorithm works on the same basis as the GST. Likewise GST, here also we fuse the individual spectral subsets of the red, blue, green and NIR band of the Hyperion data with the individual bands of the IKONOS to get four separate images. These four separate images of red, green, blue and NIR band are stacked together to acquire one single composite 34 band image which achieved the spatial resolution of IKONOS and the spectral attributes of the Hyperion data.

4.3. Performance analysis

After the pre-processing and the fusion processes, the performance analysis of the Hyperion data is done. The classification, feature extraction and the spatial and the spectral changes for the scene area between the original (IKONOS, mss and Hyperion) and the fused products are used to assess the performance of the fusion technique. The analysis is executed on the basis of the reference data taken from the ground truth for the digital classification while for the manually digitised land cover/land use classes and linear features, the composite image (IKONOS, Panchromatic with IKONOS, mss) is used for the qualitative analysis.

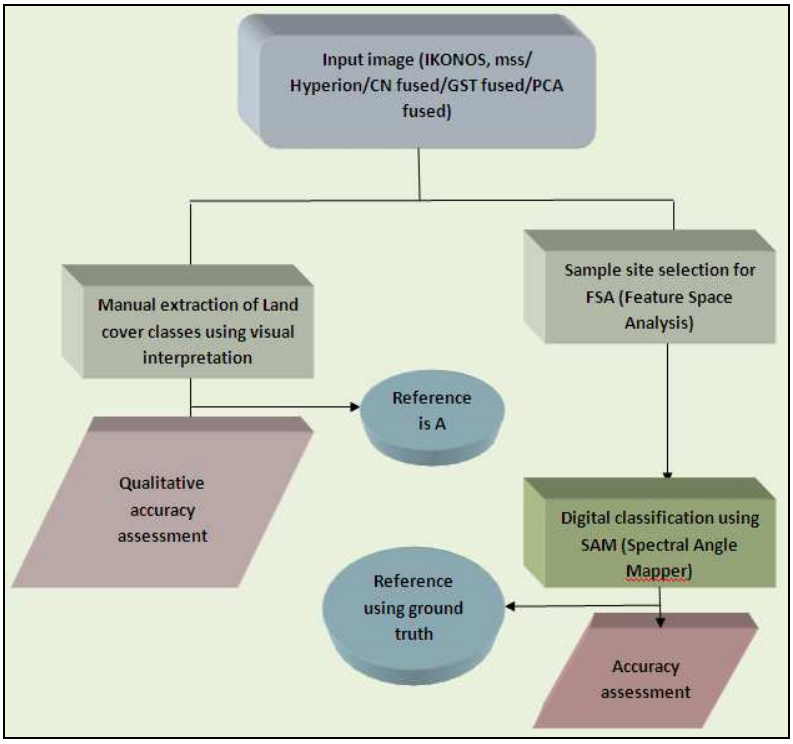

Figure 4-3 Performance analysis

4.3.1. Sample site selection for feature space analysis

Sample site selection is predominantly done for the feature space analysis (FSA) and observes the separation of the signatures in the feature space.

In the present work, the FSA (Feature Space Analysis) is performed to observe the separability of the signatures which is an input facet to the classification performed on the data sets. The present work focuses on the feature space analysis to observe the distribution of pixels before and after fusion. Here, it has been performed to observe for the separability of the various classes.

Separability analysis of the various signatures is done visually and statistically. In the present work, the separation of the signatures is seen in an n-D visualiser. The n-D visualiser is a tool in ENVI (Environment for Visualising Images) that is used for visualising the separation of the various signatures in an n-dimensional space. Statistically, this has been performed by investigating the various statistical parameters like the mean, median, maximum, minimum and the standard deviation values for the various classes in different bands.

The feature space plots show the data file values against the different band combinations. In the feature space shown downwards the distinguished ellipses are of various signatures (water, grassland, urban, bare soil, vegetation, and fallow land) that give an idea of the separability of signatures in the feature space in ERDAS (Earth Resource Data Analysis System). The well separated ellipses in the feature space intend that the signatures are substantially separated in the classified image with almost no mixing in the classes. Or, otherwise, if there is an overlap of the ellipses in the feature space, it implies the signatures are mixed in the classified image. Visually, the feature space is as follows:

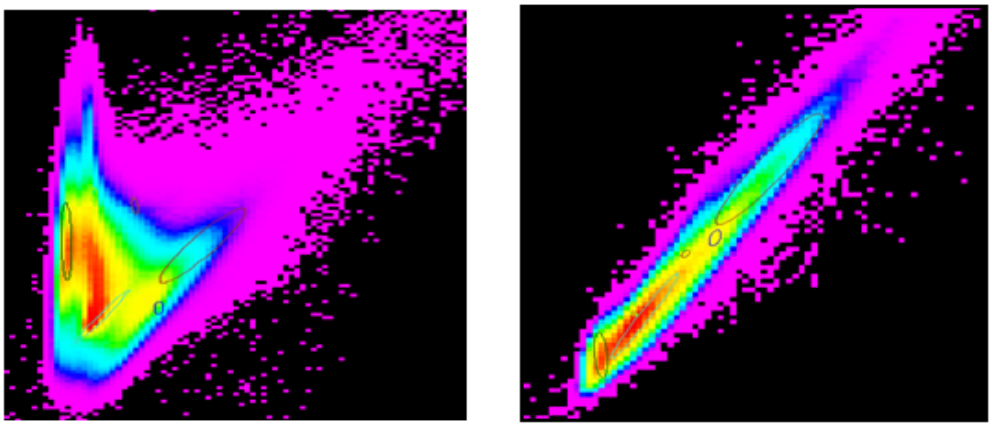

Figure 4-4 Feature space seen in between band 1 vs. band 2 & band 2 vs. Band 3 (In ERDAS)

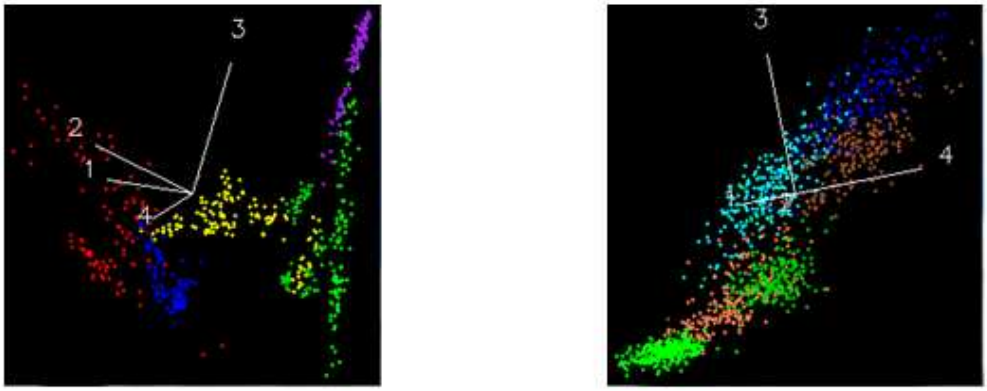

Figure 4-5 Signatures seen in an n-D visualise in IKONOS (mss) and Hyperion (In ENVI)

In the above figure, one can observe the separability of the signatures in an n-D visualiser. In the IKONOS image the signatures are remarkably separable. Generally, this is due to the reason that in the high resolution data like IKONOS the training sites (samples) can be marked with good spacing. In the Hyperion, there is an overlap and mixing of the pixels.

4.4. Classification

Image classification or the 'partition of the feature space' can be done in two ways: Supervised and Unsupervised classification.

Classification of the high-spatial resolution data like IKONOS (mss) is required because it has remarkable class separability in the feature space due to fine spatial resolution which aids for better classification of the image file.

In the context of the present work, the original and the three fused datasets are classified by the method of supervised classification using the SAM (Spectral Angle Mapper) approach. This has been adopted because we needed the spectrally unique surface materials existing within a scene. Also, SAM (Spectral Angle Mapper) approach of supervised classification is relatively insensitive to the illumination and the albedo effect which may hinder in the classification process. The selection of the classification algorithm

was also based on the characteristics of the image and the training data. For this, we marked the ROIs (Region of Interest) for the various classes in the image file by our own knowledge. After the training data has been established and the classifier algorithm has been selected, the actual classification is held out. Based on the DN-values, each individual pixel in the image is assigned to one of the pre-defined classes.

The SAM decision rule of classification classified the image into 9 classes i.e. vegetation type1, vegetation type 2, river, shrubs, urban features, grassland, fallow land, bare soil, and crops.

4.4.1. Validation

Accuracy assessment is a general term for comparing the classification to the geographical data that is assumed to be true, in order to determine the accuracy of the classification process.

In the present work, the verification of the classified images has been done by the ground truth data and the field observations. The training samples were collected from the various places in the scene area (Dehradun).

The reconnaissance survey has been carried out at the beginning of field in order to get familiar with the study area. The purpose of this field work as to accumulate training and the testing samples for some land use / land cover classes. Random sampling has been used to collect the training and test pixels for both the Hyperion EO-1 data and the IKONOS (mss) data sets. Total selected pixels were divided into two parts, one for training and one for testing or allocating the classifiers, so as to remove any possible bias resulting from the use of same set of pixels for both the testing and training phases. The collected training samples with their pictures and a short description and their geographical location (in Lat/Long) in tabular form has been shown below:

4.4.1.1. River

The river seen in the picture is Tons that flows from North West to South West direction in northern part of the Dehradun city and characterised by cyan colour. The spectrum of cyan colour is due to the silica present in the dry bed river. As the river is seasonal, water flows only during the months of July and August while during rest part of the year, the bed is dry.

4.4.1.2. Urban

The urban area is composed of areas of exhaustive use with much of the land covered with structures. Regular geometry, straight roads and characteristic cyan colour indicate urban features.

4.4.1.3. Bare soil

Soil is a layer of loose material found at the Earth's surface that is influenced by the soil forming factors: climate, relief, time, organisms and the parent material. The characteristic colour of the soil in the RGB image is light brown. Some bare soil grounds are present in the northern part of the conurbation. Even in the southern part of the sprawl, where there is abundance of the crop fields in between some bare soil is present.

4.4.1.4. Shrubs

The land cover class which is categorised under the rangeland which predominantly consists of the grasses with height less than or equal to 5 m has been assigned as the shrubs. Shrub is defined as a woody plant of relatively low height, having several stems arising from the base and lacking a single trunk; a bush. In the northern part of the Dehradun city called the Donga fan, the region is primarily covered with the shrubs. Also, at the banks of the river Tons this land cover class is mainly present. In the image, shrubs are characterised by light red colour.

4.4.1.5. Vegetation type 1 (Sal)

Vegetation of Sal (Shoria Robusta) is principally the main vegetation in the FRI region of Dehradun. Vegetation in the image data is characterised by bright red colour. The grass with height more than 2.5 m is assigned to as vegetation. In the image data sets, the interpretation key of association (of trees) also aided in identifying the vegetation.

4.4.1.6. Vegetation type 2 (Teak)

Teak (Tectona Grandis) is the second maximum vegetation present in the FRI region of the Dehradun city. This type of vegetation is also characterized by red colour with light tone. The trees of teak can gain a height more than 15 m.

4.4.1.7. Grassland

The land cover class is assigned to the category grassland as these are identified with light cyan colour in the image. Grasslands are areas where the vegetation is dominated by grasses (Poaceae) and other herbaceous (non-woody) plants (forbs). This category also comes under the vegetation class. These are identified on the ground with regular geometry.

4.4.1.8. Crop land

The terrain that is fit or used for growing crops is termed as a crop land. This land cover class is characterised by its shape (mostly rectangular in the present case). The southern part of the Dehradun city is characterised with enormous crop fields. These are characterised by shades of red cyan colour in the image data sets.

4.4.1.9. Fallow land

This land cover class is identified with the mix shades of red-cyan colour. Another characteristic of this land cover class is the shape and regular geometry. The land cover class which is deficient of any crop due to the cropping season or tillage practices is considered as the fallow land. The northern part of the Dehradun city is covered with the fallow land.

At least, 3 to 5 samples for each of the above mentioned LULC classes have been collected from the different locations of the Dehradun city for the validation of the classification results. Random sampling technique has been used for computing the overall accuracy of classified images.

Class	Latitute	Longitude
Bare soil	30°17'11.11"N	78° 0'21.90"E
	30°21'41.31"N	78° 0'36.23"E
	30°21'7.19"N	78° 0'29.51"E
Fallow Land	30°21'37.32"N	77°59'49.21"E
	30°21'55.68"N	78° 0'21.20"E
	30°21'28.67"N	78° 0'42.08"E
Crop land	30°17'11.10"N	78° 0'50.03"E
	30°17'22.21"N	78° 0'28.75"E
	30°17'37.08"N	78° 0'21.42"E
Urban	30°17'47.32"N	78° 0'49.30"E
	30°19'0.14"N	77°59'59.94"E
	30°19'31.65"N	78° 0'4.20"E
Veg Type 1	30°20'17.17"N	78° 0'25.67"E
	30°20'26.41"N	78° 0'31.72"E
	30°20'28.03"N	78° 0'23.18"E
	30°20'36.91"N	78° 0'27.59"E
	30°20'35.84"N	78° 0'35.65"E
Veg Type 2	30°20'18.30"N	78° 0'40.91"E
	30°20'23.07"N	78° 0'44.09"E
	30°20'26.74"N	78° 0'44.62"E
Grass land	30°20'35.50"N	77°59'55.10"E
	30°20'3.86"N	78° 0'2.33"E
	30°19'27.23"N	78° 0'6.98"E
Shrubs	30°21'10.62"N	78° 0'1.15"E
	30°21'16.66"N	77°59'56.54"E
	30°21'19.97"N	78° 0'16.19"E
River	30°21'33.60"N	78° 0'0.98"E
	30°21'57.37"N	78° 0'14.21"E
	30°22'4.82"N	78° 0'24.98"E

Table 4-2 Table showing the geographical location (Lat/Long) of the sample points taken for classification

4.4.2. Manual classification

Manual delineation of the LULC classes is performed on the basis of the visual inspection of the images. The Land Use and Land Cover classes are delineated by interpreting the images using the interpretation keys of tone, texture, hue, association, orientation, shape and size.

In the present work the cultural features like buildings are delineated on the ground of the shape and size. The fallow land is delineated on the basis of the association factor. The crop fields have been

delineated on the basis of the association, hue (light red) and even the geometry of the feature which in most cases is rectangular. The bare soil grounds have been mapped on the basis of the shape factor which in most cases is rectangular and the hue that is light brown. The natural features like the vegetation patch, grasslands, and shrubs are mapped on the basis of the hue (light red) and association. The natural features like vegetation are delineated roughly because in most of the cases the boundaries are not defined. In the high-spatial resolution data, IKONOS (mss), the land cover classes were easily and considerably delineated on the basis of the interpretation keys like the shape, size pattern, association, etc. To extract the same classes in the Hyperion image was difficult and cumbersome due to two reasons: firstly, due to the spectral variance among the various land cover classes like, the buildings in the urban area were not distinguished, the linear features like the roads are hard to discriminate and; secondly due to the coarse resolution it was complicated to find the exact location of the same classes.

To retrieve the same land cover classes in the Hyperion data set, the features which were delineated in the IKONOS (mss) image were initially transferred to the Hyperion image (using a tool in ENVI ROI tool box i.e. Reconcile ROIs via. Map) to obtain a rough orientation of the classes. After this, the same features were manually digitised in the Hyperion image itself by visual inspection. The interpretation keys of colour, texture, orientation, association, and pattern were used to delineate the features in the Hyperion image.

In the same way, the linear features (roads) were delineated in the IKONOS (mss) and the Hyperion images. The interpretation key of shape (linearity) has been integrated with the hue (red colour of trees present at the side of the roads in the image) to delineate the roads in the Hyperion image

4.4.2.1. Validation

The validation of the manually delineated land cover classes and the linear features has been carried out using a reference image which is obtained by fusing the IKONOS (mss) and IKONOS (Pan) image using the PCA (Principal Component Analysis) approach for fusion incorporating the nearest neighbour resampling technique. This composite image has been taken as reference because of the unavailability of the ground reference data for the evaluation of geometric accuracy.

The features which have been delineated in the original data sets (IKONOS & Hyperion), the same features have been digitised in the reference image.

Once the features have been digitised in the original datasets (IKONOS and Hyperion) and the reference data (composite image), the overlay function (same feature digitised in original and the reference image) is performed in ENVI. The area which is common and matched in both the datasets is marked as the TP (True Positive) area, the area which comes from the reference image but does not match to the area in the test image is marked as the FN (False Negative) area and the area which is in the test image but does not match with the area in the reference image is marked as the FP (False Positive) area. The TP, FP and the FN area is taken in pixels. Once we obtain TP, FP and the FN parameters, the geometric accuracy is computed i.e. Completeness and the Correctness are calculated for the various land cover/land use classes and the linear features (roads).

In the same way, the TP, FP and the FN area of the various land cover classes and the linear features extracted in the Hyperion image are acquired. Likewise, the completeness and correctness factors are investigated.

4.5. Summary

The methodology chapter gives an insight to the different processes carried out during the research work to draw out the answers of the research questions and assures us how the research objective is achieved. The chapter in general gave the overall methodology adapted in the present work with the work flow diagrams and the brief description of the various phenomenons.

5. Results and discussion

Results and discussion chapter is prepared in a way that imparts the reader with the fusion outcomes of the high-spatial resolution data, IKONOS (mss) and the Hyperion using the three merging approaches.

5.1. Evaluation method

Two approaches are used for the evaluation of product generated after applying different merging methods. The first is the visual discrimination of the various land cover classes for the evaluation of visual interpretability of merged data. In the second approach various statistical parameters were examined. These measures are (i) the difference in the various statistical parameters like the mean, median, maximum, minimum, and the standard deviation values of the different classes in different bands in the Hyperion and the merged data (ii) interpretation of the spectral profiles of the various land cover classes.

These statistical analyses are carried out for some of the classes. The third approach for evaluation is measuring the utility of merged images for classification. This is followed by making a set of training sites of various land cover classes and classifying the image using SAM (Spectral Angle Mapper) approach of supervised classification. The classification accuracy of the original (IKONOS & Hyperion) and the three merged products has also been compared for the present study.

5.1.1. Visual and statistical analysis Interpretation

Here we have put the screen shots of 11 land cover classes taken from the scene with their spectral profiles.

The spectral profiles of the various land cover classes present in the scene area like vegetation, bare soil, crop land, fallow land etc. and three fused products have been compared with the Hyperion because of its spectral resolution that ranges from 400-2500 nm and hence aids in discriminating among various land cover classes.

In the heavily vegetated area near FRI (Forest Research Institute) in Dehradun (study area), the vegetation present is of mixed type with varied tree types like Sal (Shoria Robusta), Bamboo and Teak (Tectona Grandis). This has been confirmed during the field visit in the region and through local sources. The scientific terms of the trees has been investigated through the books in the FRI library.

5.1.1.1. Vegetation type 1

The screen shot taken shows the vegetation profile of Sal (Shoria Robusta) in the three fused products and in the original Hyperion image.

Figure 5-1 Sal vegetation (type 1)

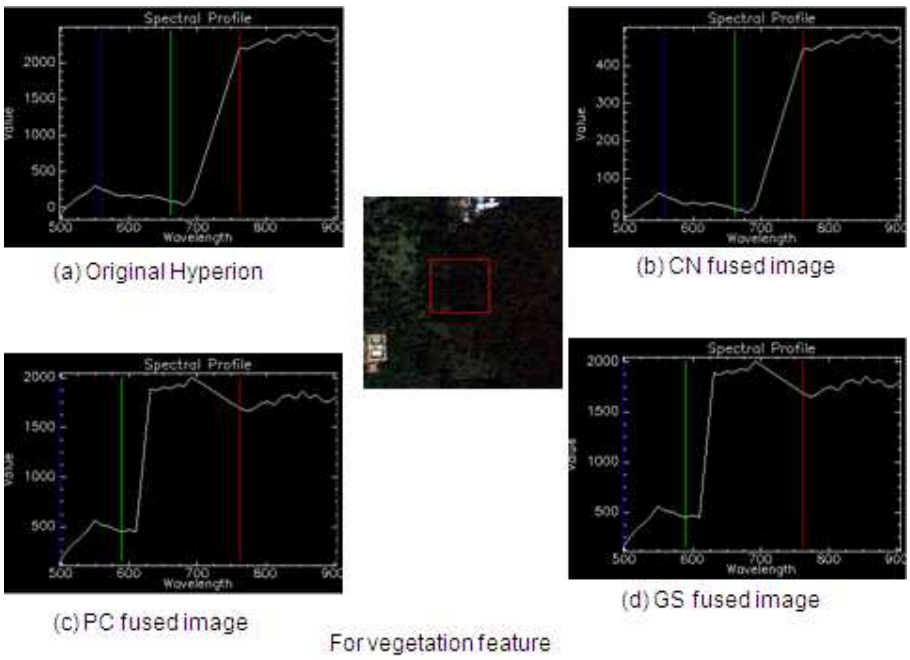

Figure 5-2 Spectral profile of Sal

In the Hyperion image, we observe that in the beginning there is a slow rise in the curve starting from the wavelength of 500 nm to a value of more than 250 and there exists a short peak in the blue region. At a wavelength of 700 nm there is a sharp rise in the curve that reaches to a value of 2000 and then there exists some small peaks in the NIR region which establishes that vegetation is best discriminated in this region. In the CN fused image, the outcomes of the spectral profile is almost similar with only one remarkable difference that is in the reflectance value. The vegetation here shows a rise in reflectance

value only up to 450-750. In the PC fused image, the results are different with respect to Hyperion and CN fused image. In the PC fused, the curve rises from 500 nm that goes up to 500. Then, again at 630 nm there is a sharp rise in the curve with a steep slope that reaches up to 2000. This rise in the curve is between green and the red region of the spectrum. In the NIR range, small peaks are present which demonstrate that in this region vegetation feature is best highlighted. The spectral profile of the GS fused image is almost similar to the PC fused image.

5.1.1.2. Vegetation type 2

The second maximum vegetation present in the FRI region of the Dehradun city is of Teak (Tectona Grandis). The spectral profile of Teak in the original Hyperion and the three fused product is here.

Figure 5-3 Teak vegetation (type 2)

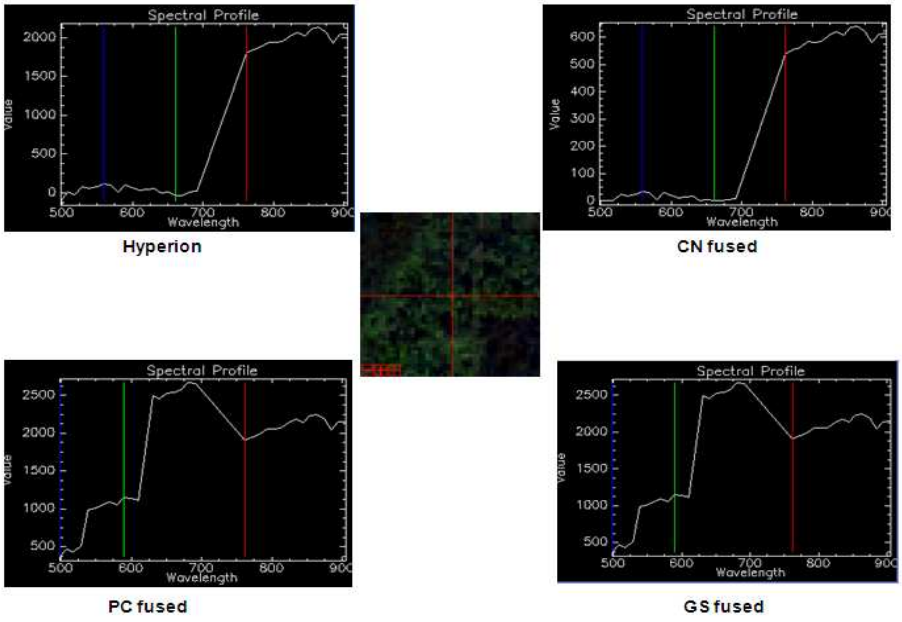

Figure 5-4 Spectral profile of Teak

In the Hyperion image, the curve starts from the negative value at 500 nm. There is almost slow rise in the curve with a flattened slope till it reaches to a value near to 0 at a wavelength of about 685 nm. Then, suddenly the curve rises linearly with a steep slope till it reaches the red region. In the NIR region, the curve shows some undulations. The spectral profile of vegetation in CN fused is almost same as in the Hyperion image. The only difference is seen at the starting where the curve runs almost parallel to the ground till it reaches to a value near to 0 at a wavelength of about 685 nm. In the PC fused image, the curve starts rising slowly till it reaches to a value near to 1000 at a wavelength of about 545 nm. In between the green and the red region, the curve shows a rise till it reaches to a value near to 2500 at 625 nm. After the curve encounters the maximum value of more than 2500 at 685 nm, the curve falls down to a value less than 2000 at red region. In the NIR region, the curve runs with a flattened slope with some undulations. The spectral profile of vegetation in the GS fused image is almost similar to the profile in the PC fused image.

5.1.1.3. Fallow land

The screen shot shows a fallow land near the river Ton in the northern part of the Dehradun city.

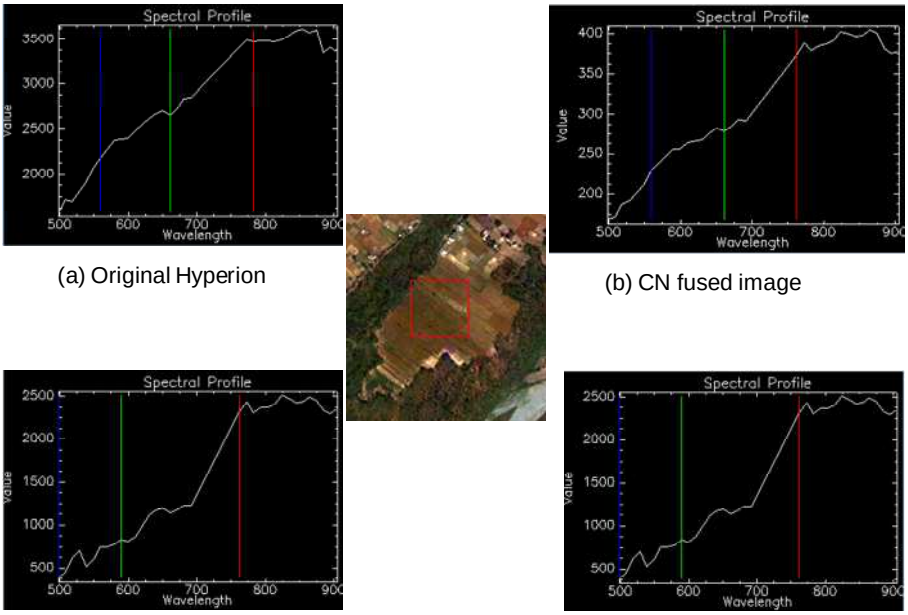

(a) Original Hyperion

(b) CN fused image

(c) PC fused image

(d) GS fused image

For fallow land

Figure 5-5 Spectral profile of Fallow land

In the Hyperion image, we observe a continuous rise in the curve up to a value of 3625. For fallow land, the rise starts from wavelength of 500 nm and the slope of the curve is not that much steep. The rise in the curve is continuous with no noteworthy dips. In the CN fused image, the events are similar to the Hyperion but there is a difference in the range of the reflectance value up to which the curve rises. The range of the values in the CN fused image is limited to 400. In the PC fused image, the curve starts rising from the wavelength of 500 nm up to 750 and then there is a small dip. The dip is not remarkable and then again the curve rises. The curve rises linearly with a steep slope in between green and the red

region up to value of 2500 and then again in the NIR region (beyond 750 nm) small pronounced peaks are present. The spectral profile of the fallow land in the GS fused image is almost comparable in the PC fused image.

5.1.1.4. Building feature type 1

The building feature shown above is near to the FRI main building. The roof top of the shown building is made of tiles of terra cotta. Terra cotta is a type of clay in which the presence of iron gives it red or orange colour.

Figure 5-6 IGFNA building near FRI

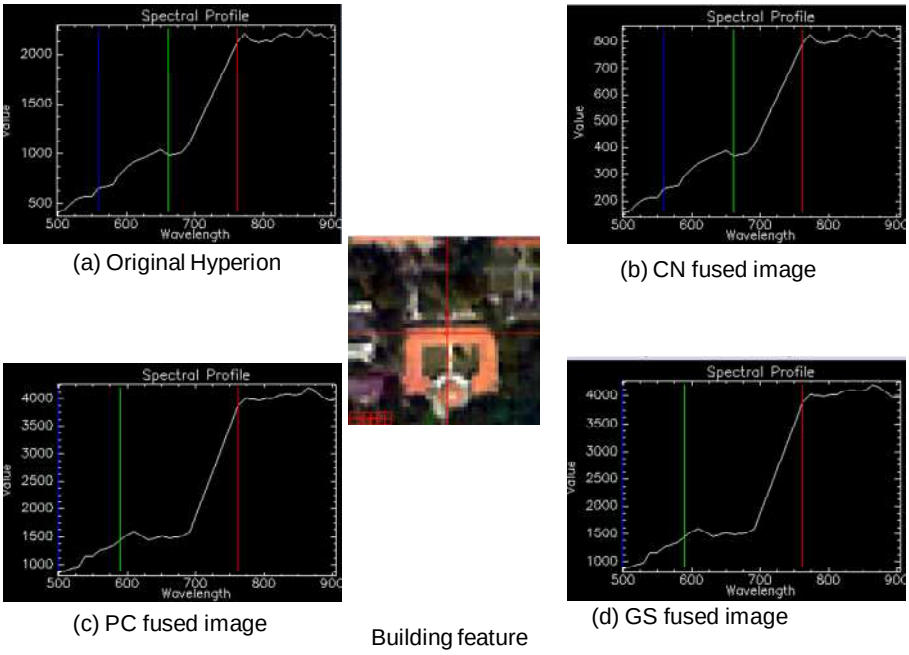

Figure 5-7 Spectral profile of Building feature type 1

In the Hyperion image, the curve starts rising slowly from the blue region up to a value of 1000 and then suddenly at the green edges the slope of the curve increases and there is a linear rise in the curve up to a value of 2500. In the NIR end small peaks are observed. Similar sort of consequences are observed in the CN fused image but the value is limited only up to 800. The results of the PC fused image are somewhat different. The building feature seen above is enhanced with values ranging more than 4000. The rise starts from the blue region that reaches to a peak at 1625. In between green and the red region of the spectrum, the rise is continuous. The curve is flattened at a value of 1500 but suddenly the curve rises at 680 nm with a steep slope that reaches a maximum value of 3900. Then after the red region, small peaks are observed. The spectrum observed for the GS fused image is same as the PC fused image.

5.1.1.5. Building feature type 2

The building feature shown down is a located in the centre of the Dehradun city in GMS road. The roof top of most of the urban features (buildings) present in the city is made of sand, concrete and clay. The presence of silica in sand accounts for the profile obtained for the given building.

Figure 5-8 Building feature type 2

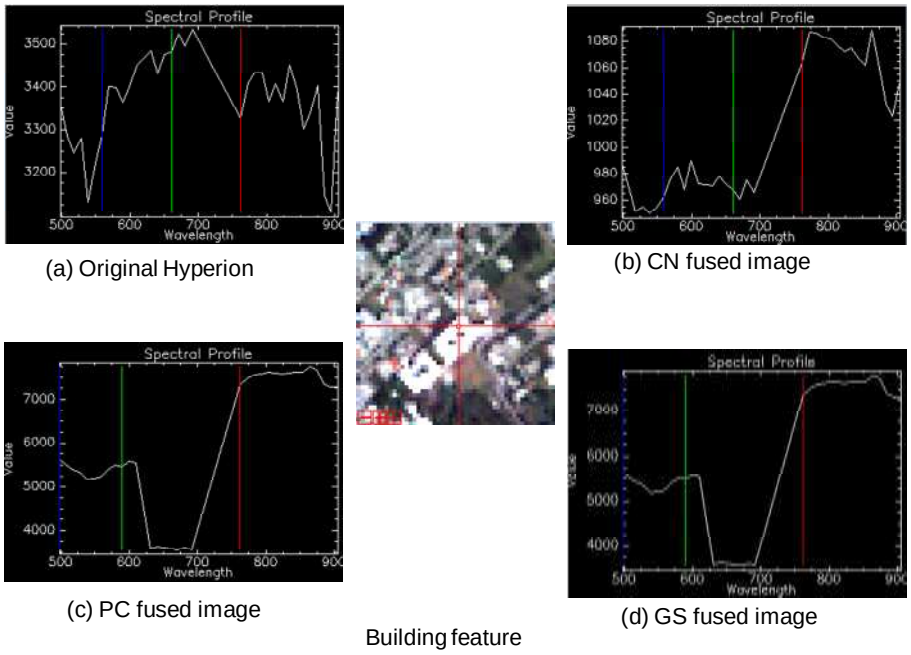

Figure 5-9 Spectral profile of building type 2

In the spectral profile of the building in the Hyperion image, the rise of the curve starts at 3350 at 500 nm. The profile show some sharp undulations i.e. peaks and dips. The spectral profile in the Hyperion show some pointer peaks. The maximum value of more than 3500 at 690 nm is encountered in between the green and the red region. After the curve reaches to a maximum value it starts falling gradually till the value less than 3350 at red region. In the NIR region, the curve shows some peaks and dips. In the CN fused image, the curve starts from the value 985 at500 nm. Then, the curve suddenly drops. In between the wavelength range of 565 to 690 nm, the curve shows some short peaks and dips. In between the green and the red region of spectrum, the curve rises sharply till it reaches a value more than 1080 at 775 nm. In the NIR region, the curve shows a gradual fall. The spectral profile of the building feature in the PC fused and the GS fused image are almost similar. The curve starts from 5500 in the blue region. Then it runs almost parallel to the ground till 620 nm. In between the green and the red region, there exists a dip. From the wavelength of about 690 nm, the curve starts rising till the red region. In the NIR region, the curve runs parallel to the ground with almost constant values.

5.1.1.6. Grounds with grass

This is located in the southern part of the Dehradun city.

Figure 5-10 Grounds with grass

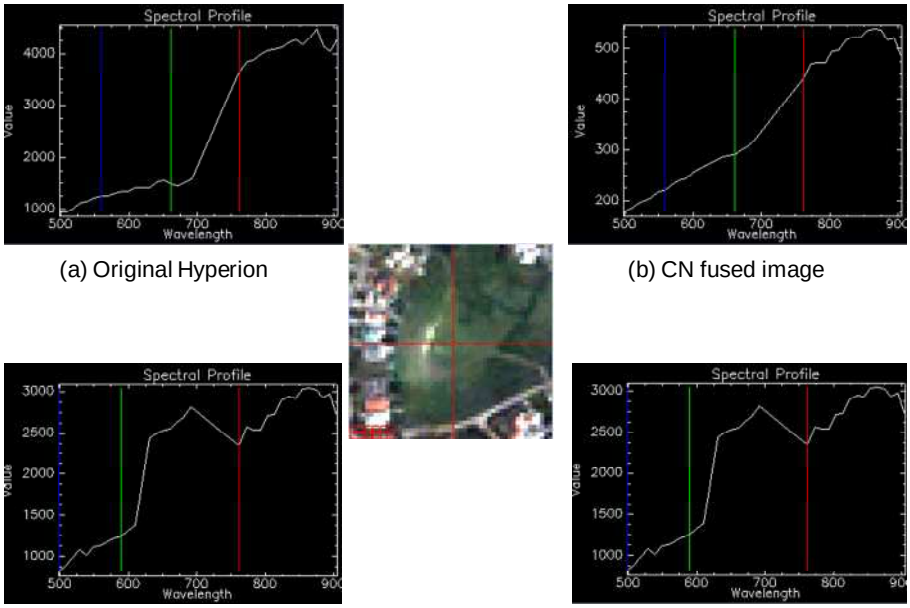

Figure 5-11 Spectral profile of grounds with grass

In the Hyperion image, the curve rises slowly with almost flattened slope till it reaches a value of 1500 at a wavelength of 700 nm but then after that the curve rises linearly with a steep slope. This slope is between green and the red region. At the red region, this sharp rise in the curve is slowed down and then after that in the NIR region the curve rises slowly with one enhanced peak at 4500 at a wavelength of 875 nm. In the CN fused image, the curve rises slowly with a stumpy slope till it reaches 475 at a wavelength of 775 nm till the red region of the spectrum. In the NIR region, we observe some peaks in the curve. In the PC fused image, the curve shows some dips. Initially, the curve rises slowly till 1350 at

a wavelength of 610 nm (approximated) then after the green end, the curve shows some variations. After the green end, the curve rises suddenly with a high slope till it reaches a value of 2750 at a wavelength of 680 nm. After 680 nm, the curve shows a decrease in the values till it reaches 2375 at the red region. In the NIR region, again the curve rises with some small peaks. The spectral profile of the grounds with grass in the GS fused image show almost the same outcomes as the PC fused image.

5.1.1.7. Bare soil

The bare soil whose profile is shown downwards is located in the southern part of the city.

Figure 5-12 Bare soil

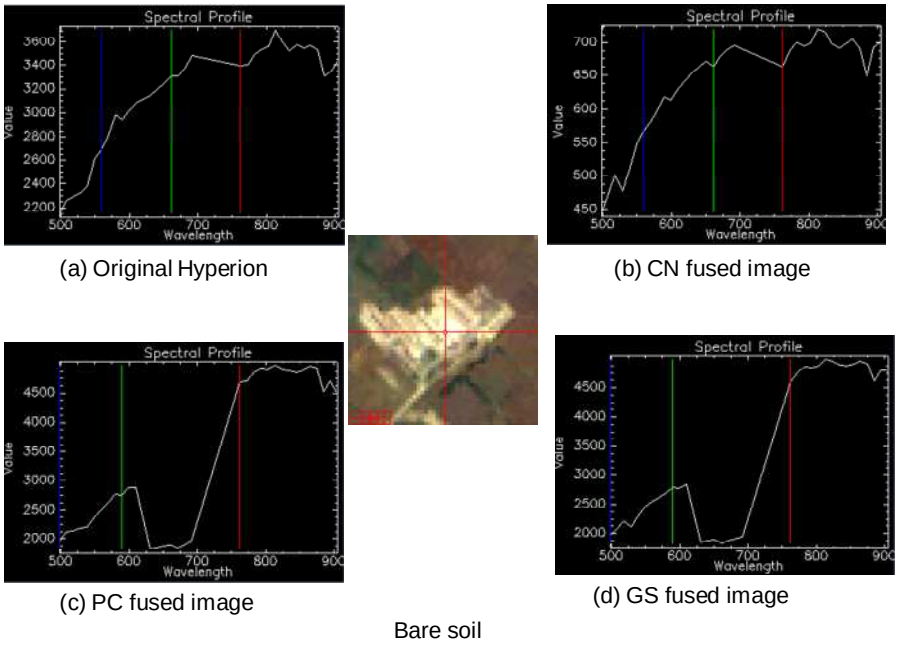

Figure 5-13 Spectral profile of bare soil

The spectral profile of the bare soil shows variations in the Hyperion image. The curve rises with a high slope and one can observe short peaks at wavelengths of 580 nm, 680 nm and highest rise at 820 nm.

The rise in the curve is not uniform as there are some dumpy peaks and dips in the curve. Only, between blue and the green region, the rise is somewhat linear with one peak at 580 nm. In between the green and the red region, one enhanced peak can be observed at 680 nm but near to the red region at a value of about 3360 there is a flat dip. In the NIR region, some undulations are present in the curve with a peak at a value of about 3680 at 820 nm. In the CN fused image, one can observe a number of dips and peaks in the curve. The curve initially rises and meets a pointed peak with a value near to 500 at 515 nm. Then, in between the blue and the green region, the curve rises with a steep slope with two peaks at a value of 612.5 and 662.5 at 580 nm and 650 nm. There is a small dip after the green end. In between the green and the red region, there is a peak at a value of about 637.5 at 680 nm. After the rise, there is a flat dip at the red region but after this dip the curve rises again in the NIR region with some flat peaks and a sharp dip at a value of 637.5 at 875 nm wavelength. In the PC and the GS fused image, the range of the reflectance value is from 2000-4500. The spectral profile of the bare soil in the PC fused image shows some remarkable outcomes. The curve first rises slowly till the green end and then there is a sudden and sharp fall in the curve till it reaches a value below 2000 at 630 nm. The dip in the curve remains constant till it reaches 2000 at 690 nm but after that the curve rises sharply with a steep slope till the value of about 4750 at the red end. After the red end, in the NIR region the curve is runs almost flat with a little dip at 4500 at 875 nm. The result of the spectral profile of the bare soil in the GS fused image is almost similar to the profile in the PC fused image with minor differences at certain points. Initially, the curve rises and a small peak is encountered at a value of about 2250 at 520 nm wavelength. The curve rises again in the same way as in the PC fused image. The curve runs almost flat below the value of about 2000 in between 630-695 nm. After this the curve rises sharply with a steep slope till the red region. In the NIR region, the outcomes are almost comparable as the PC fused image.

5.1.1.8. River

The river whose profile is shown here flows from the North East to South West direction in the scene area.

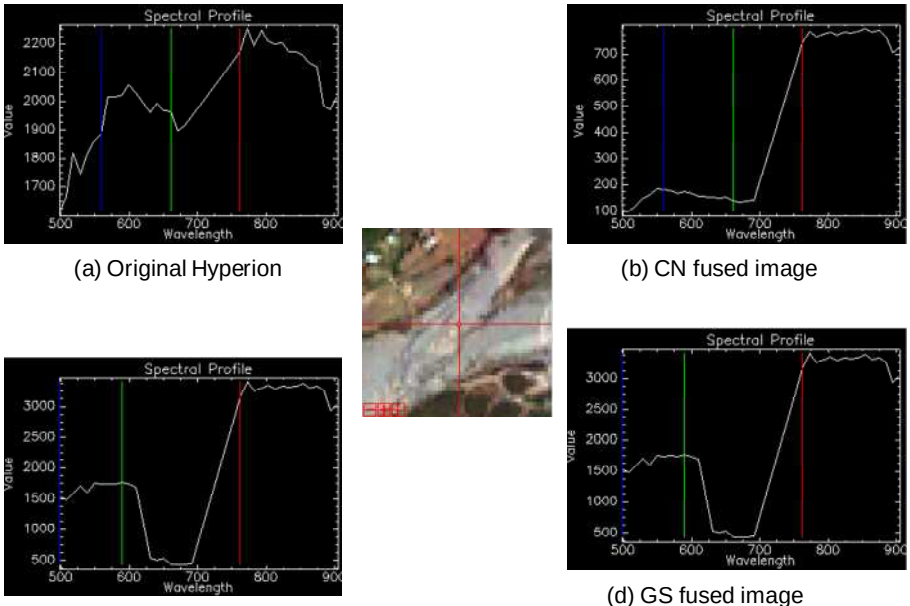

(a) Original Hyperion

(b) CN fused image

(c) PC fused image

(d) GS fused image

Water

Figure 5-14 Spectral profile of river

The spectral profile of river in the Hyperion image show lots of undulations i.e. a number of peaks and dips are observed. The curve rises sharply until it reaches a value of about 1820 at 520 nm. At 520 nm there is a pointed peak and then there is a small dip at about 530 nm. Again, the curve rises till it reaches a value of about 2050 at 590 nm. Then, suddenly the curve falls down till it reaches a value of about 1900 at 665 nm. After the fall in the curve, the curve again starts rising till it reach the red end. In the NIR region, the curve consists of two pointed peaks at 775 nm and 600 nm. After this the curve again drops to a value of about 1965 at 890 nm. In the CN fused image, the curve rises gently up to low values. There is a flattened peak at the blue region and then after the blue region the curve drops down almost flat till 690 nm. After 690 nm the curve rises sharply till the red region is encountered at 660 nm. In the NIR region, the curve runs almost flat with wide contiguous bands. In the PC fused image, the curve starts at the value of about 1500 in the blue region. The curve runs parallel to the ground till the value of about 1750 at 620 nm. After this the curve suddenly drops down and the dip encountered in the region between the blue and the red end is almost flat. At 690 nm, suddenly there is a steep rise in the curve till it reaches a value of about 3375 at 775 nm. After this in the NIR region, the curve again runs flat with small flattened peaks. The spectral profile of river in the GS fused image is almost similar to the profile in the PC fused image.

After evaluating the above profiles we observe that although the range of values in the CN fused image is not comparable to the Hyperion but in most of the cases the shape of the profile closely matches with the profile of the feature in Hyperion. So, we can infer that spectrally the CN (Colour Normalised) approach better preserves the spectral characteristics in the fused image.

In terms of the visual discreteness or the spatial characteristics of the various LULC classes in the fused images, GS (Gram-Schmidt) and the PC (Principal Component) transform are best suitable if compared to Hyperion while if compared to IKONOS there is almost no gain in the spatial quality.

5.2. Digital classification

SAM (Spectral Angle Mapper) approach of supervised classification has been utilized in the present study for the digital classification of the original datasets (IKONOS and Hyperion) and the three merged products. This approach has been considered because of the capability of determining the similarity between the endmember spectrum and the pixel spectrum in the n-dimensional space.

The ROIs (Region of Interest) for the various land cover classes are taken from the image itself using the general knowledge of the scene area. Once the ROIs are taken, the separability of the signatures is seen in the feature space. Here it has been done in the n-D visualiser. The results of the separability of the signatures in the feature space for the original and the three merged product is as follows:

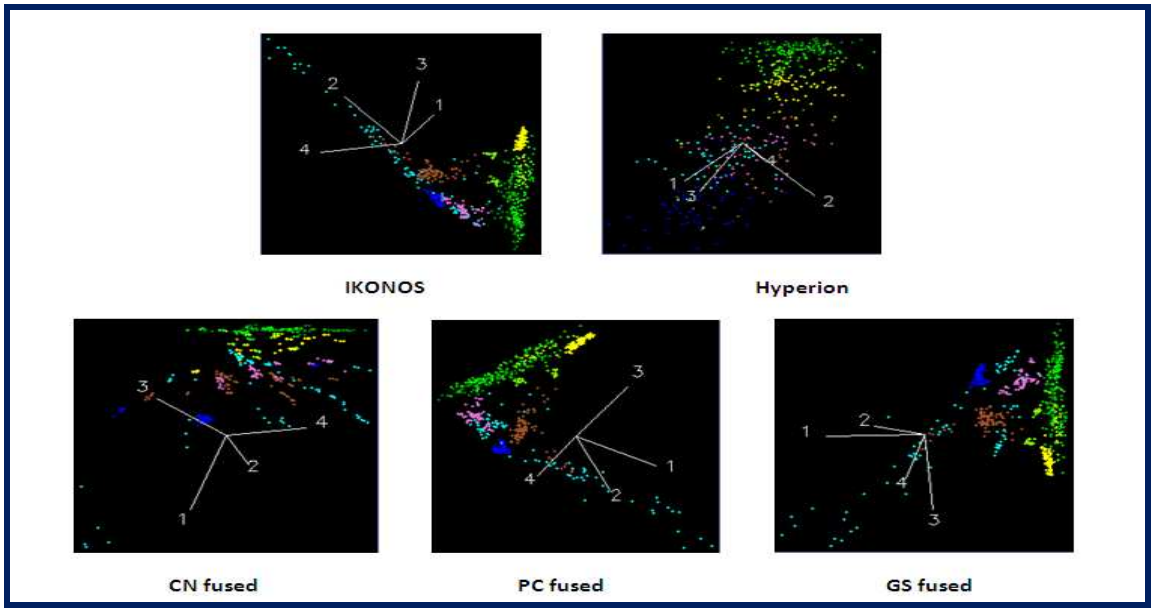

Figure 5-15 Separability as seen in n-D visualiser

From the above figure, we examine the separability of the signatures in the n-D visualiser for the original datasets (IKONOS and Hyperion) and the three fused images. As we have taken, nine various land cover classes i.e. river (in blue), vegetation type 1 (in green 1), vegetation type 2(in green 2), shrubs (in green 3), grassland (in chartreuse), fallow land (in orchid), cropland (in yellow), bare soil ground (in sienna) and the urban (in cyan), we can ascertain that in the IKONOS image the signatures are well separable. Visually, likewise, we can investigate that the results of the separability of signatures in the n- D visualiser for the GS fused, PC fused and CN fused image are better than the Hyperion.

The results of separability for the Hyperion image are not superior because of the coarser resolution the pixels were hardly differentiable into specific classes and as a result there is a concoction of the classes. Thus, the classification results for the Hyperion image are unsound. The results of separability for the CN fused image were comparable but due to the problem of spectral artifacts the signatures are intermixed .Hence, the classification results were badly affected.

As the separability of the signatures in the n-D visualiser for the IKONOS, PC fused and the GS fused image are improved the outcomes of the classification for the images were of high-quality and more effective than for Hyperion.

The outcomes of separability for some of the classes after fusion in the GS (Gram-Schmidt) and PC (Principal Component) transform increases as shown downwards.

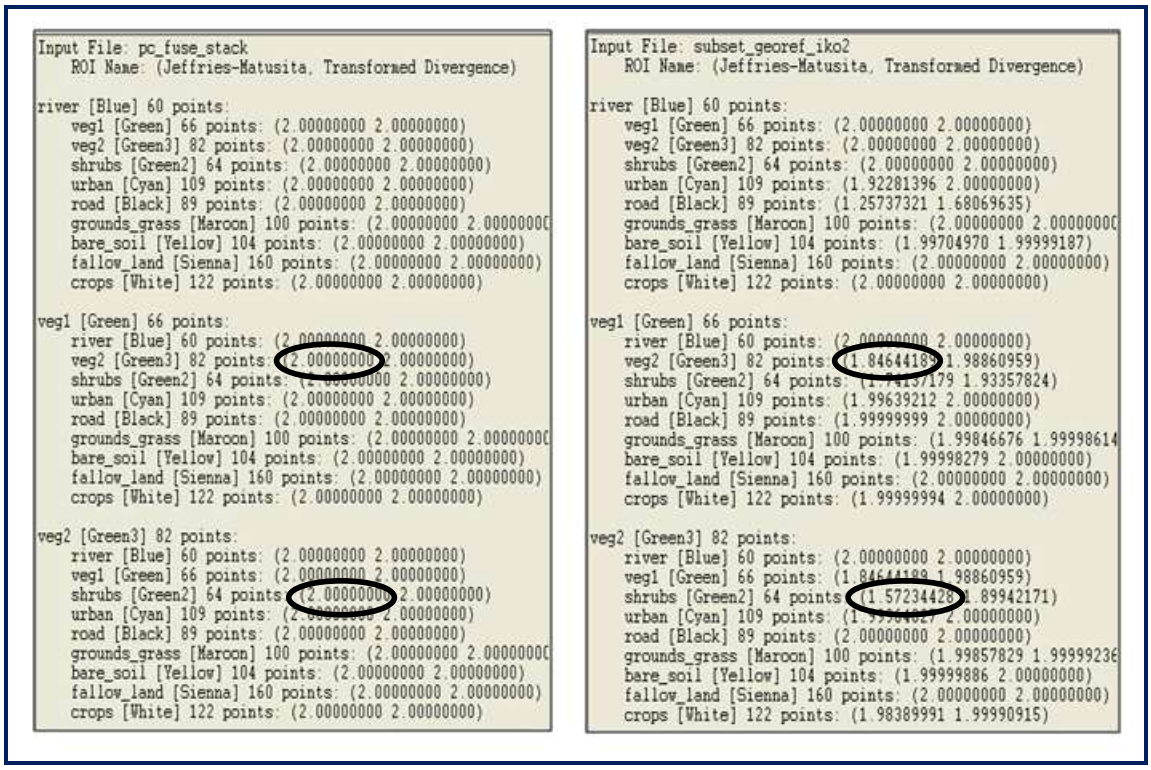

Figure 5-16 Separability report (a) PC fused image (b) IKONOS

From the above report, we can formulate that for some of the classes like for vegetation type 2 the value in the IKONOS image was 1.84644189 which increased to 2 in the PC fused image. Also, for the shrubs the value in the PC fused image increased from 1.57234428 to 2. Hence, we can resolve that the separability increases after fusion as a result of which the classification results are also improved after fusion.

The results of the separability has been analysed statistically also. The statistical analysis has been executed by comparing the parameters of the maximum, minimum, mean and standard deviation values for the different land cover classes in different bands in the original Hyperion and the three fused products. The results of the statistical analysis have been established by graphical representations as shown down. Three bands i.e. band 1, band 8 and band 17 has been chosen for the comparison of statistical parameters because these are the RGB bands and also due to their location. The bands lying in the high-frequency spectrum better preserve the statistics.

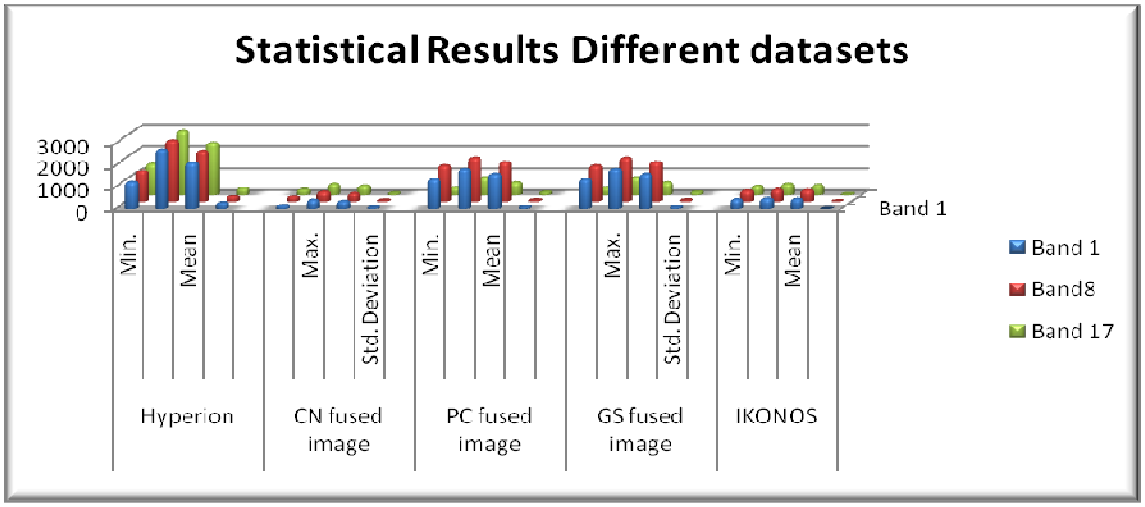

Figure 5-17 Comparison of the statistical parameters

In the above pot, the statistical parameters are depicted in four columns i.e. Minimum, Maximum, Mean and Standard Deviation.

From the above plots, we can examine that there is not notable change in the statistics in the original Hyperion and fused products. PC fused and the GS fused images demonstrate some comparable values for the mean, maximum, minimum and standard deviation but roughly have the same ability in preserving the statistics. The CN fused image show very low values for the various land cover classes in different bands. Due to the reason, the results of classification for the CN fused image were badly affected.

For the classification purpose, same ROIs (training samples) have been assigned for IKONOS and the three fused products. For the Hyperion image, different training samples for the similar land cover classes (as in IKONOS image) have been collected because of the resolution difference. The results of classification for the original data sets (IKONOS and Hyperion) and the three fused products are as follows:

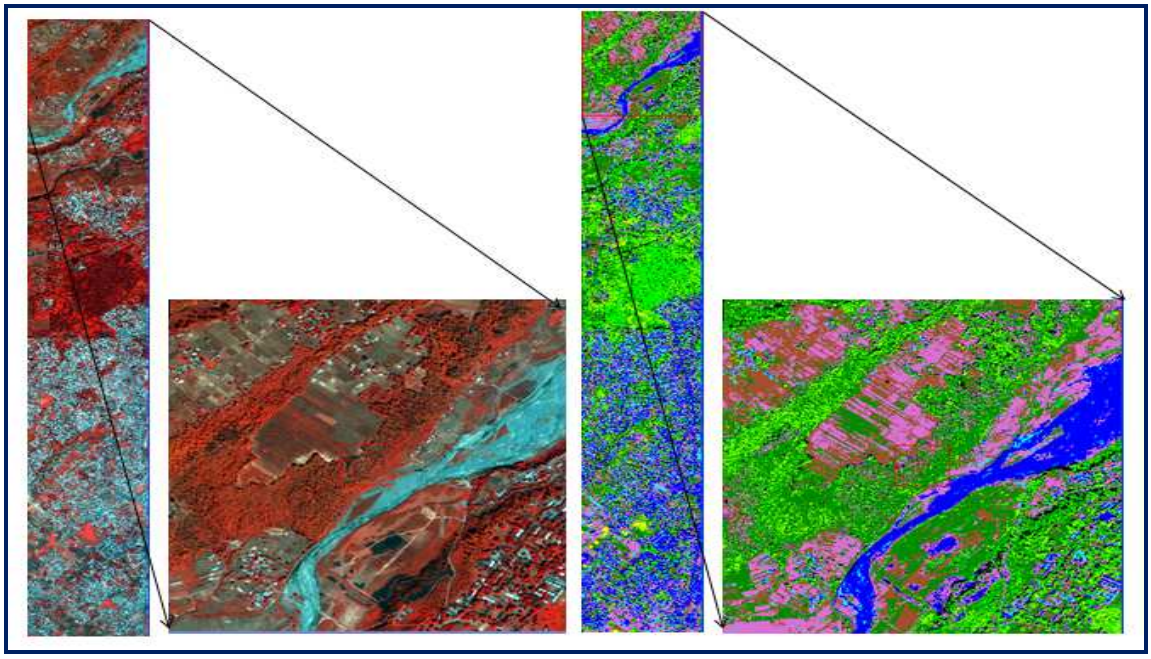

Figure 5-18 Original IKONOS and its classification

.

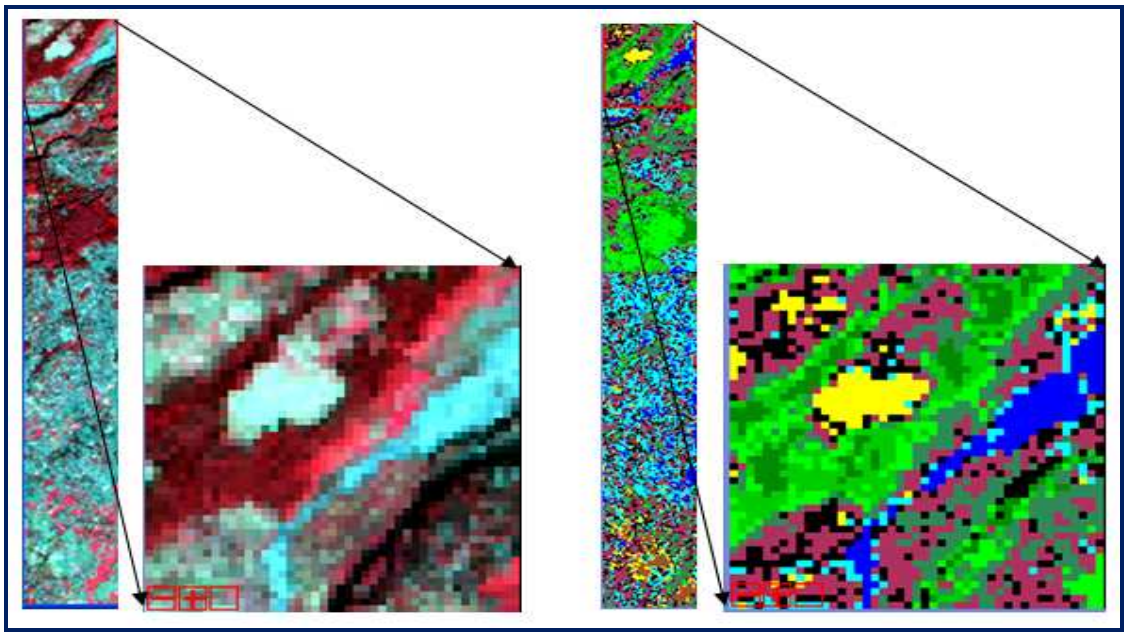

Figure 5-19 Original Hyperion and its classification.

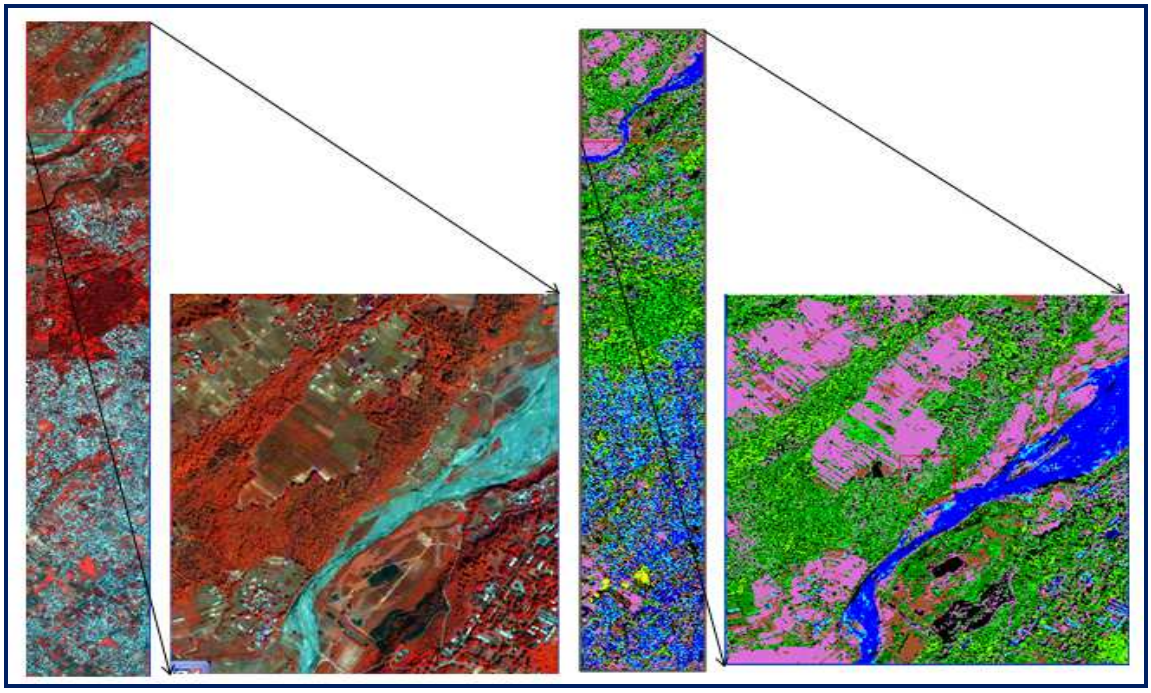

Figure 5-20 PC fused image and its classification.

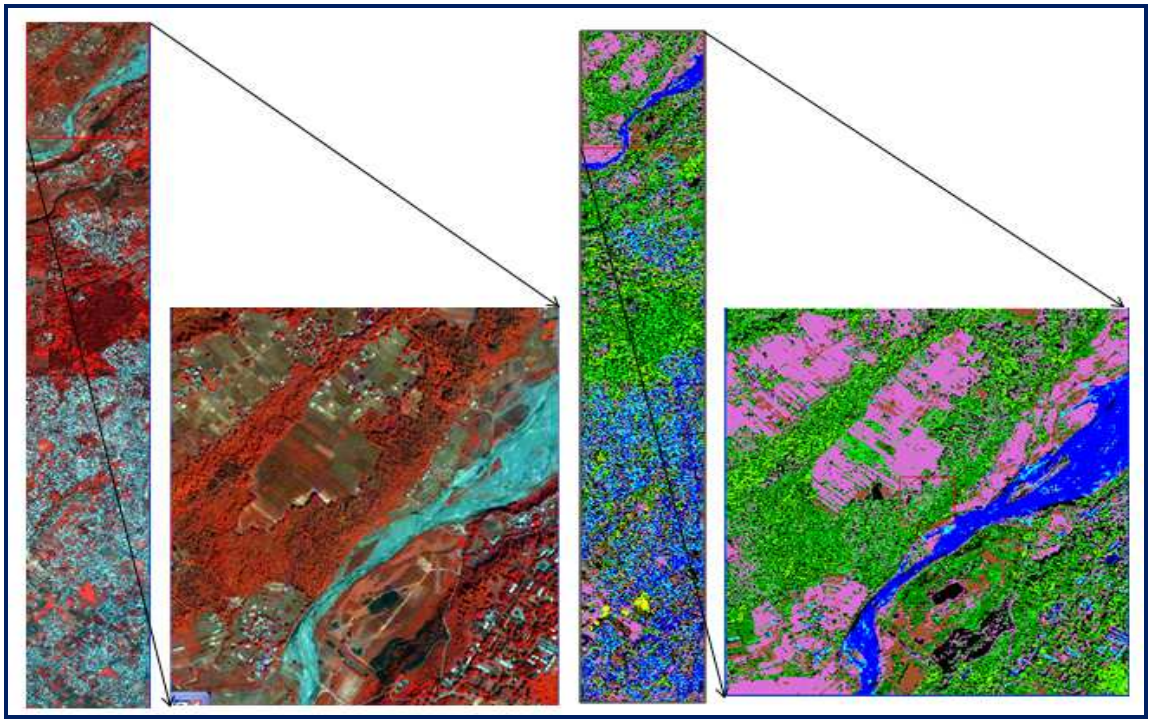

Figure 5-21 GS fused image and its classification.

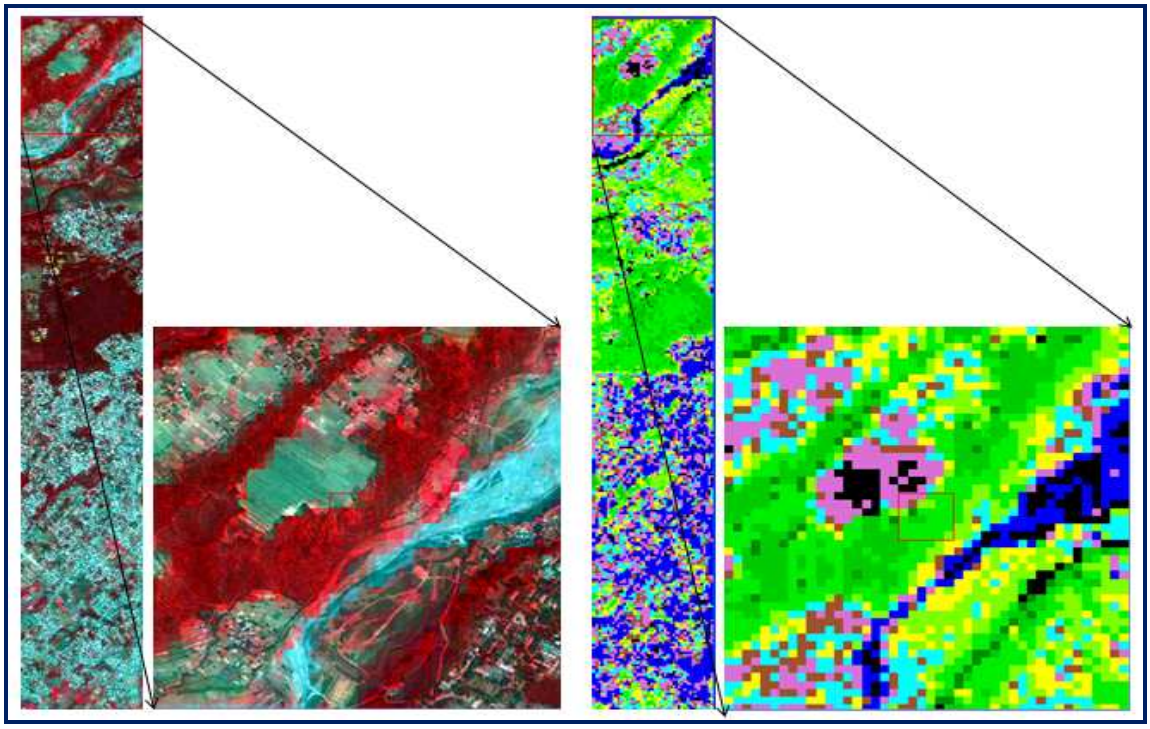

Figure 5-22 CN fused image and its classification.

The outcomes of the classification of IKONOS, Hyperion and the three merged products can be seen above. 9 land cover classes were taken i.e. urban (in cyan), vegetation type 1 (green 1), vegetation type 2 (green 2), shrubs (in green 3), grassland (in chartreuse), bare soil (in sienna), crop land (in yellow), fallow land (in orchid) and river (in blue).

In the classification outcome of images, we witness some black pixels. These black pixels are the unclassified pixels. These are left unclassified because they did not match with the pixel spectrum of any of the land cover class specified, according to the SAM (Spectral Angle Mapper) approach of supervised classification. Also, it may be due to the large angular difference (greater than .1 radians) between the known and the unknown pixel spectrum

The results of classification of the PC and GS fused image are almost similar. The results of classification for the CN fused image are very much deteriorated because of the artificial pixels that hinder in the classification process.

Also, one can observe from the classified image the spread of the blue colour in whole of the image. This is due to the silica present in the sand in the dry bed river which is the main component in the urban features (buildings) and roads.

After the classification is performed the classification accuracy has been computed for the IKONOS, Hyperion and the three merged images. For this purpose the samples have been collected from the ground itself through stringent field observations in the scene area (Dehradun). Random sampling method has been adopted for calculating the classification accuracy. 3 to 5 samples of each of the class from different locations in the Dehradun city have been collected.

The classification accuracy calculated for the IKONOS, Hyperion and the three merged products has been compared with a graphical representation.

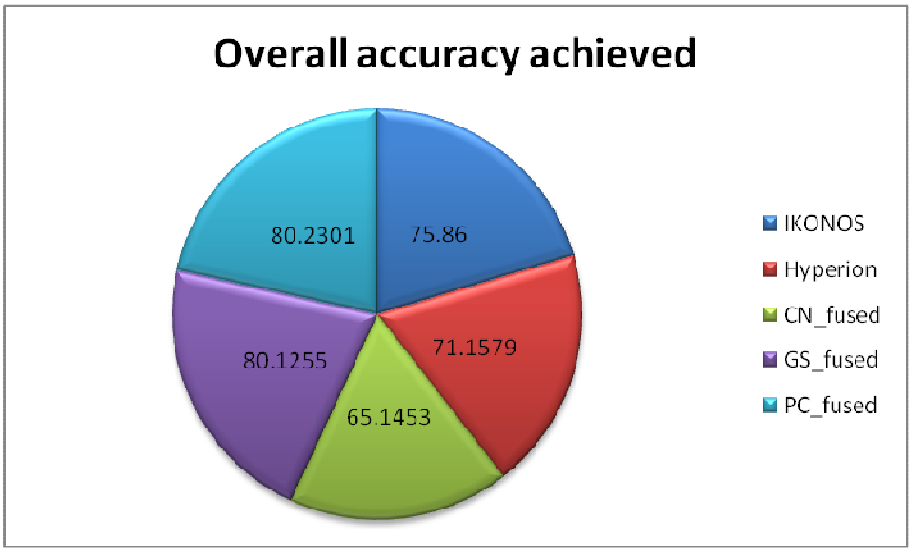

Figure 5-23 Overall accuracy achieved for different data sets

5.3. Manual classification

The classes have been delineated manually to see the consequences of the geometric accuracy and the effect of three fusion algorithms on the features extracted, before and after fusion. 21 land cover and land use classes have been delineated from the various sites in the scene area. These 21 land use and land cover classes include the linear features i.e. roads which run through the centre of the city. Two road sections at different locations have been extracted manually. The different land cover and land use classes include the fallow land, crop fields, grassland, vegetation patches at two different locations, buildings (with wooden and concrete roof top) and road sections at two different places. To extract the land cover/land use classes in the image datasets, the interpretation keys of pattern, tone, hue, shape, size, association and orientation have been exploited.

The land cover/ land use classes have been delineated easily and comfortably in high-spatial resolution IKONOS (mss) image. In turn, it was hard and complicated to extract the same LULC (Land Use and Land Cover) classes at the exact location in the Hyperion image. To extract the LULC classes in the Hyperion image, the LULC classes extracted in the IKONOS (mss) image were reassigned to the Hyperion image (using a tool in ENVI i.e. Reconcile ROIs via. Map in the ROI tool box) to obtain an approximate orientation of the classes. Roughly, once we obtain the location of the LULC classes in the Hyperion image, the interpretation keys were utilized to delineate the same LULC classes in the Hyperion image.

Once the LULC classes have been delineated in the original datasets (IKONOS and Hyperion), the same ROIs (samples) from the IKONOS image were communicated to the three fused images (CNT, GST and the PCT) since after fusion they encompass the same resolution as that of the IKONOS.

After the features are extracted in the image files, the next step was to extract the TP (True Positive), FP (False Positive) and the FN (False Negative) area for every delineated class. To acquire the TP, FP and the FN area for the various LULC classes in the image files, a composite image (merged IKONOS, mss and IKONOS, Pan) has been used as the reference image. The similar LULC classes have been

delineated in the reference image also. The two layers (of similar classes in the test and the reference image) are overlaid to obtain the TP, FP and the FN area. The area which is common and matches in both the test (input image) and the reference image is pertained as the TP (True Positive) area, the area which is coming from the reference image but does not match with the area of the class in the test image is termed as the FN (False Negative) and the area which lies in the test image but does not match with the area covered by the reference image is termed as the FP (False Positive) area. The TP, FP and FN area is taken in terms of the pixels. Once we acquire TP, FP and the FN area, the completeness and correctness has been calculated for the various LULC classes.

The LULC classes taken in the images data sets (IKONOS, Hyperion and the three fused products) are as follows:

Features	*TP(True Positive)*	*FP (False Positive)*	*FN (False Negative)*	*Completeness = TP/(TP+FN)(in %)*	*Correctness=TP/(TP+FP)(in %)*
Fallow_land_A	168	35	62	73.04	82.75
Fallow_land_B	22	8	16	57.89	73.33
Bare_soil_field_A	11	3	9	55	78.57
Bare_soil_field_B	8	2	12	40	80
Bare_soil_field_C	7	1	6	53.84	87.5
Building type 1_A	3	4	2	60	42.857
Building type 1_B	6	6	2	75	50
Building type 1_C	3	5	3	50	37.5
Building type 2_A	4	1	2	66.66	80
Building5 type 2_B	2	1	1	66.66	66.66
Building type 2_C	3	3	1	75	50
Vegetation patch type 1	15	8	6	71.42	65.21
Vegetation patch type 2	29	8	10	74.35	78.37
Grassland_A	18	15	5	78.26	54.54
Grassland_B	25	7	3	89	78
Crop_field_A	33	14	5	86.89	70.21
Crop_field_B	19	12	5	79.16	61.29
Crop_field_C	15	6	10	60	71.42
Crop_field_D	8	7	3	72.72	53.33
Road_A	28	17	20	58.33	62.2
Road_B	30	21	28	51.724	58.82

Table 5-1 List of the LULC classes taken in the image datasets.

Some of the LULC classes absorbed like the fallow land, grassland, bare soil field, crop field and the road have been prearranged with different terminology like the fallow_land_A and fallow_land_B or building_type1_A etc. This intends that the similar LULC class have been delineated at different locations from the scene area.

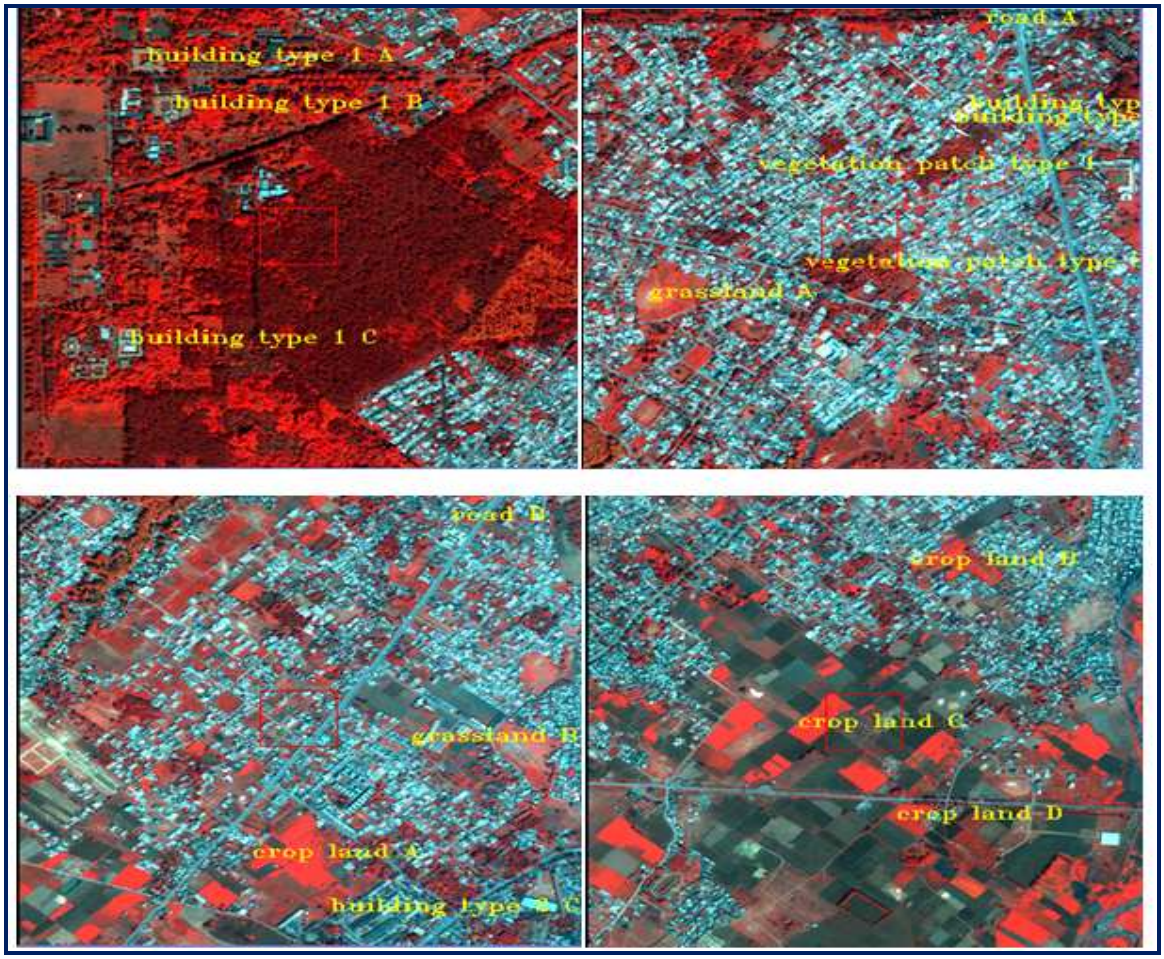

Figure 5-24 LULC classes taken for the manual delineation

Above figure shows the screenshots taken from the IKONOS image with the LULC classes marked at different locations in the scene. The screen shots of the IKONOS image is taken in four sections because whole image could not draw closer LULC classes in a single strip.

Some of the classes like the building type 1 and building type 2 have been differentiated on the material basis. Building type 1 means the material of the roof top is made of terra cotta tiles (composed of clay in which the presence of iron give them a reddish tint) and building type 2 means the material of the roof top is of concrete and cement (mainly composed of silica). Likewise, vegetation type 1 means mostly the trees present in an extracted patch are of Sal (Shoria Robusta) and vegetation type 2 means the trees in the extracted patch are of Teak (Tectona Grandis). Two or three crop fields are extracted at different locations and likewise, two road sections are extracted at different places in the region. Hence, the suffix of A, B, C and D has been assigned to the LULC classes.

The features delineated in the image datasets are as follows:

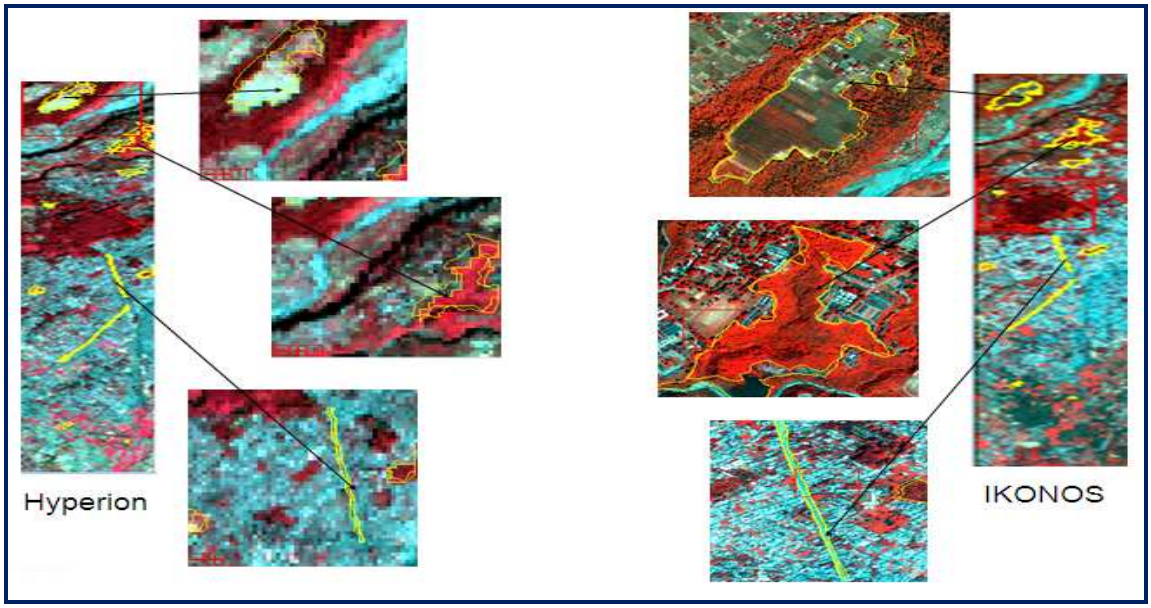

Figure 5-25 Some LULC classes extracted in the original data sets.

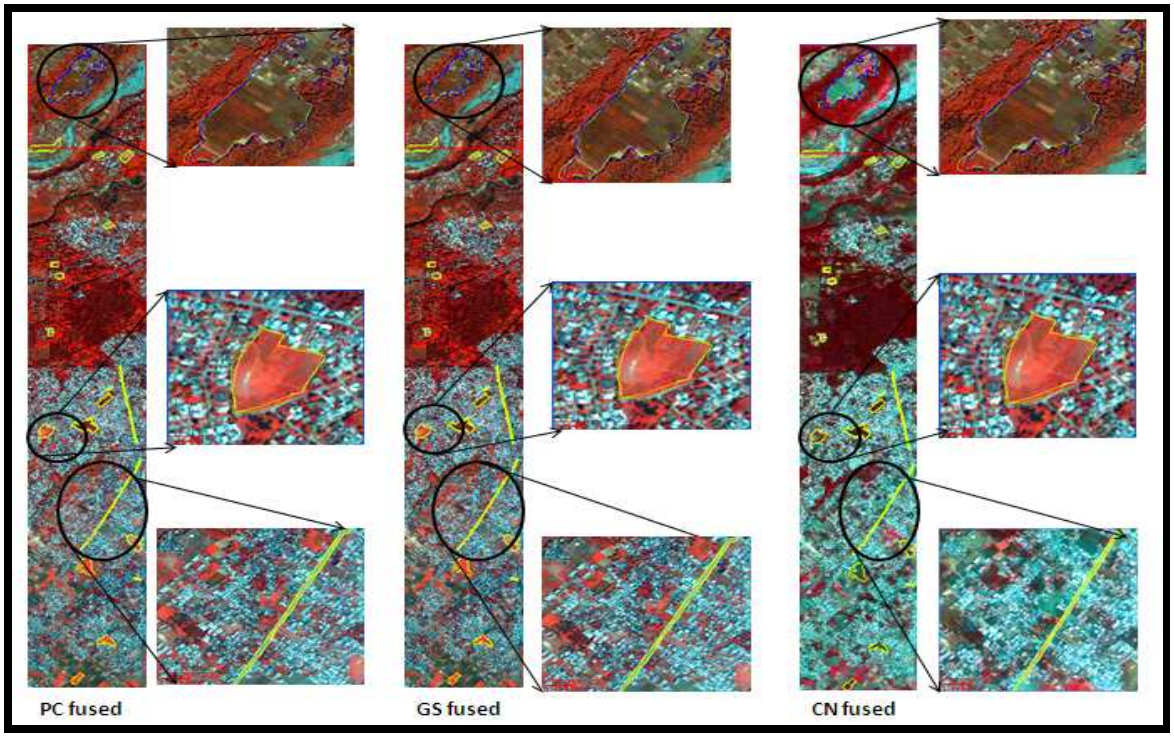

Figure 5-26 Same LULC classes in the three fused images

The TP, FP and the FN area extracted in the images data sets is as follows:

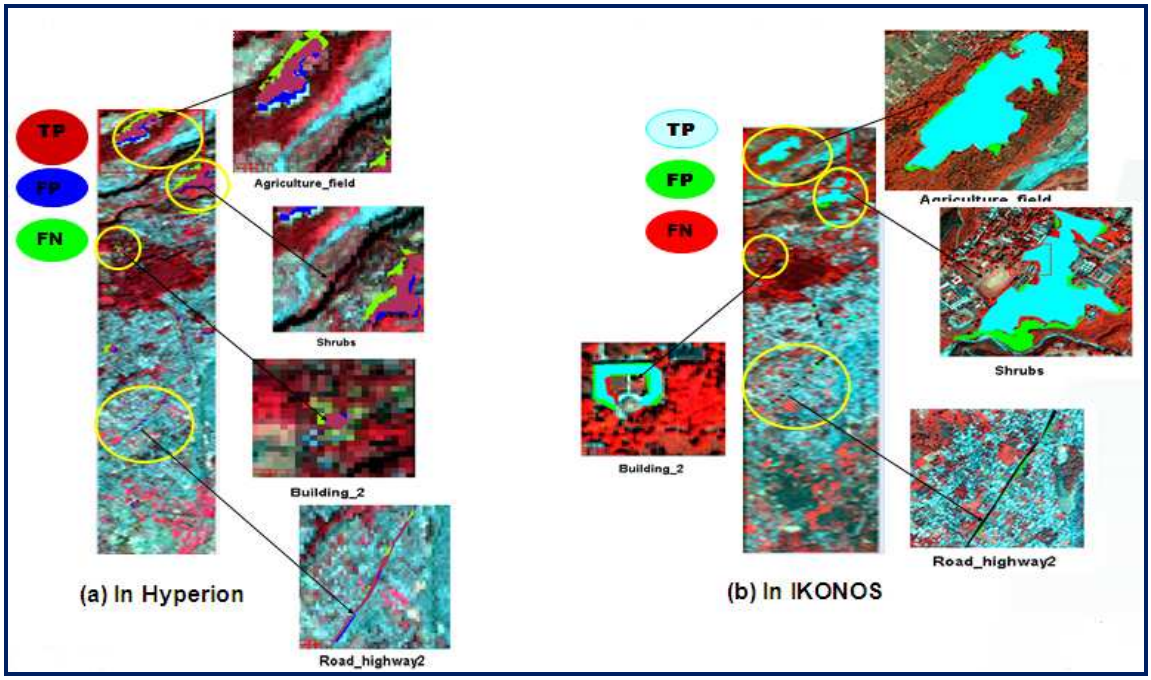

Figure 5-27 TP, FP and the FN area demarcated in the original data sets.

In the same manner, the TP, FP and the FN area is acquired for the fused images by reassigning the same LULC samples to the three fused products.

To investigate that if there is a gain in the geometric accuracy of the LULC classes before and after fusion, the outcomes of the completeness and correctness for the various LULC classes in the three fused products is compared with the completeness and correctness parameters calculated for the high-spatial resolution IKONOS, mss image. This comparison has been executed with the IKONOS image because IKONOS has better spatial resolution. The results are highlighted using graphical representations:

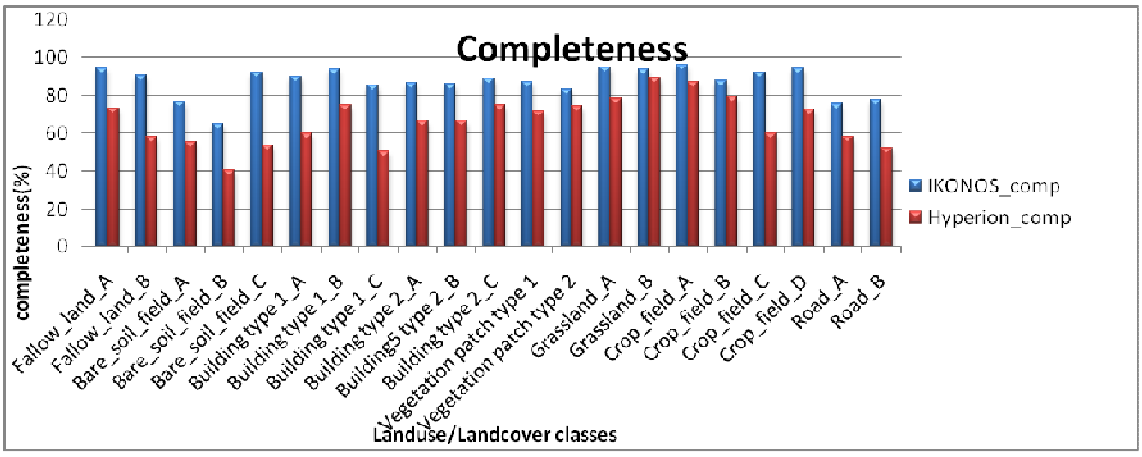

Figure 5-28 Completeness comparison, IKONOS vs. Hyperion

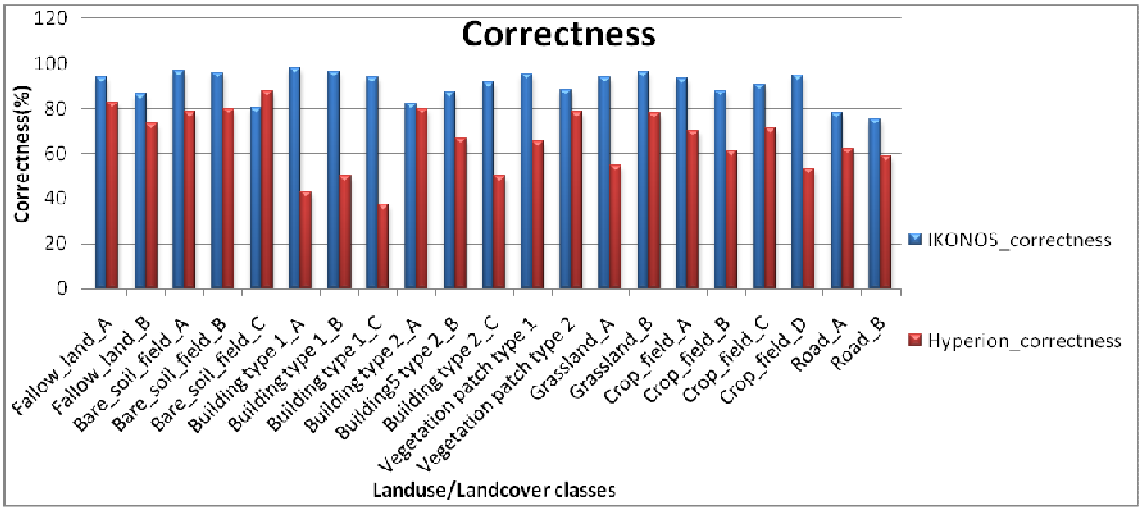

Figure 5-29 Correctness comparison, IKONOS vs. Hyperion

The graphs shown above demonstrate the completeness and correctness calculated for IKONOS vs. Hyperion. The comparison of the graphs verify that in terms of quality the LULC classes delineated in the high-resolution image IKONOS have high values for completeness and correctness. Particularly, for the man made features like the building, the difference is quite remarkable. This is due to the fact that the man made features like the buildings have superior geometry and defined boundaries instead of the natural features like vegetation or the bare soil which can not be marked in defined area because of the spread. Even for the landcover classes like grassland and crop fields the difference is remarkable because of the geometry of the classes.

For the manually delineated linear features i.e. the roads the values of completeness and correctness are quite small in both the data sets (IKONOS, Hyperion) because of the trees present on both the sides of the road which hinder in the delineation process and thus less area is captured. Even the building feature type 2 show low value of correctness in both the data sets (IKONOS, Hyperion) as compared to the building feature type 1 because of the shadow of the trees present at that location in the scene which obstruct the extraction phenomenon in the images.

When the same samples (ROIs) are passed from the IKONOS image to the three fused products, we observe that there is no gain in the completeness and correctness of the various LULC classes. This is due to the reason that the three fused images achieve the same resolution of the IKONOS image. The comparison of the completeness and correctness of the various LULC classes in the three fused products with the IKONOS has been plotted in graphs.

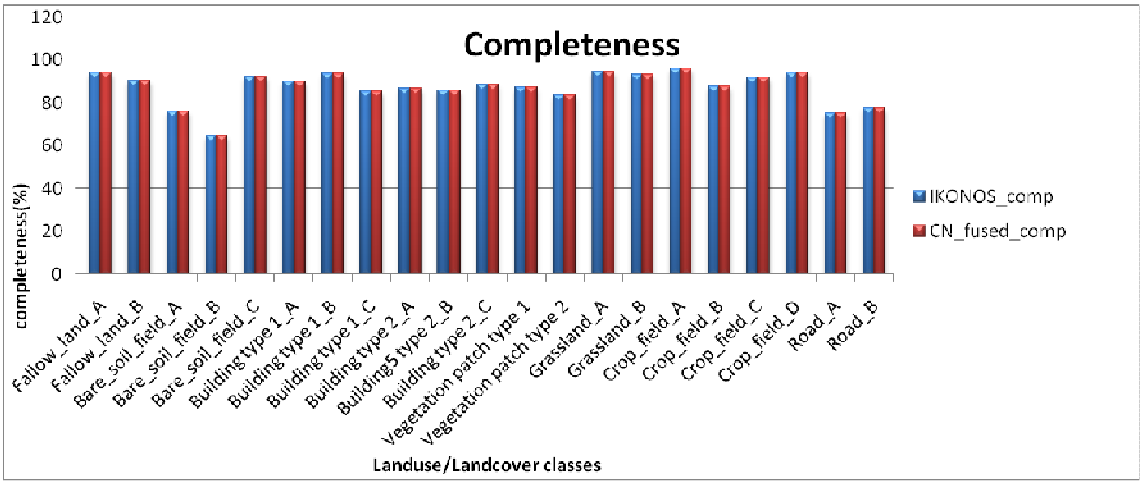

Figure 5-30 Completeness comparison in IKONOS vs. CN fused.

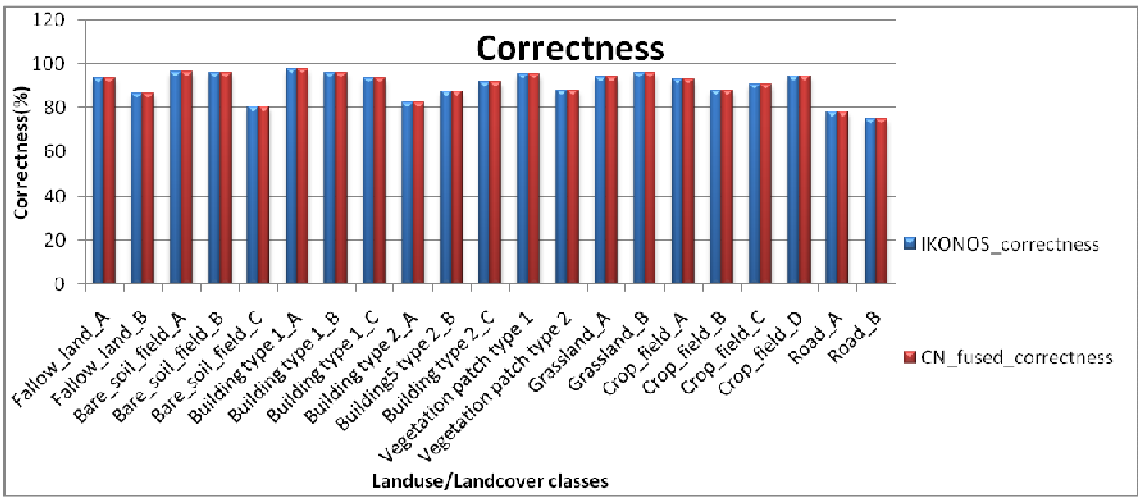

Figure 5-31 Correctness comparison in IKONOS vs. CN fused

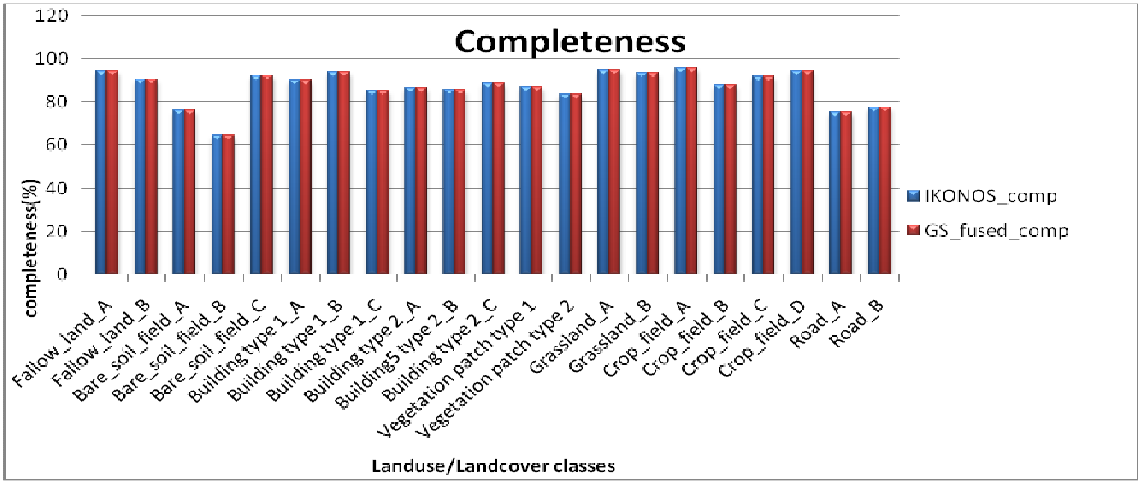

Figure 5-32 Completeness comparison in IKONOS vs. GS fused.

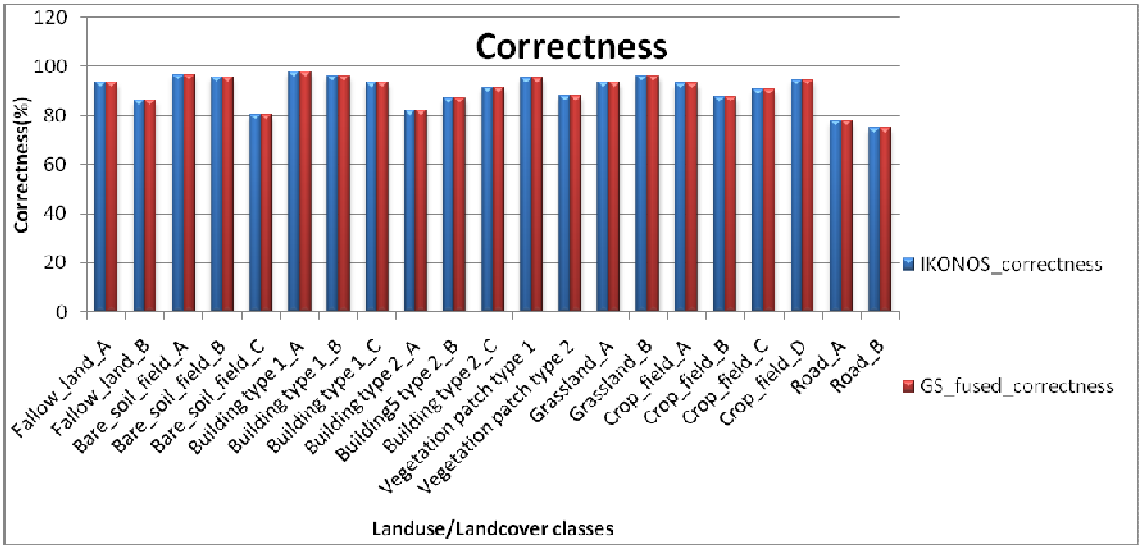

Figure 5-33 Correctness comparison in IKONOS vs. GS fused.

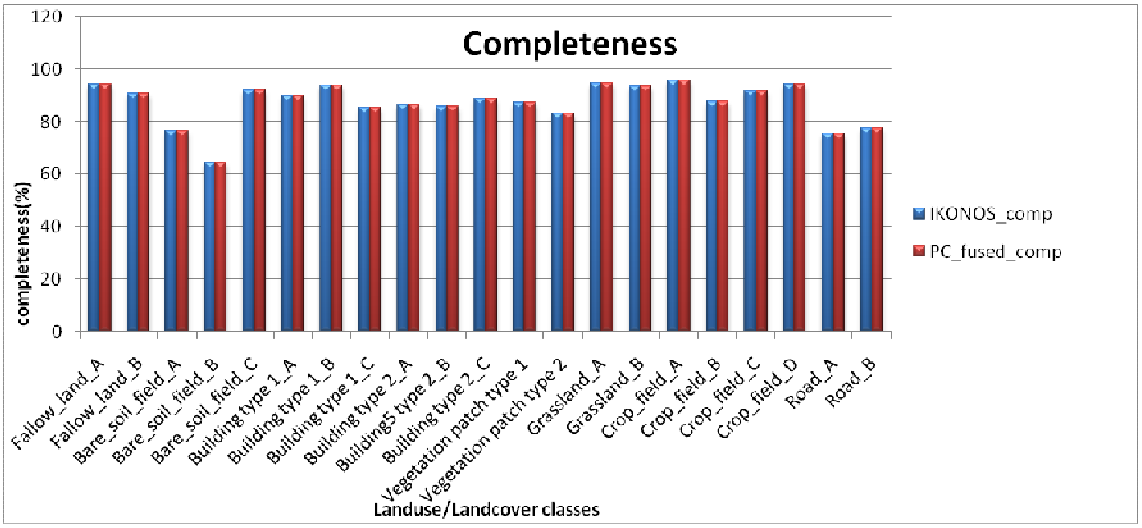

Figure 5-34 Completeness comparison in IKONOS vs. PC fused.

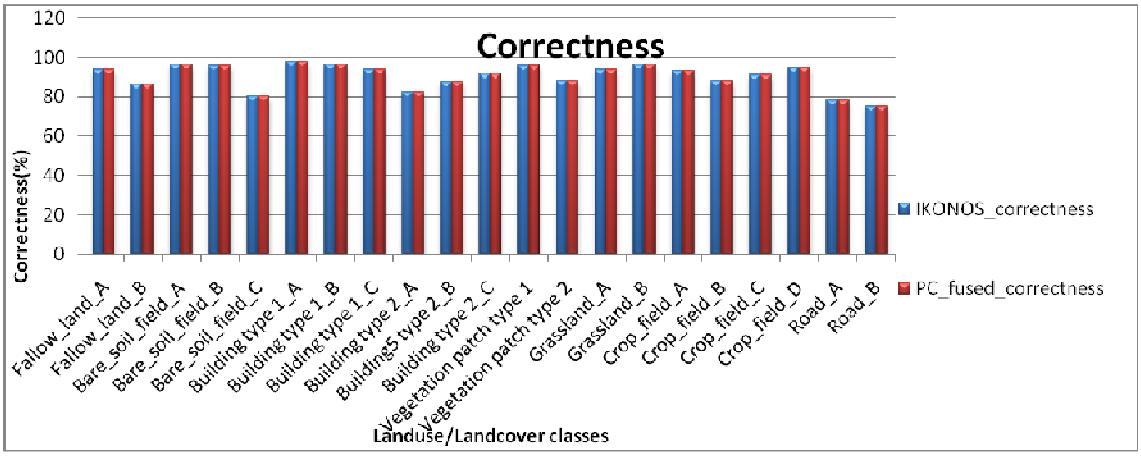

Figure 5-35 Correctness comparison in IKONOS vs. PC fused.

The comparison of the above graphs show that there is a gain in the completeness and correctness of the various LULC classes after fusion using the three merging techniques (GST, PCT and CNT) if compared to the Hyperion image but no gain if compared to the IKONOS, mss image.

5.4. Performance analysis of the three fused images with the original IKONOS and Hyperion images

The performance assessment is accomplished by probing the spatial and the spectral changes in the three fused products with respect to the original IKONOS and the Hyperion image.

5.4.1. Spatial evaluation

The spatial quality of the image refers to ability to identify the features present in the image data distinctly. In the present context, the spatial quality of the fused image is examined on the ground of the two quality measures i.e. completeness and correctness. The samples (ROIs) that have been delineated in the original data set (IKONOS), the same ROIs have been passed to the three merged images for investigating the spatial enhancement in the merged images.

To assess the spatial quality of the merged images some LULC classes have been examined. The outcomes investigate that there is an increase in the spatial quality of the images after fusion using any of the three techniques in comparison to the Hyperion but no gain in comparison to the IKONOS image. Once we extract the TP, FP and the FN areas for the various LULC classes in the data sets, completeness and the correctness are computed. The completeness and correctness computed for the LULC classes in the IKONOS image and the three merged images are the same. For the cultural class like the buildings, the completeness and correctness shows large values while for the natural land cover classes like the bare soil or the vegetation patches which do not have the defined boundaries, the values are comparatively low.

The linear features, roads have remarkably low values as compared to other features. This is due to the trees present at the sides of the road that obstruct in the delineation process.

5.4.2. Spectral evaluation

The spectral evaluation of the features is performed to examine and assess the spectral enhancement in the three fused images as compared to the Hyperion image. The spectral enhancement in the features is assessed by observing and investigating the spectral profiles of the various LULC classes.

The outcomes of the profile show enhancement in the spectral characteristics of the features in the CN fused image as compared to the GS and PC fused image. Although, the value range of the CN fused image is limited as compared to the Hyperion, the shape of the profiles for most of the features obtained in the CN fused image match more closely to the shape of the profiles of the same features in the Hyperion image.

The spectral profiles obtained for the vegetation show variations within a single pixel. The study of the spectral profile of the vegetation show variations and hence confirms the presence of varied vegetation in the region. During the field survey in the Dehradun city it was established that in the FRI region of Dehradun, vegetation content of Sal (Shoria Robusta), Teak (Tectona Grandis) and Bamboo is predominantly present. For the man-made feature like buildings some observations has been established. The spectral profile of IGFNA building situated near to the FRI main building show some variations from the remaining buildings. The reason for the difference in the profile was due to material difference of the roof top. The IGFNA building located near FRI has the roof top constructed of terra cotta tiles and the other buildings present in the scene are mostly of concrete in which the presence of silica affects the spectral profile. Thus, in the fused image the enhancement in the spectral characteristics has been observed for some of the classes which confirm that fused images better preserve the spectral properties of the Hyperion data.

5.4.3. Feature Space Analysis (FSA) and Classification

The FSA performed on the original and the three fused data sets show that after fusion using the three merging techniques the separability for some of the land cover/ land use classes like the shrubs, bare soil, vegetation increases after fusion. The same ROIs have been assigned to the original and the three merged images.

The increase in separability of the classes (signatures) in the feature space directly affects the classification and overall accuracy acquired for the image data sets. The overall accuracy obtained for the fused image is higher than IKONOS and Hyperion image. Specially, for the homogenous class like vegetation, the increase in accuracy is comparable. The results of classification for the CN fused image are speculative due to the reason of the spectral artifacts .Hence; the overall accuracy computed is quite low.

5.5. Discussion

Qualitative assessment of the fused images for classification and feature extraction requires the evaluation of the fused images on the ground of the spatial or the spectral enhancement. The spatial quality of the fused images has been judged by the computation of the quality measures of completeness and correctness while the spectral enhancement can be approximated by the analysis of the spectral profiles and also by comparing the statistical parameters of mean, maximum, minimum, and standard deviation values of the various LULC classes in different bands.

The qualitative analysis has been carried out for the various LULC classes present in the Dehradun city like the vegetation patches, bare soil, grassland, buildings, etc. In the first experiment, the completeness of the various LULC classes is compared to the completeness of the LULC classes extracted in the IKONOS image. The samples (or ROISs) that are extracted from the IKONOS image, the same samples have been specified to the three fused images. The results of the comparison prove that there is no gain in the spatial quality of three fused images if compared to the IKONOS image .The TP (True Positive), FP (False Positive) and the FN (False Negative) area gained in the IKONOS image is equivalent to the TP, FP and the FN area in the three fused image. In the second experiment, the correctness of the various LULC classes is compared to the correctness of the LULC classes extracted in the IKONOS image. After passing the same samples to the three fused images, the outcomes show no gain in the correctness factor in any of the three merged images also.

The spectral evaluation is based on the spectral profiles obtained for the various LULC classes. From the profiles of some of the LULC classes shown in the chapter "Results & Discussion", we observe that the shape of the profiles for most of the LULC classes in CN fused image closely match to the shape of the profiles of the LULC classes in the Hyperion image. This establishes that the CN fused image better preserves the spectral characteristics as in the original Hyperion image.

Separability analysis performed in the present work demonstrates that separability for some of the classes (or signatures) in the feature space increases after fusion and as a result of this, the classification accuracy obtained for the GS (Gram-Schmidt) and the PC (Principal Component) fused image is greater than the classification accuracy of the IKONOS and Hyperion images. The classification results of CN fused images were badly affected due to the problem of spectral artifacts.

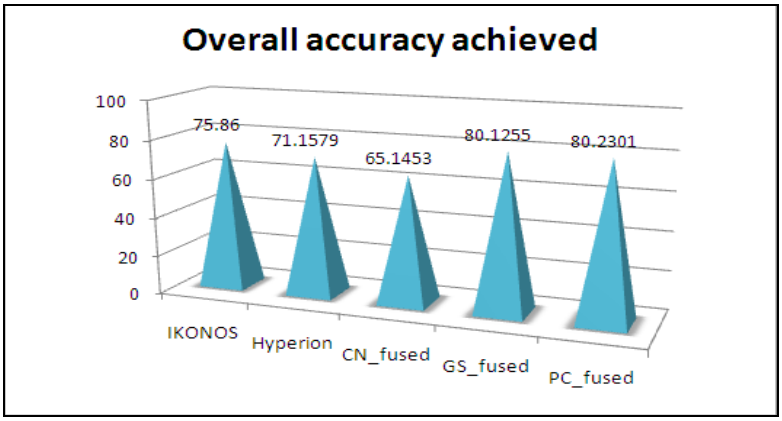

Figure 5-36 Overall accuracy comparison.

6. Conclusions and further recommendations

6.1. Overall conclusion

The main objective of the present study was the performance analysis of the high-resolution and hyperspectral data fusion for classification and feature extraction. To accomplish this objective, fusion of multispectral (IKONOS, mss) and hyperspectral (Hyperion) using the three techniques i.e. GST (Gram-Schmidt Transform), PCT (Principal Component Transform) and CNT (Colour Normalised Transform) has been performed. In terms of the spatial quality, there is remarkable enhancement in features if compared to the Hyperion but if compared to the high-spatial resolution data (IKONOS), there is no gain. The quality measures of completeness and correctness has been computed to quantify the spatial enhancement. The comparison of the outcomes of the completeness and correctness calculated for the LULC classes show no gain in manual classification after fusion using any of the three merging techniques. The comparison of the separability analysis done to the original data sets and the three fused products, show that the separability for some of the classes increases after fusion and hence the classification accuracy achieved is higher. The results of the CN fused image were badly affected due to the artificial pixels that hindered in the classification process. The spectral quality evaluation was performed by examining the spectral profiles of LULC classes. The outcomes of the spectral evaluation show that CN fused image better preserve the spectral characteristics in comparison to the GS and the PC fused images.

6.1.1. Sub-conclusions

In order to render the answers of the research questions framed in the present study, different experiments were carried out. Most of the work has been completed in ENVI (Environment for Visualising Images) because of its potential to handle the hyperspectral data and particular tools are available for feature extraction and classifying the hyperspectral data.

- Is there a gain in classification and feature extraction from the fusion of high spatial resolution and hyperspectral data, i.e. is there a gain in geometric accuracy while the high thematic information is kept?

Ans. No, there is no gain in the geometric accuracy of the LULC classes after fusion using the three merging techniques while the high thematic accuracy is kept.

The fusion of IKONOS, mss with the Hyperion using the three merging techniques of Gram-Schmidt, Principal Component and the Colour Normalised transform resulted in images with the spatial resolution similar to the IKONOS, mss. When some samples (ROIs) of LULC classes were delineated in the IKONOS image, the same ROIs has been passed to the three merged products and the TP, FP and the FN area was obtained in terms of pixels. The quality measures of completeness

and correctness calculated for the LULC classes in the three merged products show no gain in geometric accuracy after fusion.

- What is the effect of fusion regarding the separability of the classes in the feature space?

Ans. The separability of the classes in feature space increases after fusion using the three merging techniques. Particularly, for some of the classes like vegetation, bare soil, crops, shrubs, and grasslands the separability increases and as a result of this the classification results are enhanced. The separability of the signatures has been visualised in the n-D visualiser. The assessment of the n-D visualiser shows that the classes are well separable in the feature space after fusion. Hence, the classification accuracy of the GS and the PC fused images is higher than the IKONOS. The results of classification done to the CN fused image are badly affected due to the spectral artifacts and hence the classification accuracy is low.

- How do the results of classification and feature extraction depend on the selected algorithm?

Ans. This is an extension of the second answer. In terms of the spatial evaluation, the results of the three fused images are almost comparable and hence the outcomes of the completeness and correctness computed for the LULC classes in the three merged images are the same. It implies that there is no gain in terms of the feature extraction using any of the three merging techniques.
The second issue is of the effect of the three merging techniques on the digital classification processes. In the present study, SAM (Spectral Angle Mapper) approach of supervised classification is used to classify the original data sets and the three merged images. As we discover that the results of separability of signatures (classes) in the feature space do not differ much in the three merging techniques, the classification results of the three merged products are almost similar. Statistically, there is not much remarkable difference in the statistical parameters of mean, maximum, minimum and standard deviation of the classes in different bands except for the CN fused image for which the values are quite low. The results of classification do not differ much in the GS and the PC fused image .The results of classification done to the CN fused image are badly affected due to the spectral artifacts.

Data	Overall accuracy
Hyperion	71.1579
IKONOS, mss	75.86
GS fused image	80.1255
PC fused image	80.2301
CN fused image	65.1453

Table 6-1 Table showing the overall accuracy in all the data sets

6.2. Recommendations

Some of the factors to be considered for further detailed work in the direction of multispectral/hyperspectral image fusion are:

- Resolution difference between multispectral and the hyperspectral data.
- Scene area (homogenous patch should be taken for better classification and feature extraction). Also, the urban pattern of the scene should be regular and customary for better segmentation and feature extraction processes.
- Methods of atmospheric correction for the Hyperion data.
- Standard classification methods for Hyperion data of a heterogeneous scene with large spectral variations in some of the LULC classes.
- Some other algorithms to merge the multispectral/hyperspectral data to enhance the details after fusion.

These parameters should be considered in more detail in future studies.

7. References

Aarthy, R.S. and Sanjeevi, S., 2007. Spectral studies of lunar equivalent rocks-A prelude to lunar mineral mapping. Indian society of Remote Sensing, 35(2): 141- 152.

Aiazzi, B., Alparone, L., Baronti, S. and Selva, M., 2006. MS + Pan Image Fusion by an Enhanced Gram-Schmidt Spectral Sharpening, Italy. www.igik.edu.pl/earsel2006/abstracts/data_fusion/aiazzi_baronti.pdf

Ali Darvishi, B., Kuppas, M. and Erasmi, S., 2005. Hyper-spectral/High resolution Data fusion: Assessing the quality of EO1 - Hyperion/spot-Pan and Quickbird-MS fused Images in spectral Domain.

Bakker, H.W. et al., 2004. Principals of Remote Sensing. The international institute for Geo-Information Science and Earth Observation(ITC), Enschede.

Chen, C.-M., Hepner, G.F. and R.R., F., 2003. Fusion of Hyperspectral and radar data using the IHS transformation to enhance urban surface features. ISPRS Journal of photogrammetry and Remote Sensing, 58(2003): 19-30.

Eckert, S. and Kneubuhler, M., 2004. Application of hyperion data to agricultural land classification and vegetation properties estimation in switzerland. Remote Sensing Laboratories(RSL), ZURICH. http://cartesia.org/geodoc/ISPRS2004/comm7/papers/170.pdf

Gomez, B.R., Jazaeri, A. and Kafatos, M., 2001. Wavelet-based hyperspectral and multispectral image fusion. www.scs.gmu.edu/~rgomez/fall01/fusionpaper.pdf

Greiwe, A. and Ehlers, M., 2008. COMBINED ANALYSIS OF HYPERSPECTRAL AND HIGH RESOLUTION IMAGE DATA IN AN OBJECT ORIENTED CLASSIFICATION APPROACH, Germany. www.isprs.org/commission8/workshop_urban/greiwe.pdf

Huang, R. and He, M., April,2005. Band Selection Based on Feature Weighting for Classification of Hyperspectral Data. IEEE transactions on geoscience and remote sensing, 2(2).

Jensen, J.R., 1996. Introductory Digital Image Processing- A Remote Sensing Perspective. Prentice-Hall.

Lee, R.J. and Davies, A.G., 2004. Autonomous vegetation cover scene classification of EO-1 Hyperion Hyperspectral data. Lunar and planetary Science XXXV(2004). http://eo1.gsfc.nasa.gov/new/SensorWebExp/JPL-Papers/Lee-Aut-Veg.pdf

Lillesand, M.T. and Kiefer, W.R., 2000. Remote sensing and image interpretation. John Wiley and sons, New york.

Ling, Y., Ehlers, M., Usery, l.E. and Marguerite, M., 2006. FFT-enhanced IHS transform method for fusing high-resolution satellite images. ISPRS Journal of photogrammetry and Remote Sensing, 61(2007): 381-392.

Owojori, A. and Xie, H., 2008. LANDSAT IMAGE-BASED LULC CHANGES OF SAN ANTONIO, TEXAS USING ADVANCED ATMOSPHERIC CORRECTION AND OBJECT-ORIENTED IMAGE ANALYSIS APPROACHES, San Antonio. http://www.isprs.org/commision8/workshop_urban/owojori.pdf

Pohl, C. and Genderen Van, j.l., 1998. Multisensor image fusion in remote sensing : concepts, methods and applications. International journal of remote sensing 19(5): 823-854.

San, B.T. and Suzen, M.L., 2007. COMPARISON OF ATMOSPHERIC CORRECTION TECHNIQUES
FOR HYPERION DATA, Turkey. http://www.isprs2007ist.itu.edu.tr/prog_8may07.pdf

Sanjeevi, S., 2008. Multisensor Image Fusion. In: S.A. Aggarwal and H. Pande (Editors), Advanced Image Processing. Photogrammetry and remote sensing Division Indian institute of remote sensing, Dehradun.

Shih, T.-Y., 2004. On The Atmospheric Correction for a Hyperion Scene Taiwan. www.aars.org/acrs/proceedings/ACRS2004/Papers/HDP04.2.htm

Shippert, P., 2008. Introduction to Hyperspectral Image Analysis. http://satjournal.tcom.ohiou.edu/pdf/shippert.pdf

Varshney, P.k. and Arora, M.K., 2004. Advanced Image Processing Techniques for Remotely Sensed Hyperspectral data. Springer-Verlag Berlin Heidelberg New York.

Wiedemann, C., Heipke, C. and Mayer, H., 1998. EMPIRICAL EVALUATION OF AUTOMATICALLY EXTRACTED ROAD AXES. www.ipk.bv.tum.de/site_lpf/site_new/ download/ pub/1998/Weidemann_eemev98.ps.gz